Supramolecular Polymerization Provides Non-Equilibrium Product Distributions of Imine-Linked Macrocycles

Michael J. Strauss, Austin M. Evans, Ioannina Castano, Rebecca L. Li, and William R. Dichtel*

Department of Chemistry, Northwestern University, Evanston, IL, 60208 USA

Supplementary Information

Correspondence Address
Professor William R. Dichtel Department of Chemistry Northwestern University 2145 Sheridan Road Evanston, IL 60208 United States wdichtel@northwestern.edu

Table of Contents

A. Materials and Instrumentation S-6
- **I.** Materials
- **II.** Instrumentation

B. Synthetic Procedures S-8

C. ^{1}H and ^{13}C NMR of Monomers S-17

D. Dilution Experiments: Macrocycle and Nanotube Characterization S-18
- **I.** Characterization of **MC 1**
- **II.** Characterization of **MC 2**

E. Kinetic Experiments: Macrocycle and Nanotube Characterization S-38
- **I.** Characterization of **MC 1** Kinetics
- **II.** Characterization of **MC 2** Kinetics

F. Scrambling Experiments: Macrocycle and Nanotube Characterization S-45

G. Competition Experiments: Macrocycle and Nanotube Characterization S-54

H. Monomer Exchange Experiments: Macrocycle and Nanotube Characterization S-63
- **I.** Monomer Exchange of **MC 2**
- **II.** Monomer Exchange of **MC 1**
- **III.** Monomer Exchange of 5-Br-IDA MC

I. Small Molecule ^{1}H NMR Studies S-73
- **I.** Small Molecule Competition ^{1}H NMR Study
- **II.** Small Molecule 'Scrambling' ^{1}H NMR Study

J. References S-77

List of Schemes, Tables, and Figures in Supporting Information

Schemes in Supporting Information — **Page No.**

Scheme S1. Overall Synthesis of **S1** (DAPB) S-9
Scheme S2. Synthesis of **MC 1** and Corresponding Dilution Experiments S-10
Scheme S3. Synthesis of **MC 2** and Corresponding Dilution Experiments S-11
Scheme S4. Scrambling Experiments Between **MC 1** and **MC 2** S-12
Scheme S5. Competition Experiments Between **MC 1** and **MC 2** S-13
Scheme S6. Monomer Exchange Experiments Beginning with **MC 2** S-14
Scheme S7. Monomer Exchange Experiments Beginning with **MC 1** S-15
Scheme S8. Synthesis of 5-Br-IDA Macrocycles S-16
Scheme S9. Monomer Exchange Experiments Beginning with 5-Br-IDA MC S-17
Scheme S10. Small Molecule Competition Experiment S-74
Scheme S11. Small Molecule 'Scrambling' Experiment S-76

Tables in Supporting Information — **Page No.**

Table S1. Concentrations Used to Probe Dilution Effects on **MC 1** Synthesis S-10
Table S2. Concentrations Used to Probe Dilution Effects on **MC 2** Synthesis S-11
Table S3. Concentrations Used to Probe Dilution Effects on Scrambling Reactions S-12
Table S4. Concentrations Used to Probe Dilution Effects on Competition Reactions S-13

Figures in Supporting Information — **Page No.**

Figure S1. ^{1}H NMR ($CDCl_3$, 500 MHz, 298 K) of **S1** S-18
Figure S2. ^{13}C NMR ($CDCl_3$, 126 MHz, 298 K) of **S1** S-18
Figure S3. GPC of **MC 1** Synthesis at 25 mM S-19
Figure S4. MALDI-MS of **MC 1** Synthesis at 25 mM S-19
Figure S5. FT-IR of **MC 1** Synthesis at 25 mM S-20
Figure S6. ^{1}H NMR (THF-d_8, 500 MHz, 298 K) of **MC 1** S-20
Figure S7. GPC of **MC 1** Synthesis at 12.5 mM S-21
Figure S8. GPC of **MC 1** Synthesis at 8.5 mM S-21
Figure S9. GPC of **MC 1** Synthesis at 6.4 mM S-22
Figure S10. GPC of **MC 1** Synthesis at 5.1 mM S-22
Figure S11. GPC of **MC 1** Synthesis at 3.4 mM S-23
Figure S12. Overlaid GPC Traces from All Dilution Experiments S-23
Figure S13. MALDI-MS of **MC 1** Synthesis at 12.5 mM S-24
Figure S14. MALDI-MS of **MC 1** Synthesis at 8.5 mM S-24
Figure S15. MALDI-MS of **MC 1** Synthesis at 6.4 mM S-25
Figure S16. MALDI-MS of **MC 1** Synthesis at 5.1 mM S-25
Figure S17. MALDI-MS of **MC 1** Synthesis at 3.4 mM S-26
Figure S18. AFM Image of **MC 1** Synthesis at 3.4 mM S-26
Figure S19. SEM Image of **MC 1** Synthesis at 3.4 mM S-27
Figure S20. TEM Image of **MC 1** Synthesis at 25 mM S-27
Figure S21. *In*-Situ WAXS Pattern of **MC 1** Synthesis at 25 mM S-28
Figure S22. GPC of **MC 2** Synthesis at 25 mM S-29
Figure S23. MALDI-MS of **MC 2** Synthesis at 25 mM S-29
Figure S24. FT-IR of **MC 2** Synthesis at 25 mM S-30
Figure S25. ^{1}H NMR (THF-d_8, 500 MHz, 298 K) of **MC 2** S-30

Figure S26. GPC of **MC 2** Synthesis at 12.5 mM S-31
Figure S27. GPC of **MC 2** Synthesis at 8.5 mM S-31
Figure S27. GPC of **MC 2** Synthesis at 6.4 mM S-32
Figure S29. GPC of **MC 2** Synthesis at 5.1 mM S-32
Figure S30. GPC of **MC 2** Synthesis at 3.4 mM S-33
Figure S31. Overlaid GPC Traces from All Dilution Experiments S-33
Figure S32. MALDI-MS of **MC 2** Synthesis at 12.5 mM S-34
Figure S33. MALDI-MS of **MC 2** Synthesis at 8.5 mM S-34
Figure S34. MALDI-MS of **MC 2** Synthesis at 6.4 mM S-35
Figure S35. MALDI-MS of **MC 2** Synthesis at 5.1 mM S-35
Figure S36. MALDI-MS of **MC 2** Synthesis at 3.4 mM S-36
Figure S37. AFM Image of **MC 2** Synthesis at 3.4 mM S-36
Figure S38. SEM Image of **MC 2** Synthesis at 3.4 mM S-37
Figure S39. TEM Image of **MC 2** Synthesis at 25 mM S-37
Figure S40. *In*-Situ WAXS Pattern of **MC 2** Synthesis at 25 mM S-38
Figure S41. GPC of **MC 1** Synthesis After 2 Minutes S-39
Figure S42. GPC of **MC 1** Synthesis After 15 Minutes S-39
Figure S43. GPC of **MC 1** Synthesis After 30 Minutes S-40
Figure S44. GPC of **MC 1** Synthesis After 60 Minutes S-40
Figure S45. GPC of **MC 1** Synthesis After 120 Minutes S-41
Figure S46. Overlaid GPC Traces of **MC 1** Synthesis S-41
Figure S47. GPC of **MC 2** Synthesis After 2 Minutes S-42
Figure S48. GPC of **MC 2** Synthesis After 15 Minutes S-42
Figure S49. GPC of **MC 2** Synthesis After 30 Minutes S-43
Figure S50. GPC of **MC 2** Synthesis After 60 Minutes S-43
Figure S51. GPC of **MC 2** Synthesis After 120 Minutes S-44
Figure S52. Overlaid GPC Traces of **MC 2** Synthesis S-44
Figure S53. GPC of **MC 2** Synthesis After 2 Minutes at Reduced Acid Loading S-45
Figure S54. GPC of Scrambling Experiment at 25 mM S-46
Figure S55. GPC of Scrambling Experiment at 12.5 mM S-46
Figure S56. GPC of Scrambling Experiment at 8.5 mM S-47
Figure S57. GPC of Scrambling Experiment at 6.4 mM S-47
Figure S58. GPC of Scrambling Experiment at 5.1 mM S-48
Figure S59. Overlaid GPC Traces from All Scrambling Experiments S-48
Figure S60. MALDI-MS of Scrambling Experiment at 25 mM S-49
Figure S61. MALDI-MS of Scrambling Experiment at 12.5 mM S-49
Figure S62. MALDI-MS of Scrambling Experiment at 8.5 mM S-50
Figure S63. MALDI-MS of Scrambling Experiment at 6.4 mM S-50
Figure S64. MALDI-MS of Scrambling Experiment at 5.1 mM S-51
Figure S65. MALDI-MS of Scrambling Experiment at 3.4 mM S-51
Figure S66. MALDI-MS of a 1:1 Mixture of **MC 1** and **MC 2** S-52
Figure S67. ^{1}H NMR (THF-d_8, 500 MHz, 298 K) of the Scrambling Experiment S-52
Figure S68. AFM Image of the Product of the Scrambling Reaction S-53
Figure S69. SEM Image of the Product of the Scrambling Reaction S-53
Figure S70. TEM Image of the Product of the Scrambling Reaction S-54
Figure S71. *In*-Situ WAXS Pattern of the Scrambling Reaction at 25 mM S-54

Figure S72. GPC of Competition Experiment at 25 mM S-55
Figure S73. GPC of Competition Experiment at 12.5 mM S-55
Figure S74. GPC of Competition Experiment at 8.5 mM S-56
Figure S75. GPC of Competition Experiment at 6.4 mM S-56
Figure S76. GPC of Competition Experiment at 5.1 mM S-57
Figure S77. Overlaid GPC Traces from All Competition Experiments S-57
Figure S78. MALDI-MS of Competition Experiment at 25 mM S-58
Figure S79. MALDI-MS of Competition Experiment at 12.5 mM S-58
Figure S80. MALDI-MS of Competition Experiment at 8.5 mM S-59
Figure S81. MALDI-MS of Competition Experiment at 6.4 mM S-59
Figure S82. MALDI-MS of Competition Experiment at 5.1 mM S-60
Figure S83. ^{1}H NMR (THF-d_8, 500 MHz, 298 K) of the Competition Experiment S-60
Figure S84. AFM Image of the Product of the Competition Reaction S-61
Figure S85. SEM Image of the Product of the Competition Reaction S-61
Figure S86. TEM Image of the Product of the Competition Reaction S-62
Figure S87. *In*-Situ WAXS Pattern of the Competition Reaction at 25 mM S-62
Figure S88. GPC of the Monomer Exchange Reaction Beginning with **MC 2** S-63
Figure S89. MALDI-MS of the Monomer Exchange Reaction Beginning with **MC 2** S-63
Figure S90. FT-IR of the Monomer Exchange Reaction Beginning with **MC 2** S-64
Figure S91. ^{1}H NMR (THF-d_8, 500 MHz, 298 K) of the Monomer Exchange Reaction Beginning with **MC 2** S-64
Figure S92. AFM Image of the Monomer Exchange Beginning with **MC 2** S-65
Figure S93. SEM Image of the Monomer Exchange Beginning with **MC 2** S-65
Figure S94. TEM Image of the Monomer Exchange Beginning with **MC 2** S-66
Figure S95. *In*-Situ WAXS Pattern of the Monomer Exchange Reaction Beginning with **MC 2** S-66
Figure S96. GPC of the Monomer Exchange Reaction Beginning with **MC 1** S-67
Figure S97. MALDI-MS of the Monomer Exchange Reaction Beginning with **MC 1** S-67
Figure S98. FT-IR of the Monomer Exchange Reaction Beginning with **MC 1** S-68
Figure S99. ^{1}H NMR (THF-d_8, 500 MHz, 298 K) of the Monomer Exchange Reaction Beginning with **MC 1** S-68
Figure S100. Comparison of ^{1}H NMR spectra of **MC 1**, **MC 2,** and the Product of Monomer Exchange Beginning with **MC 1** S-69
Figure S101. ^{1}H NMR Quantification of Monomer Exchange S-69
Figure S102. AFM Image of the Monomer Exchange Beginning with **MC 1** S-70
Figure S103. SEM Image of the Monomer Exchange Beginning with **MC 1** S-70
Figure S104. TEM Image of the Monomer Exchange Beginning with **MC 1** S-71
Figure S105. *In*-Situ WAXS Pattern of the Monomer Exchange Reaction Beginning with **MC 1** S-71
Figure S106. GPC of 5-Br-IDA Macrocycles S-72
Figure S107. MALDI-MS of 5-Br-IDA Macrocycles S-72
Figure S108. GPC of 5-Br-IDA Macrocycle Monomer Exchange S-73
Figure S109. MALDI-MS of 5-Br-IDA Macrocycle Monomer Exchange S-73
Figure S110. Stacked ^{1}H NMR Spectra from Small Molecule Competition Reaction S-74
Figure S111. Normalized Integrations of Key Protons in Small Molecule Competition Reaction S-75

Figure S112. Stacked ^{1}H NMR Spectra from Small Molecule 'Scrambling' Reaction S-76
Figure S113. Mass Spectrum of the Results from the Small Molecule 'Scrambling' Reaction S-77
Figure S114. Normalized Integrations of Key Protons in Small Molecule 'Scrambling' Reaction S-77

A. Materials and Instrumentation.

I. Materials

Reagents were purchased from commercial grade suppliers and used without further purification. All measurements presented ≤3 mg were delivered via a stock solution of the appropriate monomer. Anhydrous solvents (Toluene, THF, DMF, DCM) were obtained from a solvent purification system (JC Meyer System). Reaction progress was monitored by thin layer chromatography (TLC) carried out on EMD 250 μm silica gel 60-F254 plates. Visualization was performed by UV light irradiation.

II. Instrumentation.

Nuclear Magnetic Resonance (NMR). Isolated ^{1}H and ^{13}C NMR spectra were acquired on a Bruker AvanceIII-500 MHz spectrometer with a CryoProbe 5mm DCH w/ Z-Gradient, or on a 400 MHz Agilent DD MR-400 spectrometer using an AutoX 5mm probe w/ Z-Gradient. All kinetic NMR experiments were carried out on a Bruker AvanceIII HB Nanobay-400 MHz spectrometer using a BBFO Smart probe w/ Z-Gradient. All spectra were recorded at 25°C unless specified otherwise. All spectra were calibrated using residual solvent as an internal reference ($CDCl_3$: 7.26 ppm for ^{1}H NMR, 77.00 for ^{13}C NMR; THF-d_8: 3.58, 1.73 ppm for ^{1}H NMR, 67.57, 25.37 ppm for ^{13}C NMR).

Infrared Spectroscopy (IR). Infrared spectra were recorded on a Nicolet iS10 FT-IR spectrometer equipped with a diamond ATR attachment and are uncorrected.

Matrix Assisted Laser Desorption Ionization Time of Flight (MALDI-TOF) Mass Spectrometry. MALDI-TOF mass spectra were recorded on a Bruker AutoFlex III with a 2,5-dihydroxybenzoic acid (DHB) matrix. All measurements were taken in reflectron positive (RP) mode.

Gel Permeation Chromatography (GPC). Gel permeation chromatography (GPC) was performed in stabilized, HPLC-grade tetrahydrofuran using an Agilent 1260 Infinity II system with variable-wavelength diode array (254, 450, and 530 nm) and refractive index detectors, guard column (Agilent PLgel; 5μm; 50 x 7.5 mm), and three analytical columns (Agilent PLgel; 5μm; 300 x 7.5 mm; 105, 104, and 103 Å pore sizes). The instrument was calibrated with narrow dispersity polystyrene standards between 640 Da and 2300 kDa (Polymer Standards Service GmbH). All runs were performed at 1.0 mL/min flow rate and 40 ºC. All samples were dissolved in THF (1 mg/mL) and sonicated for 10 minutes before being filtered through a 0.45 μm syringe filter (PTFE membrane). All chromatograms were obtained using the refractive index detector.

Atomic Force Microscopy (AFM). Atomic force microscopy (AFM) was conducted using the facilities at the Northwestern Atomic and Nanoscale Characterization Experiment Center (NUANCE) on a SPID Bruker FastScan AFM under the non-contact mode in air. AFM samples

were prepared by drop casting reaction mixtures onto silicon native oxide substrates and allowed to dry for 4 hours before imaging.

Scanning Electron Microscopy (SEM). Scanning electron microcopy (SEM) was conducted using the facilities at Northwestern's Electron Probe Instrumentation Center (EPIC) on an SEM Hitachi SU8030 microscope with an accelerating voltage of 15 kV. SEM samples were prepared by drop casting reaction mixtures onto silicon native oxide substrates and allowed to dry for 4 hours. The samples were then mounted onto a flat aluminum sample holder and coated with 3 nm of Osmium before images were taken.

Transmission Electron Microscopy (TEM). Transmission electron microscopy (TEM) images were obtained using the facilities at Northwestern's Atomic and Nanoscale Characterization Experimental Center (NUANCE) using a JEOL ARM300F GrandARM TEM operating at 300 kV, equipped with a Gatan OneView-IS camera. Samples were prepared by drop casting 4 μL of the macrocyclization reaction solution onto a lacey carbon copper grid (Ted Pella 01885-F). The samples sat on the grids in ambient conditions for ~10 seconds, and then were wicked dry with filter paper.

***In-Situ* Wide-Angle X-Ray Scattering (WAXS).** Wide-Angle X-Ray Scattering (WAXS) patterns were collected simultaneously at sector 5-ID-D of the Advanced Photon Source at Argonne National Laboratory. A beam energy of 17.0 KeV was used for all experiments. Patterns were collected with single 10 second frames on a series of 3 Pilatus 2D detectors which were then radially integrated. All samples were conducted in 0.5 mm borosilicate capillaries with a wall thickness of 0.01 nm available from Charles Supper Scientific. For the time resolved XRD experiments, patterns were baselined and then background subtracted from the starting time pattern to produce corrected patterns. The predominant diffraction pattern was then integrated and plotted against the time of each pattern.

Sonication. Sonication was performed with a Branson 3510 ultrasonic cleaner with a power output of 100 W and a frequency of 42 kHz.

Centrifugation. Centrifugation was performed with a Fisherbrand Mini-Centrifuge operating at 6000 rpm.

B. Synthetic Procedures

Scheme S1. Overall synthesis of **S1** (DAPB).

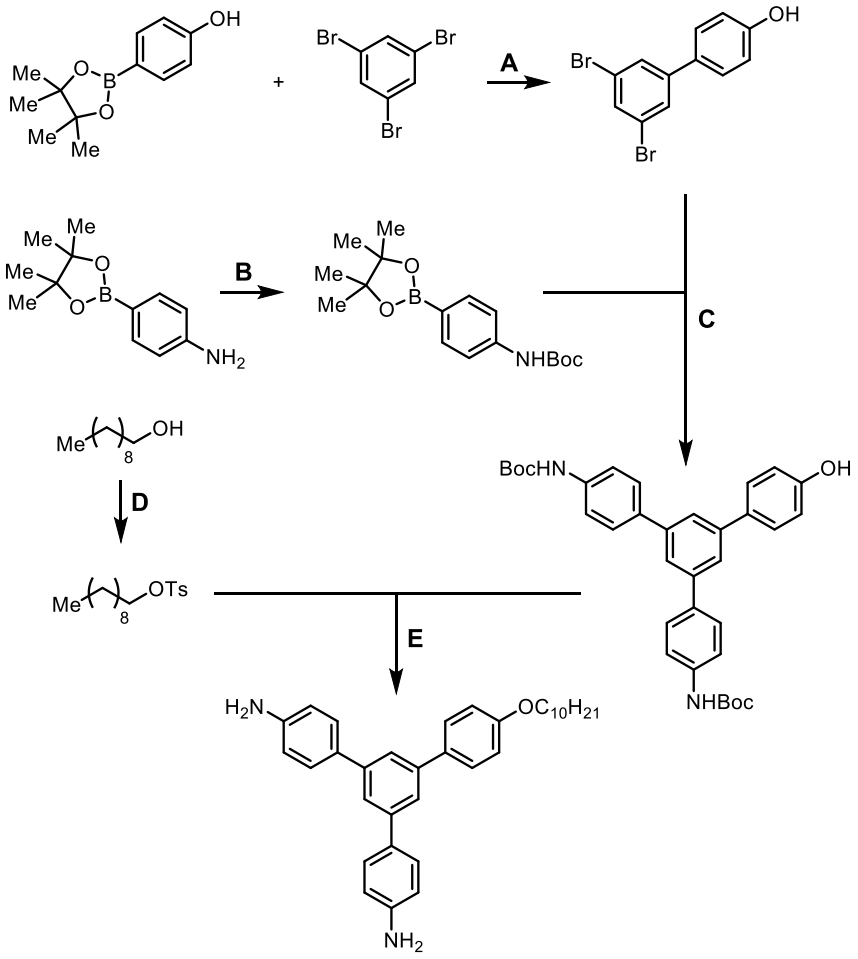

Synthesis of S1:

S1 was prepared using a reported procedure.[1,2] All characterization of synthetic intermediates were consistent with previous reports. (A) $Pd(PPh)_3$, K_2CO_3, PhMe:EtOH:H_2O (3:1:1), 115°C; (B) Boc_2O, PhMe, 90°C; (C) $Pd(OAc)_2$, SPhos, K_3PO_4, PhMe:H_2O (10:1), 80°C; (D) TsCl, Et_3N, CH_2Cl_2; r.t.; (E) K_2CO_3, DMF, 100°C, then CF_3CO_2H, CH_2Cl_2, r.t. (2 steps).

Scheme S2. Synthesis of **MC 1** and Corresponding Dilution Experiments.

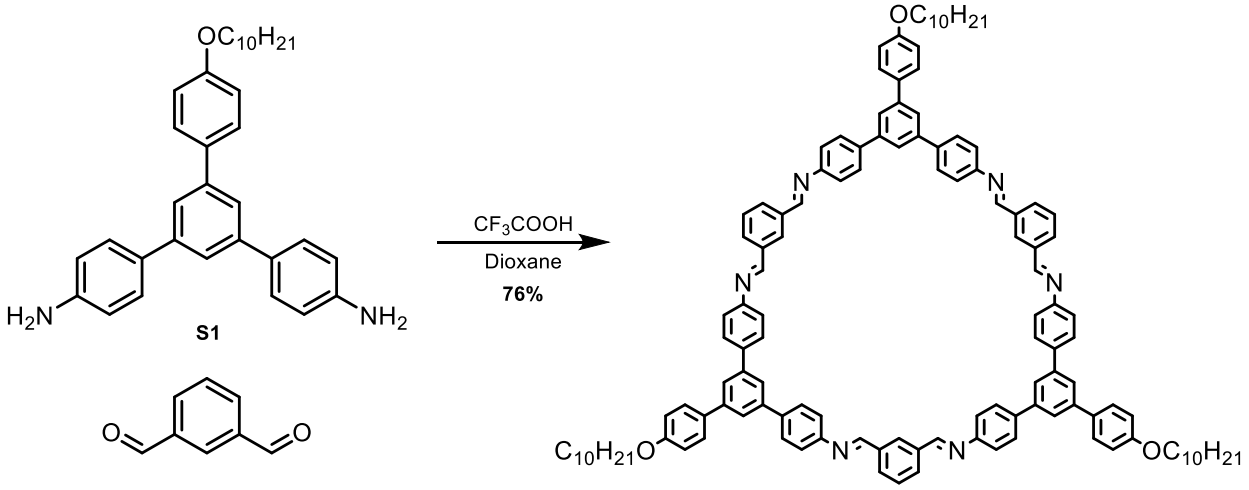

Synthesis of MC 1:

S1 (3 mg, 0.006 mmol) and isophthalaldehyde (IDA) (0.84 mg, 0.006 mmol, 1.0 equiv) were combined in 1,4-dioxane (0.243 mL, 25 mM with respect to **S1**) and sonicated until completely dissolved. 20 μL of a 0.2 M solution of CF_3CO_2H in 1,4-dioxane (0.003 mmol, 0.5 equiv) was then added. The solution immediately turned yellow and a precipitate began to form. The solution was then left undisturbed at room temperature for 36 h. After 36 h., the reaction mixture was neutralized with Et_3N (0.5 mL) and poured into Et_2O (c.a. 2 mL). The precipitate was isolated by centrifugation and subsequently rinsed with additional Et_2O (3x2 mL). The resulting solid was dried under high vacuum at room temperature to yield **MC 1** (2.8 mg, 78%) as a light-yellow solid. For all kinetic traces of **MC 1** formation, the acid loading was reduced to 0.05 equivalents.

Table S1. Concentrations used to probe dilution effects on **MC 1** synthesis.

Concentration of S1 (mM)	Volume Dioxane (mL)	Yield (mg)	Yield (%)
25.00	0.153	2.80	78%
12.50	0.397	3.10	86%
8.50	0.626	2.70	75%
6.40	0.861	2.60	72%
5.10	1.103	2.40	67%
3.40	1.691	2.50	69%

Scheme S3. Synthesis of **MC 2** and Corresponding Dilution Experiments.

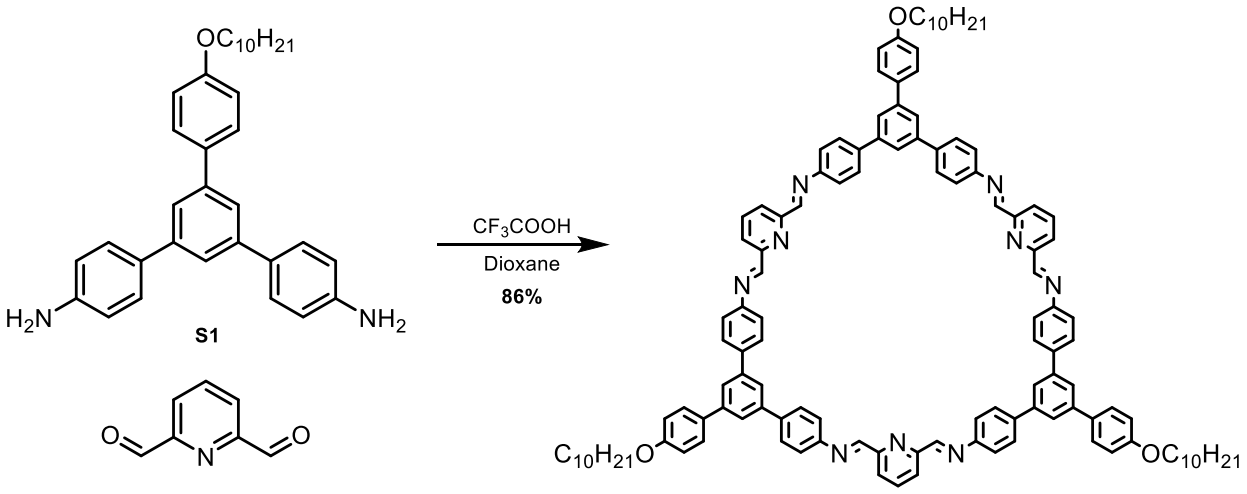

Synthesis of MC 2:

S1 (3 mg, 0.006 mmol) and 2,6-pyridinedicarboxaldehyde (0.84 mg, 0.006 mmol, 1.0 equiv) were combined in 1,4-dioxane (0.243 mL, 25 mM with respect to **S1**) and sonicated until completely dissolved. 20 μL of a 0.2 M solution of CF_3CO_2H in 1,4-dioxane (0.003 mmol, 0.5 equiv) was then added. The solution immediately turned yellow and a precipitate began to form. The solution was then left undisturbed at room temperature for 36 h. After 36 h., the reaction mixture was neutralized with Et_3N (0.5 mL) and poured into Et_2O (c.a. 2 mL). The precipitate was isolated by centrifugation and subsequently rinsed with additional Et_2O (3x2 mL). The resulting solid was dried under high vacuum at room temperature to yield the desired **MC 2** (3.1 mg, 86%) as a light brown solid. For all kinetic traces of **MC 2** formation, the acid loading was reduced to 0.05 equivalents.

Table S2. Concentrations used to probe dilution effects on **MC 2** synthesis.

Concentration of S1 (mM)	Volume Dioxane (mL)	Yield (mg)	Yield (%)
25.00	0.153	3.10	86%
12.50	0.397	3.40	94%
8.50	0.626	3.00	83%
6.40	0.861	3.10	86%
5.10	1.103	3.10	86%
3.40	1.691	3.10	86%

Scheme S4. Scrambling Experiments Between **MC 1** and **MC 2**.

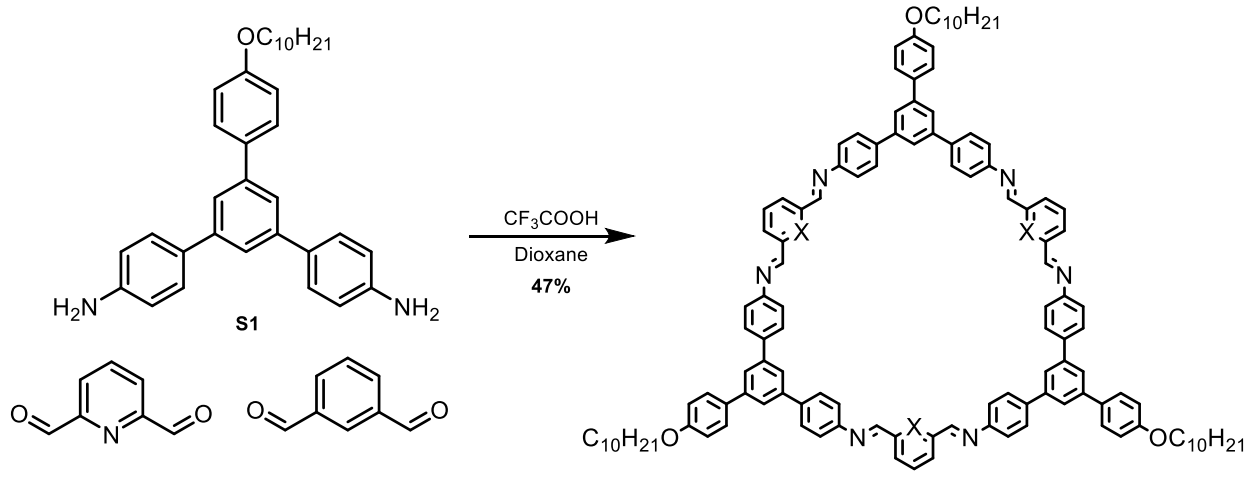

Macrocycle Scrambling Experiment:

S1 (3 mg, 0.006 mmol) and a 1:1 mixture of isophthalaldehyde:2,6-pyridinedicarboxaldehyde (0.84 mg, 0.006 mmol, 1.0 equiv) were combined in 1,4-dioxane (0.243 mL, 25 mM with respect to **S1**) and sonicated until completely dissolved. 40 µL of a 2.0 M solution of CF_3CO_2H in 1,4-dioxane (0.060 mmol, 10.0 equiv) was then added. The solution immediately turned yellow and a precipitate began to form. The solution was then left undisturbed at room temperature for 36 h. After 36 h., the reaction mixture was neutralized with Et_3N (0.5 mL) and poured into Et_2O (c.a. 2 mL). The precipitate was isolated by centrifugation and subsequently rinsed with additional Et_2O (3x2 mL). The resulting solid was dried under high vacuum at room temperature to yield the desired macrocycles (1.7 mg, 47%) as a light brown solid.

Table S3. Concentrations used to probe dilution effect on macrocycle scrambling reactions. Yields are established assuming **S1** could react fully to yield macrocycles. Macrocycles were isolated by precipitating the solid yielded from the reaction into CH_2Cl_2 and drying under high vacuum.

Concentration of S1 (mM)	Volume Dioxane (mL)	Yield (mg)	Yield (%)
25.00	0.153	1.70	47%
12.50	0.397	1.50	42%
8.50	0.626	1.40	39%
6.40	0.861	1.30	36%
5.10	1.103	1.40	39%

Scheme S5. Competition Experiments Between **MC 1** and **MC 2**.

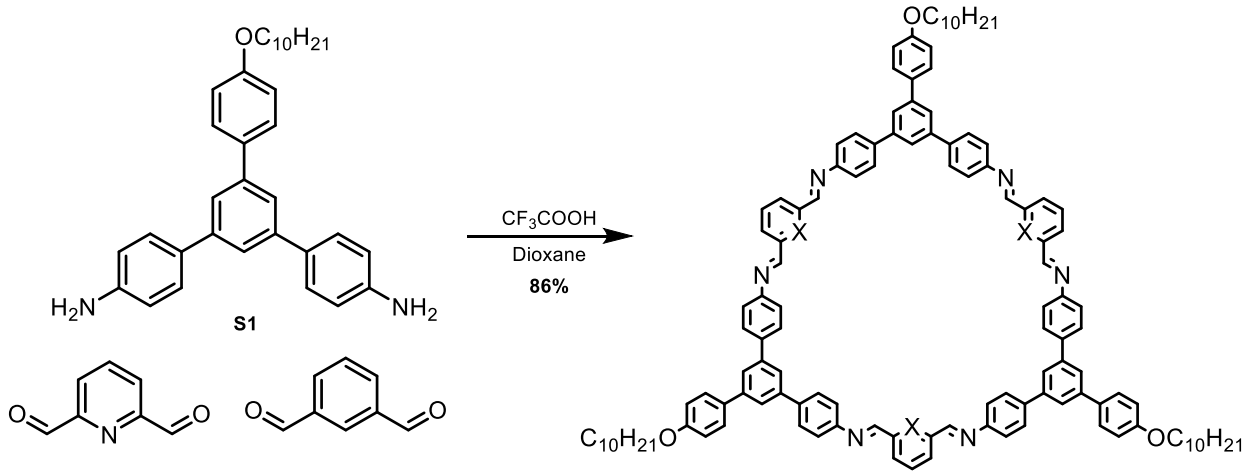

Macrocycle Competition Experiment:

S1 (3 mg, 0.006 mmol) and a 1:1 mixture of isophthalaldehyde:2,6-pyridinedicarboxaldehyde (1.68 mg, 0.012 mmol, 2.0 equiv) were combined in 1,4-dioxane (0.243 mL, 25 mM with respect to **S1**) and sonicated until completely dissolved. 40 μL of a 2.0 M solution of CF_3CO_2H in 1,4-dioxane (0.060 mmol, 10.0 equiv) was then added. The solution immediately turned yellow and a precipitate began to form. The solution was then left undisturbed at room temperature for 36 h. After 36 h., the reaction mixture was neutralized with Et_3N (0.5 mL) and poured into Et_2O (c.a. 2 mL). The precipitate was isolated by centrifugation and subsequently rinsed with additional Et_2O (3x2 mL). The resulting solid was dried under high vacuum at room temperature to yield the desired macrocycles (3.1 mg, 86%) as a light brown solid.

Table S4. Concentrations used to probe dilution effect on macrocycle competition reactions.

Concentration of S1 (mM)	Volume Dioxane (mL)	Yield (mg)	Yield (%)
25.00	25.00	3.10	86%
12.50	12.50	3.30	92%
8.50	8.50	3.20	89%
6.40	6.40	3.40	94%
5.10	5.10	3.30	92%

Scheme S6. Monomer Exchange Experiments Beginning with **MC 2**.

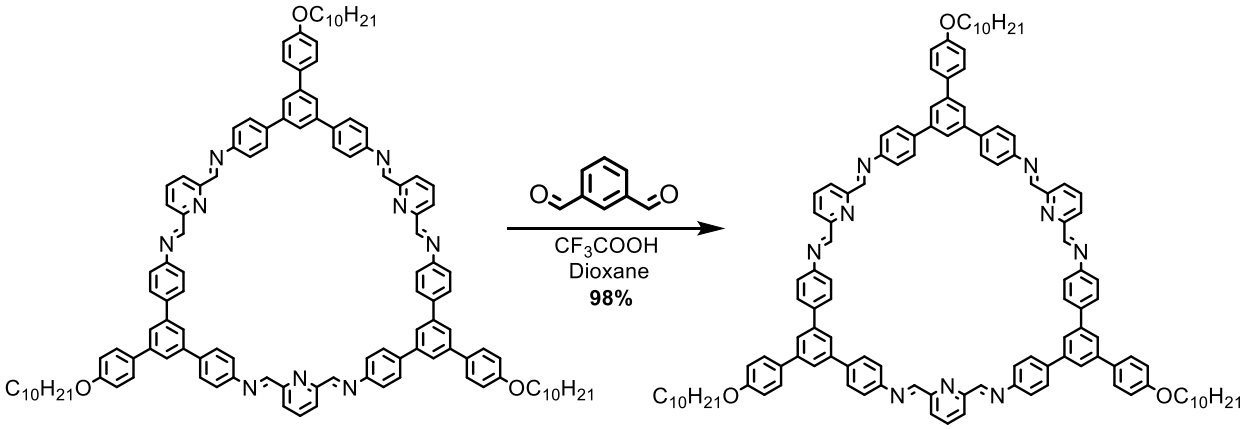

Macrocycle Monomer Exchange Experiment:

MC 2 (15 mg, 0.008 mmol) was sonicated in 1,4-dioxane (4 mL) until completely dispersed. After dispersion of the original macrocycle, isopthalaldehyde (11.3 mg, 0.080 mmol, 10.0 equiv) and CF_3CO_2H (2.0 M in dioxane, 160 μL, 10 equiv) was then added. The solution was then allowed to sit undisturbed at room temperature for 3 days. After 3 days, the reaction mixture was neutralized with Et_3N (2 mL) and poured into Et_2O (c.a. 10 mL). The precipitate was isolated by centrifugation and subsequently rinsed with Et_2O (3x10 mL). The resulting solid was dried under high vacuum at room temperature to yield the desired macrocycle (14.7 mg, 98%) as a light brown solid.

Scheme S7. Monomer Exchange Experiments Beginning with **MC 1**.

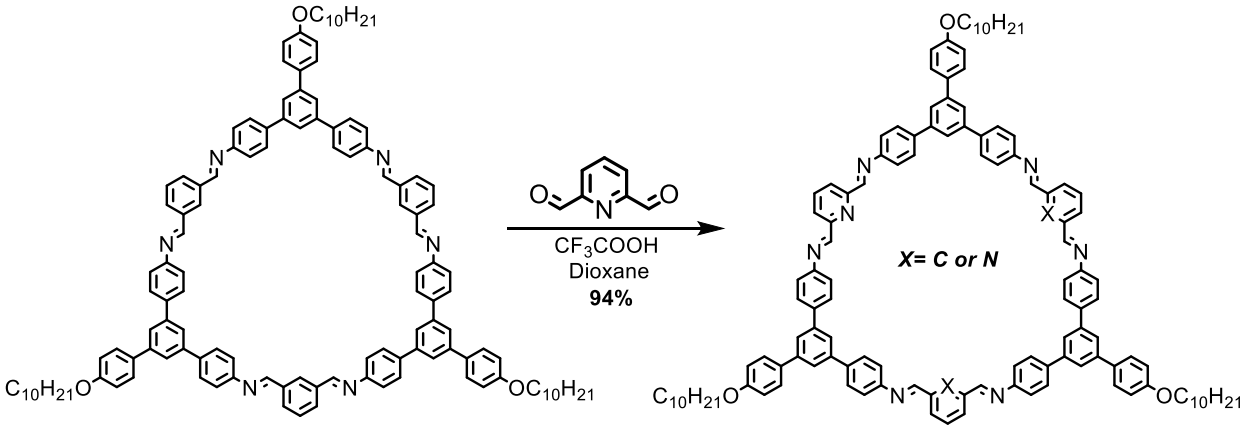

Macrocycle Monomer Exchange Experiment:

MC 1 (15 mg, 0.008 mmol) was sonicated in 1,4-dioxane (4 mL) until completely dispersed. After dispersion of the original macrocycle, pyridine-2,6-dicarboxaldehyde (11.3 mg, 0.080 mmol, 10.0 equiv) and CF_3CO_2H (2.0 M in dioxane, 160 μL, 10 equiv) was then added. The solution was then allowed to sit undisturbed at room temperature for 3 days. After 3 days, the reaction mixture was neutralized with Et_3N (2 mL) and poured into Et_2O (c.a. 10 mL). The precipitate was isolated by centrifugation and subsequently rinsed with Et_2O (3x10 mL). The resulting solid was dried under high vacuum at room temperature to yield the desired macrocycle (14.1 mg, 96%) as a light brown solid.

Scheme S8. Synthesis of 5-Br-IDA Macrocycles.

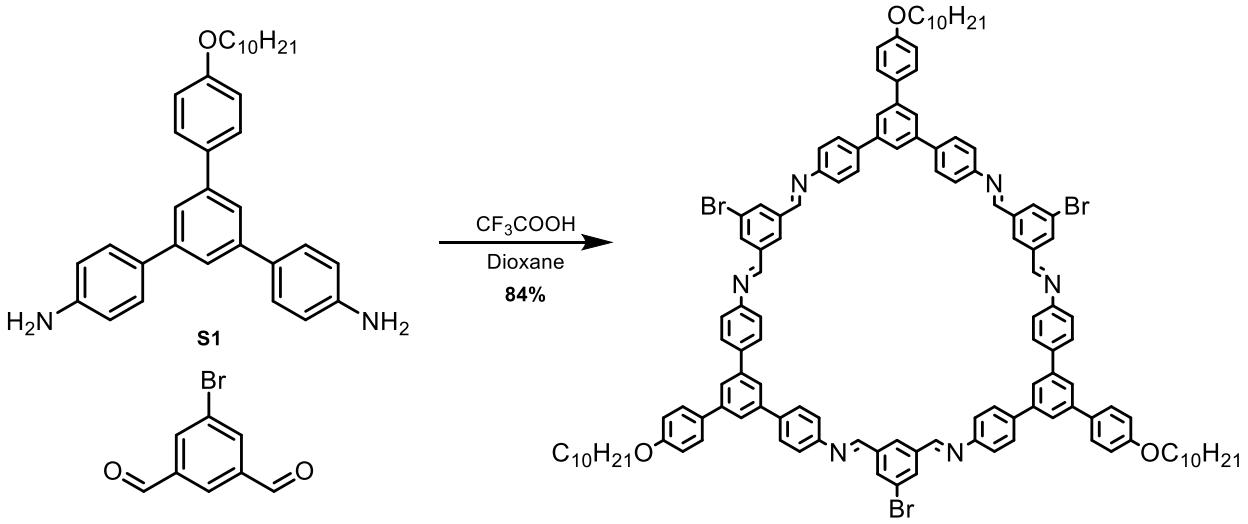

Synthesis of 5-Br-IDA Macrocycles:

S1 (25 mg, 0.055 mmol) and 5-bromoisophthalaldehyde (11 mg, 0.055 mmol, 1.0 equiv) were combined in 1,4-dioxane (2.2 mL, 25 mM with respect to S1) and sonicated until completely dissolved.12.5 μL of a 2 M solution of CF_3CO_2H in 1,4-dioxane (0.028 mmol, 0.5 equiv) was then added. The solution immediately turned yellow and a precipitate began to form. The solution was then left undisturbed at room temperature for 36 h. After 36 h., the reaction mixture was neutralized with Et_3N (1.0 mL) and poured into Et_2O (c.a. 5 mL). The precipitate was isolated by centrifugation and subsequently rinsed with additional Et_2O (3x5 mL). The resulting solid was dried under high vacuum at room temperature to yield the desired 5-Br-IDA macrocycle (26 mg, 84%) as a light-yellow solid.

Scheme S9. Monomer Exchange Control Experiment Beginning with 5-Br-IDA Macrocycles.

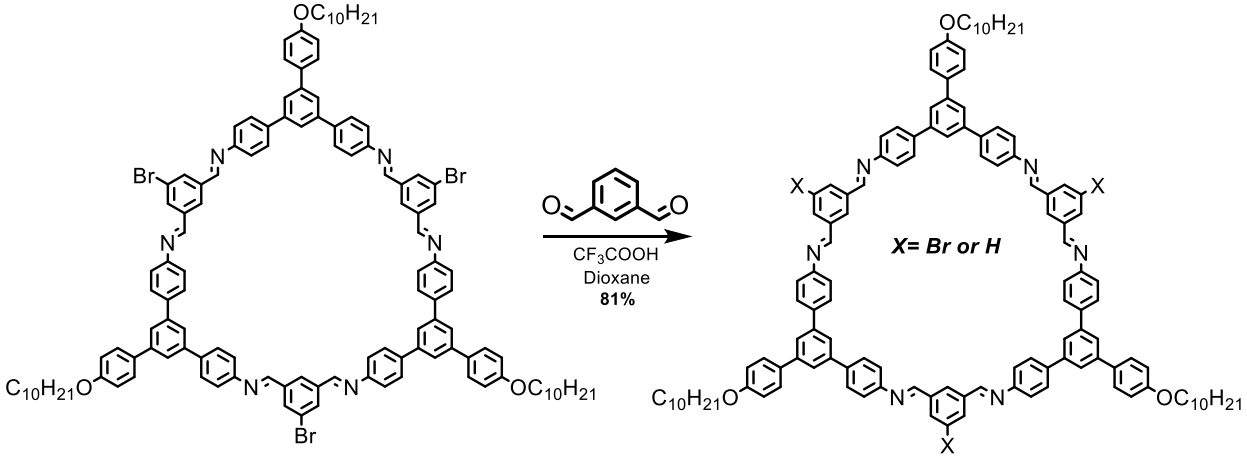

Macrocycle Monomer Exchange Experiment:

A sample of 5-Br-IDA macrocycles (13.1 mg, 0.007 mmol) were sonicated in 1,4-dioxane (4 mL) until completely dispersed. After dispersion of the original macrocycle, isophthalaldehyde (2.6 mg, 0.021 mmol, 3.0 equiv) and CF_3CO_2H (2.0 M in dioxane, 140 µL, 10 equiv) was added. The solution was then allowed to sit undisturbed for 3 days at room temperature. After 3 days, the reaction mixture was neutralized with Et_3N (2 mL) and poured into Et_2O (c.a. 10 mL). The precipitate was isolated by centrifugation and subsequently rinsed with Et_2O (3x10 mL). The resulting solid was dried under high vacuum at room temperature to yield the desired macrocycle (10.6 mg, 81%) as a yellow solid.

C. ^{1}H and ^{13}C NMR Spectra

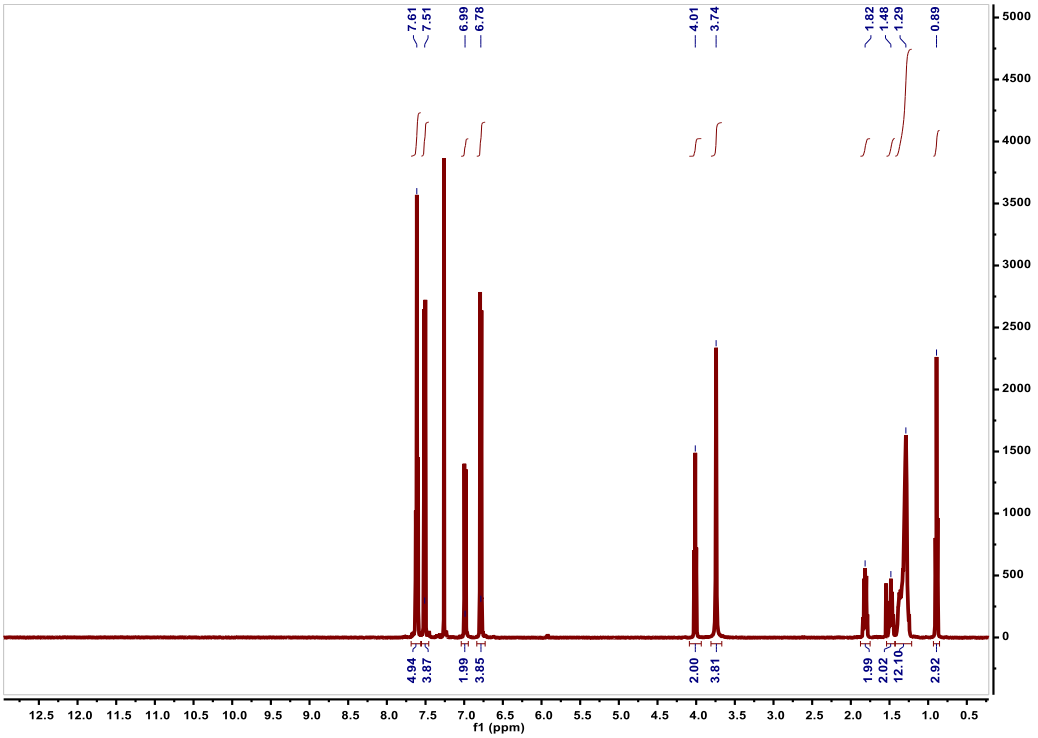

Figure S1. ^{1}H NMR ($CDCl_3$, 500 MHz, 298 K) of **S1**.

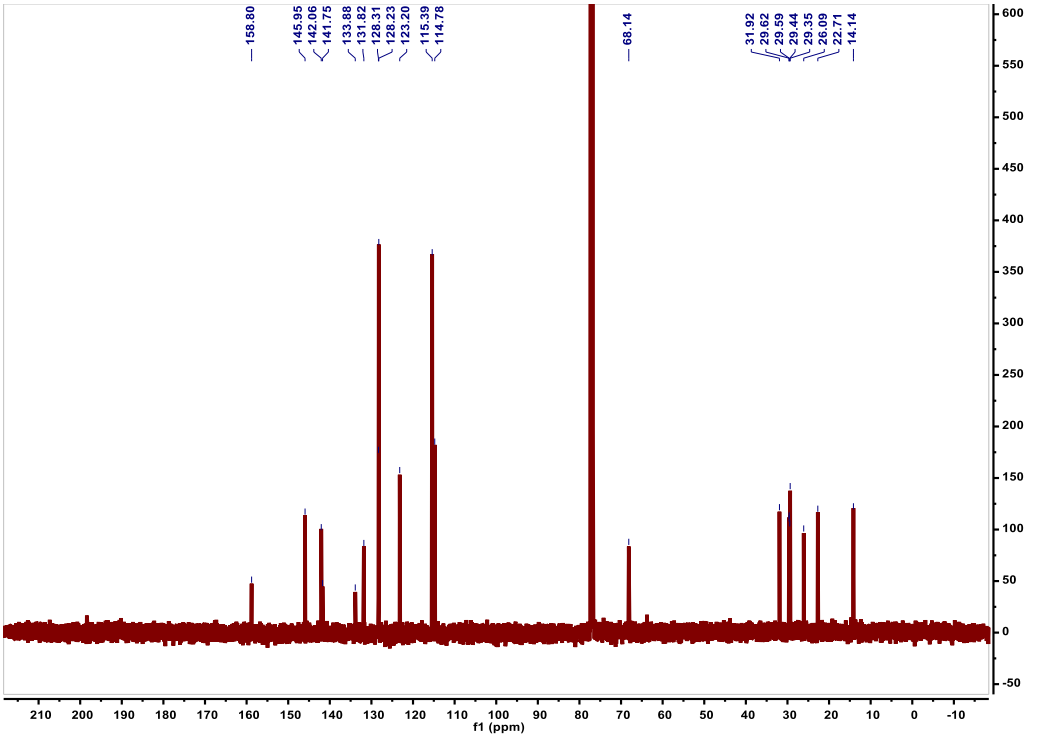

Figure S2. ^{13}C NMR ($CDCl_3$, 126 MHz, 298 K) of **S1**.

D. Dilution Experiments Macrocycle and Nanotube Characterization

I. Characterization of MC 1

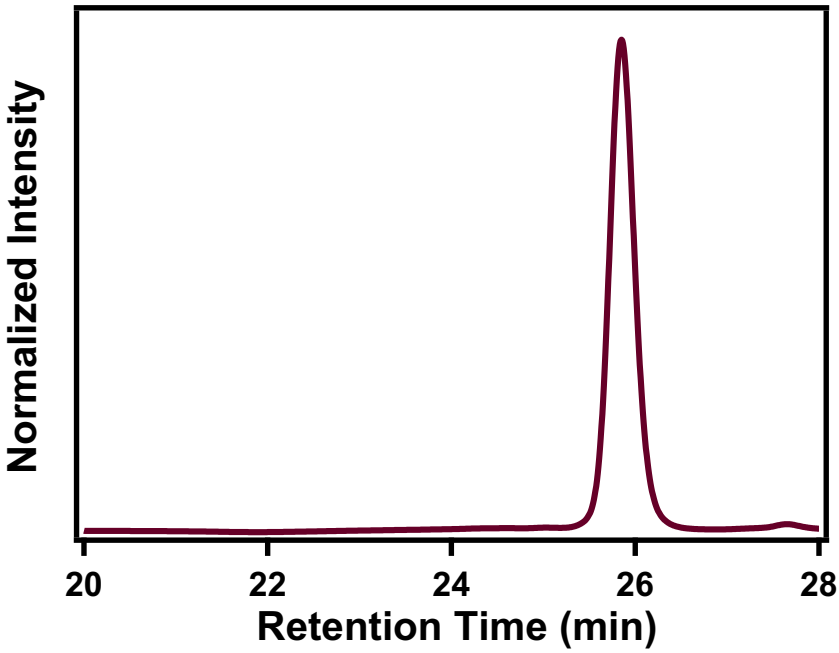

Figure S3. GPC of **MC 1**, synthesized at 25 mM, in THF showing a single narrow elution band corresponding to successful macrocyclization.

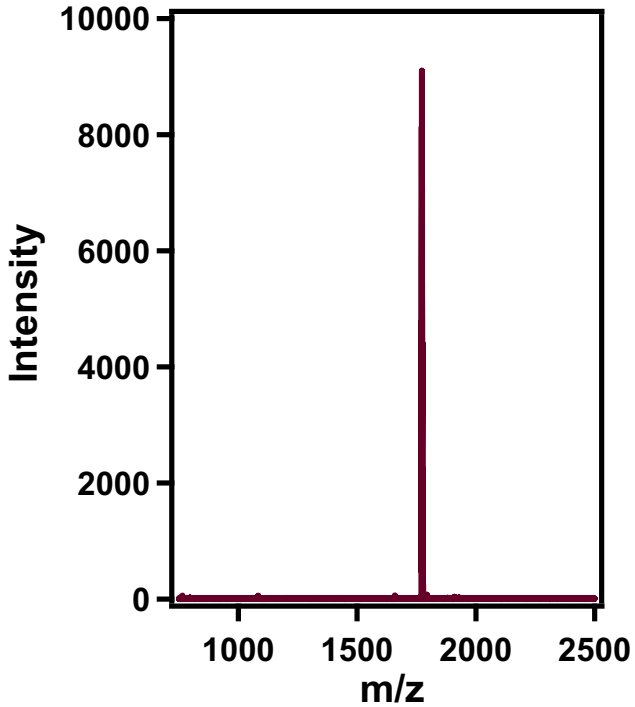

Figure S4. MALDI-MS of **MC 1**, synthesized at 25 mM, showing the desired $[M+H]^+$ adduct (*m/z*=1771.68).

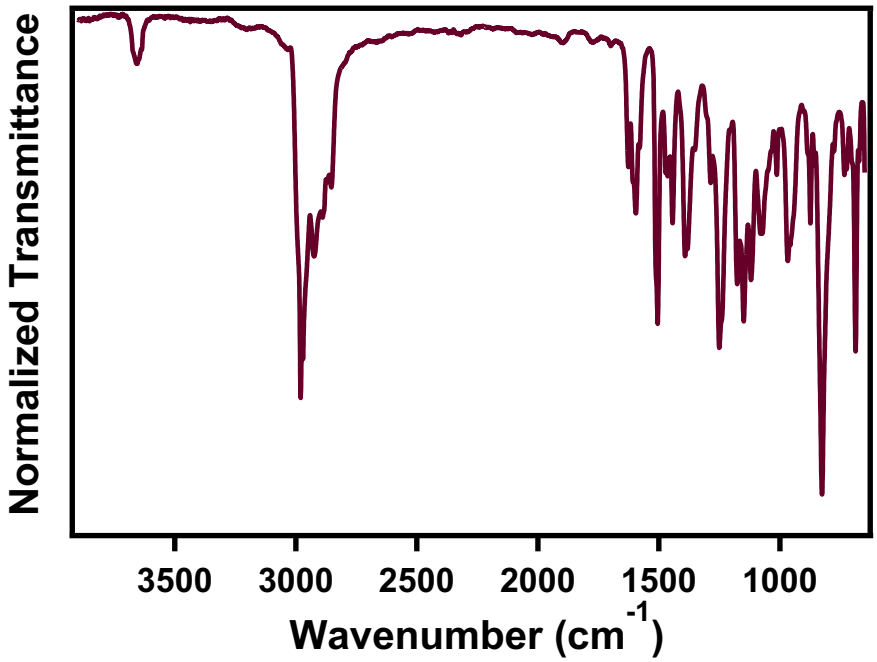

Figure S5. FT-IR spectra of **MC 1** synthesized at 25 mM with respect to **S1**. The observations made in this spectra are consistent with previous reports.[1-2]

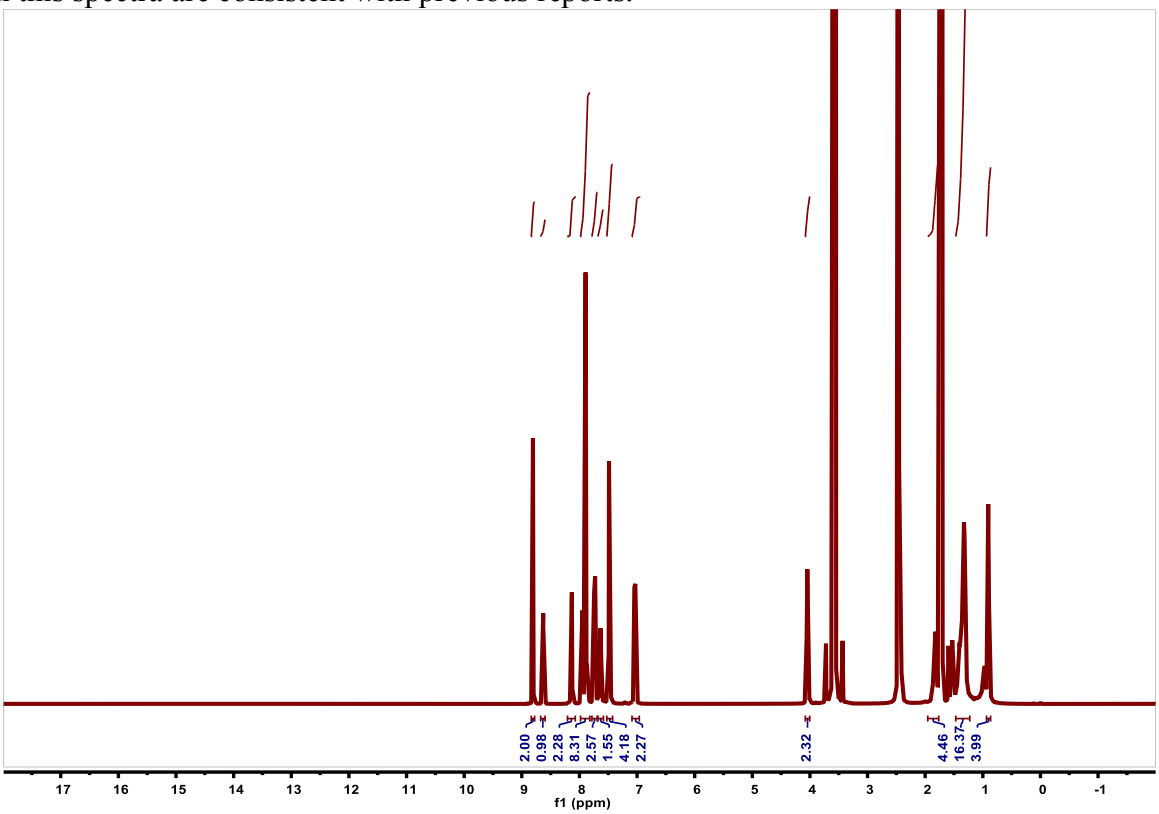

Figure S6. ^{1}H NMR (THF-d_8, 500 MHz, 298 K) of **MC 1**.

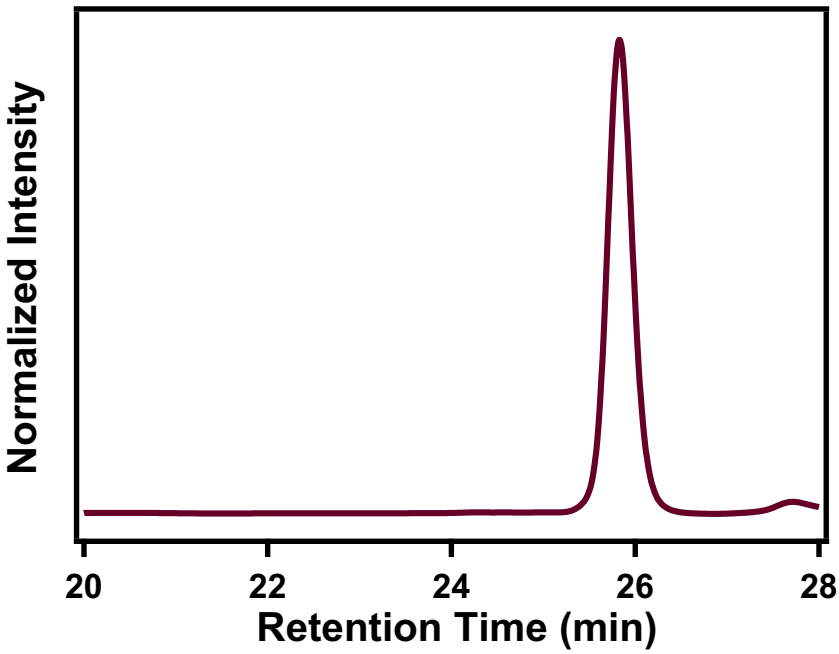

Figure S7. GPC of **MC 1**, synthesized at 12.5 mM, in THF showing a single narrow elution band corresponding to successful macrocyclization.

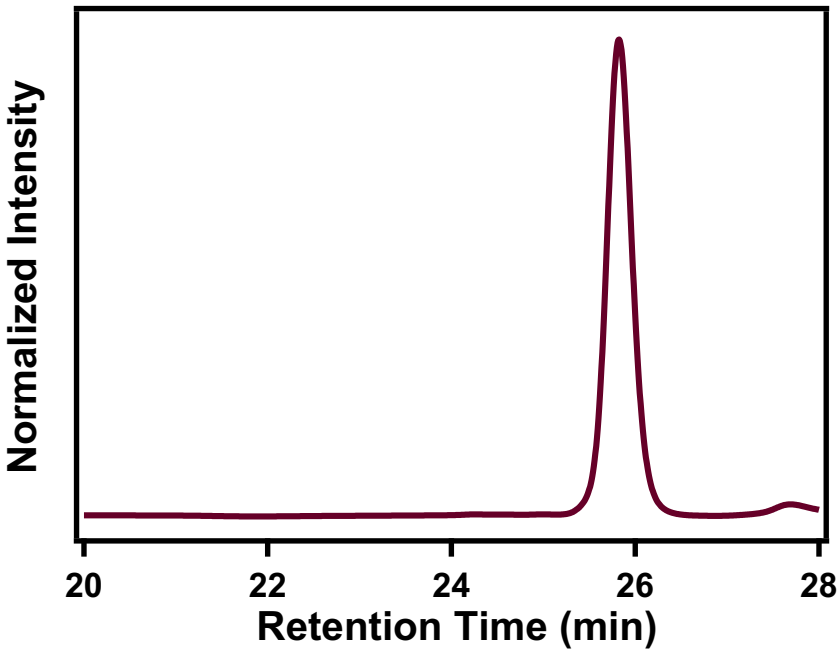

Figure S8. GPC of **MC 1**, synthesized at 8.5 mM, in THF showing a single narrow elution band corresponding to successful macrocyclization.

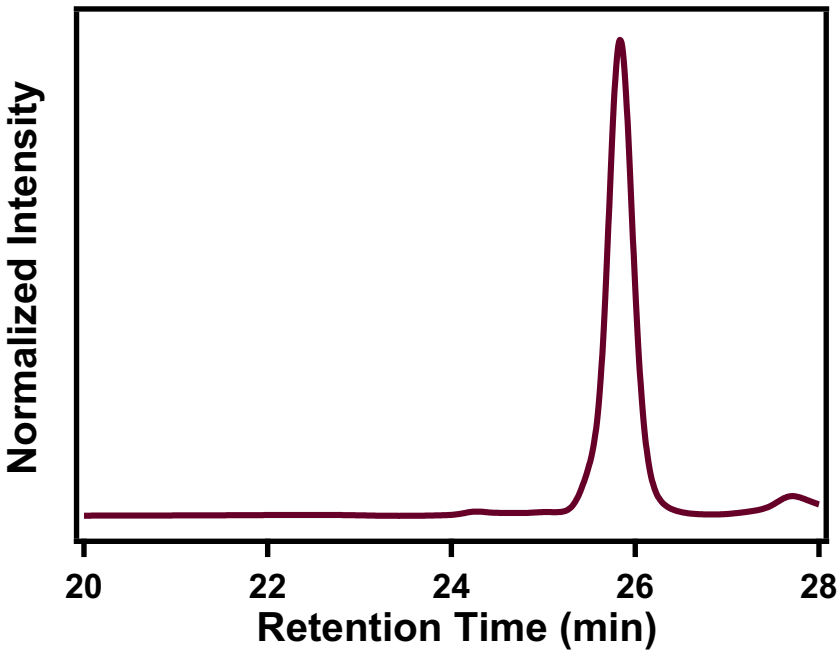

Figure S9. GPC of **MC 1**, synthesized at 6.4 mM, in THF showing a single narrow elution band corresponding to successful macrocyclization.

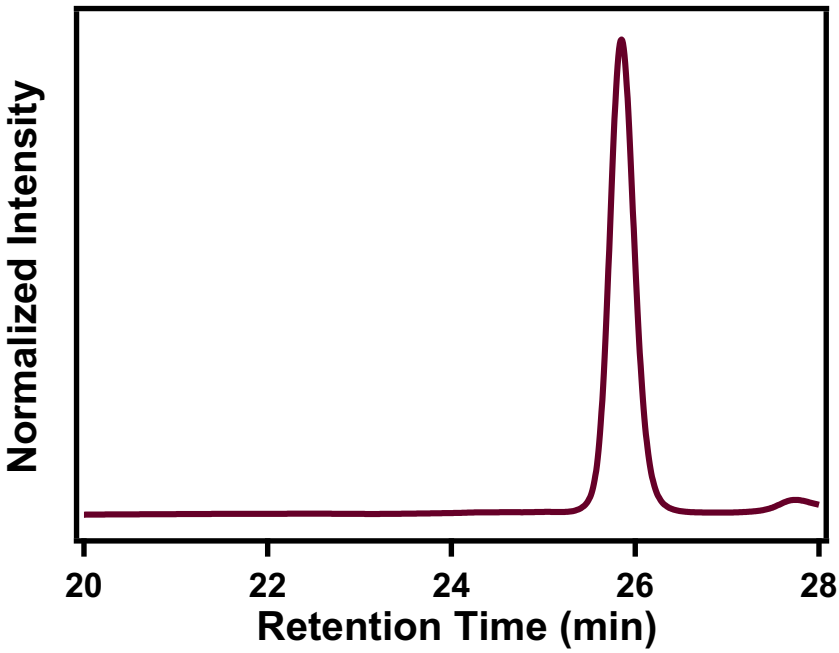

Figure S10. GPC of **MC 1**, synthesized at 5.1 mM, in THF showing a single narrow elution band corresponding to successful macrocyclization.

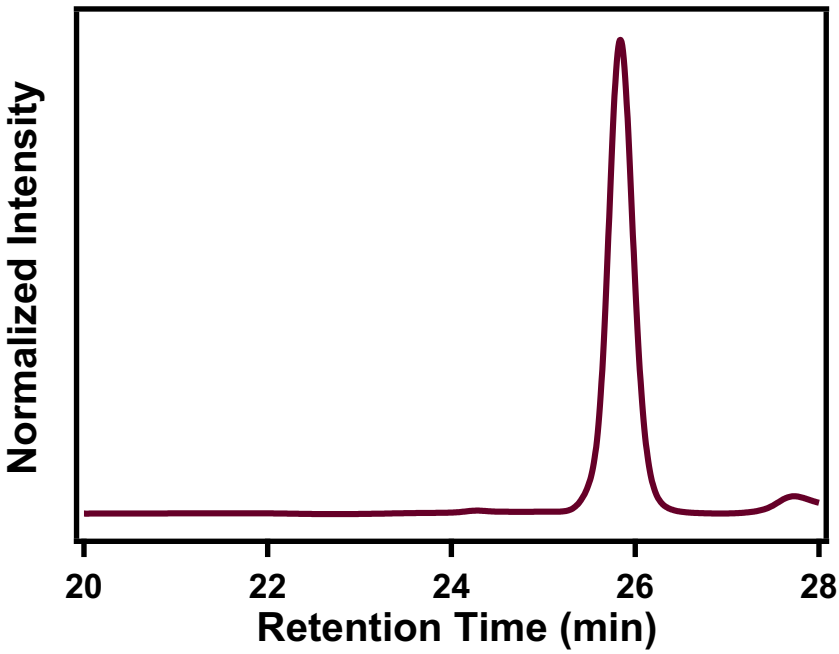

Figure S11. GPC of **MC 1**, synthesized at 3.4 mM, in THF showing a single narrow elution band corresponding to successful macrocyclization.

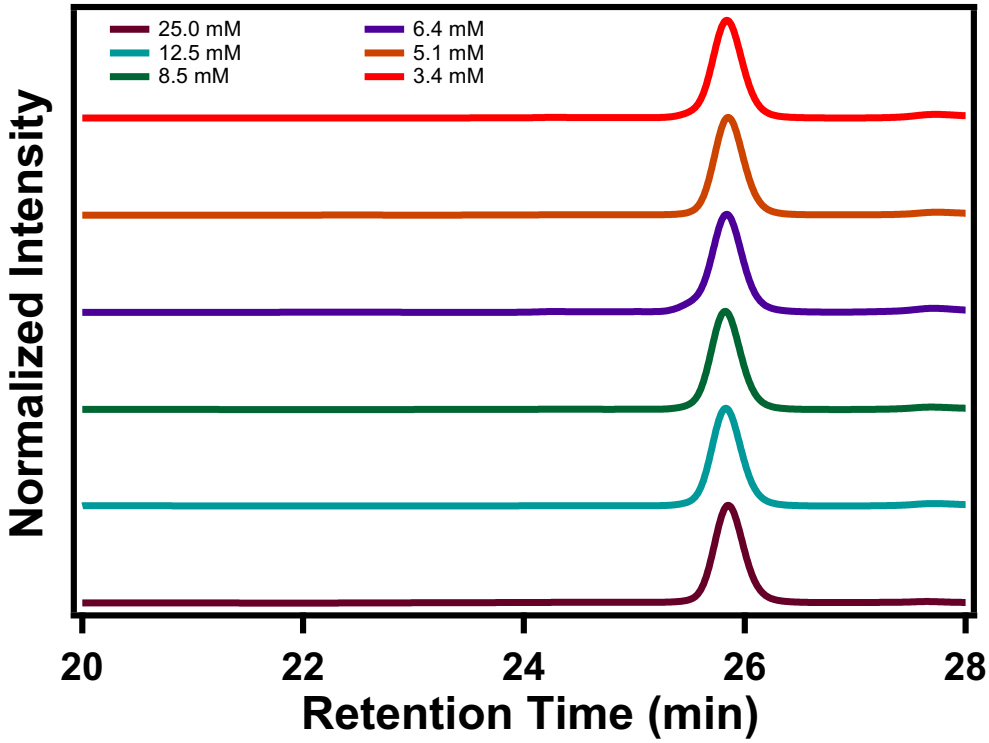

Figure S12. Overlaid GPC traces from all diluted syntheses of **MC 1**, showing no concentration dependence on macrocycle formation.

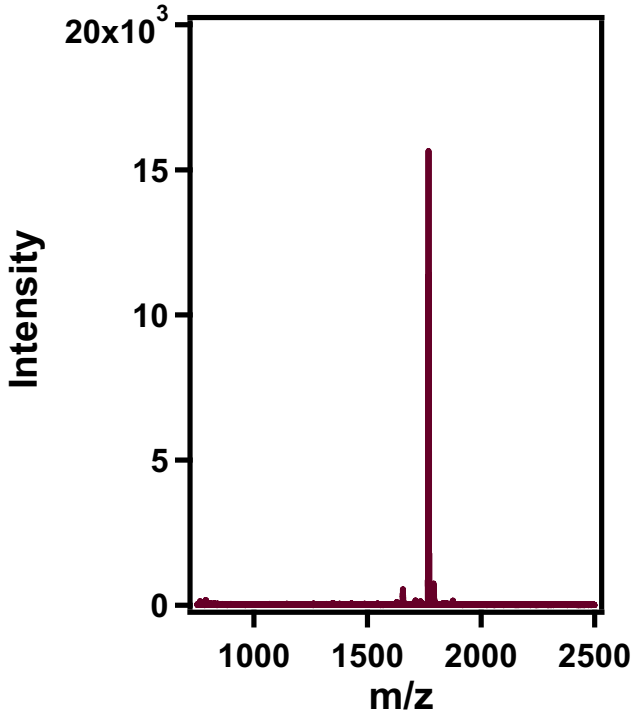

Figure S13. MALDI-MS of **MC 1**, synthesized at 12.5 mM, showing the desired $[M+H]^+$ adduct (*m/z*=1771.67).

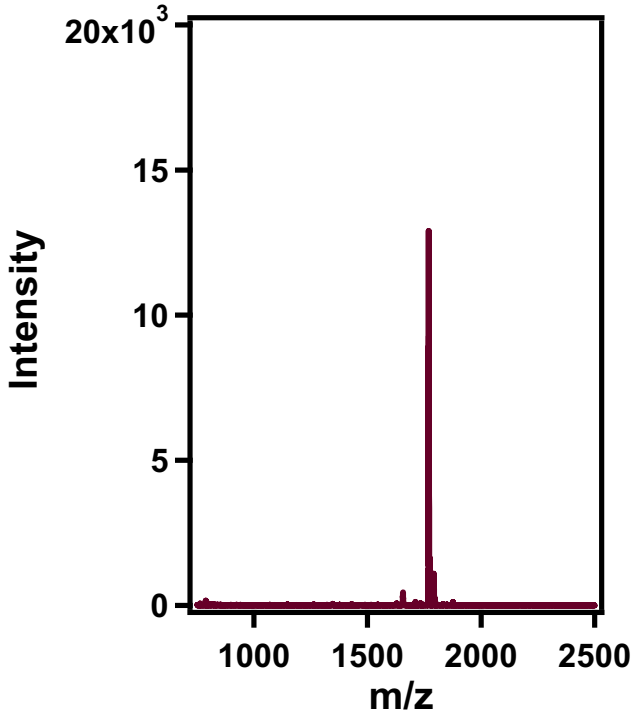

Figure S14. MALDI-MS of **MC 1**, synthesized at 8.5 mM, showing the desired $[M+H]^+$ adduct (*m/z*=1771.74).

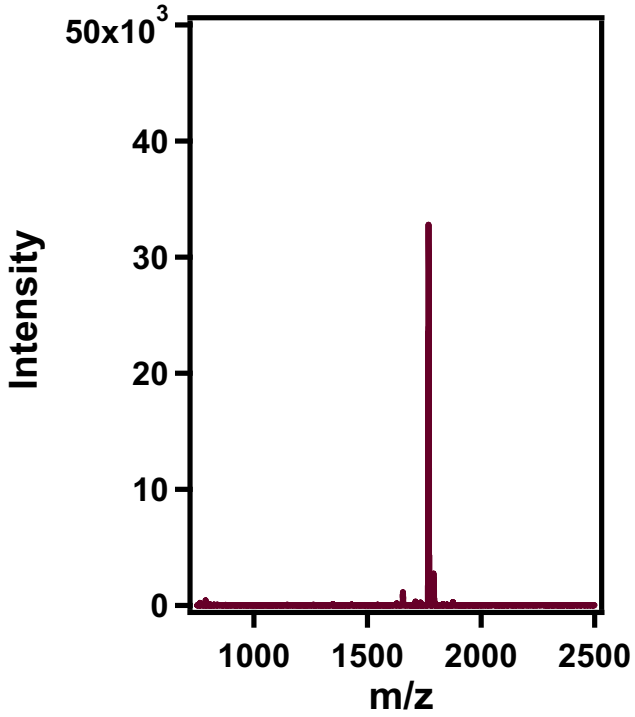

Figure S15. MALDI-MS of **MC 1**, synthesized at 6.4 mM, showing the desired $[M+H]^+$ adduct (*m/z*=1771.64).

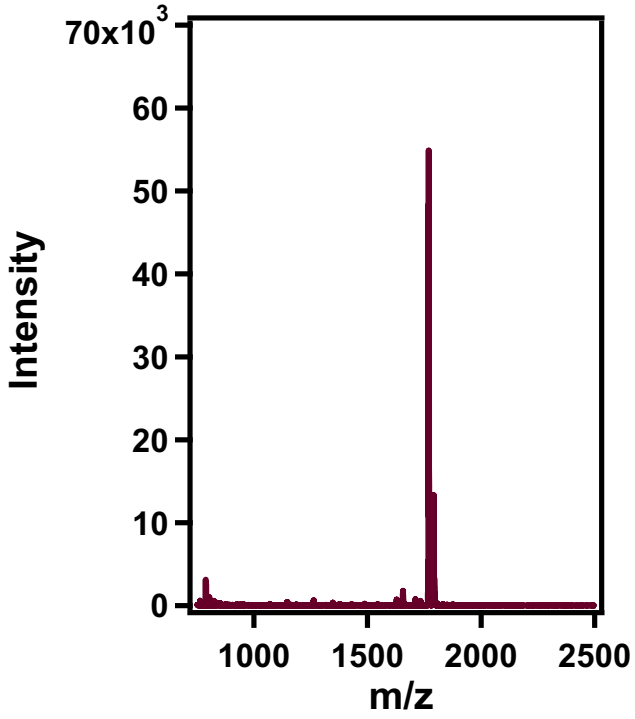

Figure S16. MALDI-MS of **MC 1**, synthesized at 5.1 mM, showing the desired $[M+H]^+$ adduct (*m/z*=1771.68).

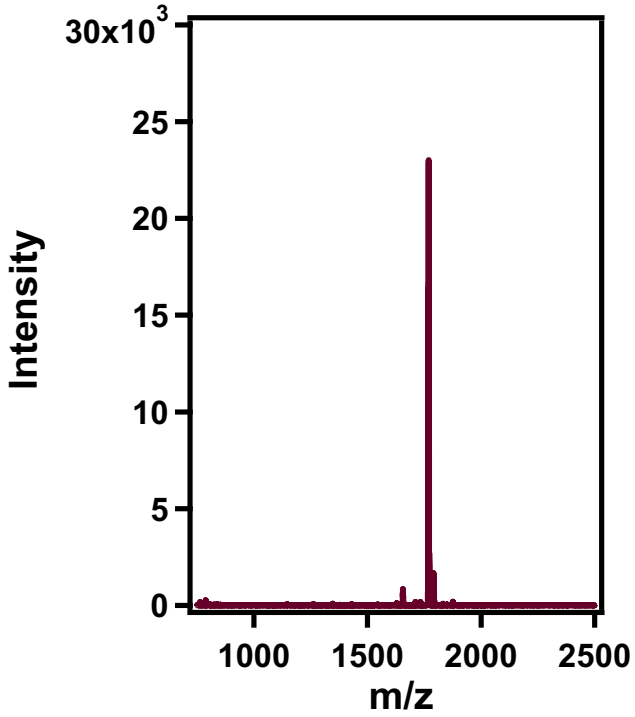

Figure S17. MALDI-MS of **MC 1**, synthesized at 3.4 mM, showing the desired $[M+H]^+$ adduct (*m/z*=1771.66).

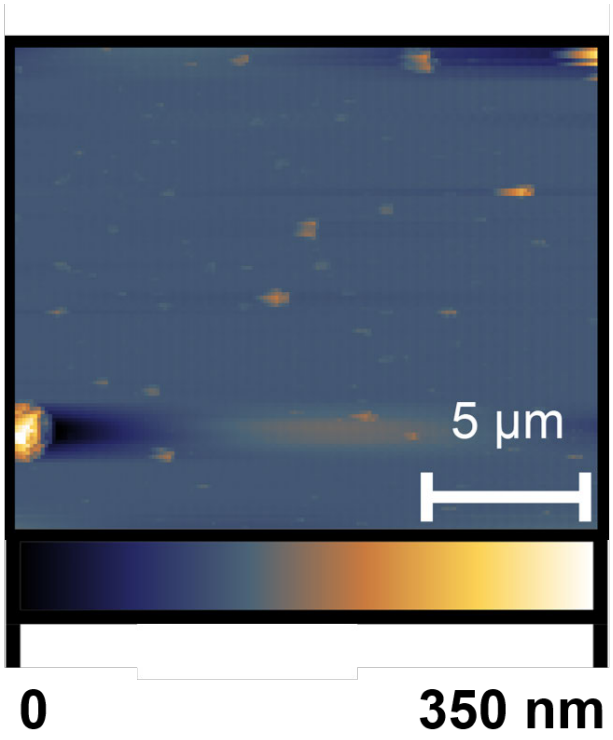

Figure S18. Atomic force microscopy image of a drop cast aliquot of from the **MC 1** reaction at 3.4 mM showing a lack high-aspect ratio assemblies but rather ill-defined aggregates.

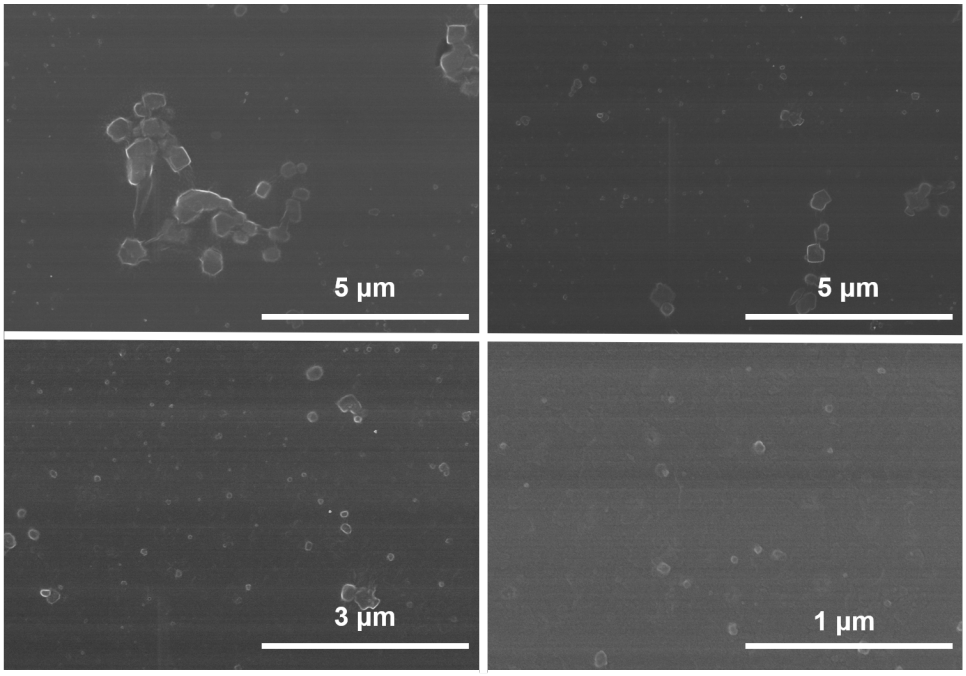

Figure S19. Scanning electron microscopy images of a drop cast aliquot of from the **MC 1** reaction at 3.4 mM showing no formation of high-aspect ratio assemblies but rather ill-defined aggregates.

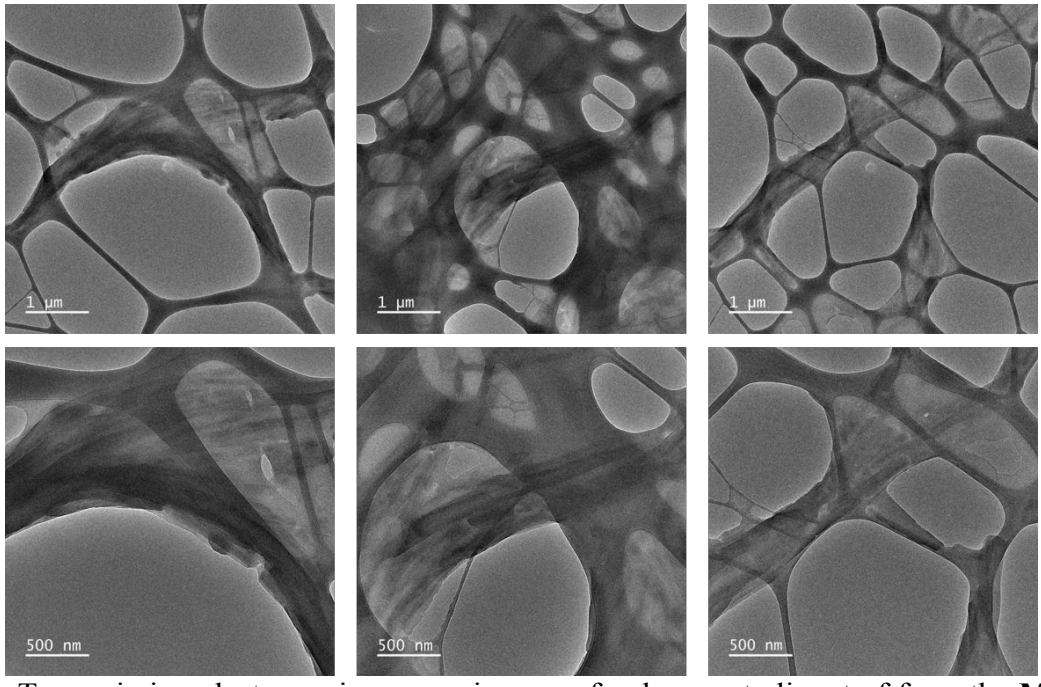

Figure S20. Transmission electron microscopy images of a drop cast aliquot of from the **MC 1** reaction at 25 mM showing the formation of low aspect ratio aggregates, like what has been previously reported in the literature.[1]

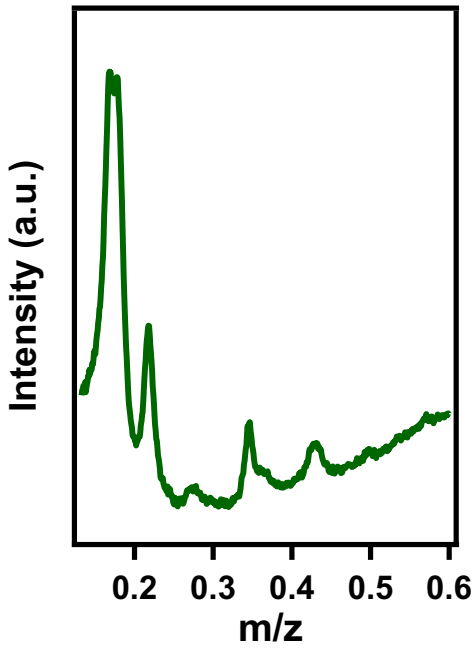

Figure S21. *In-Situ* WAXS pattern of the **MC 1** reaction run at 25 mM.

II. Characterization of MC 2

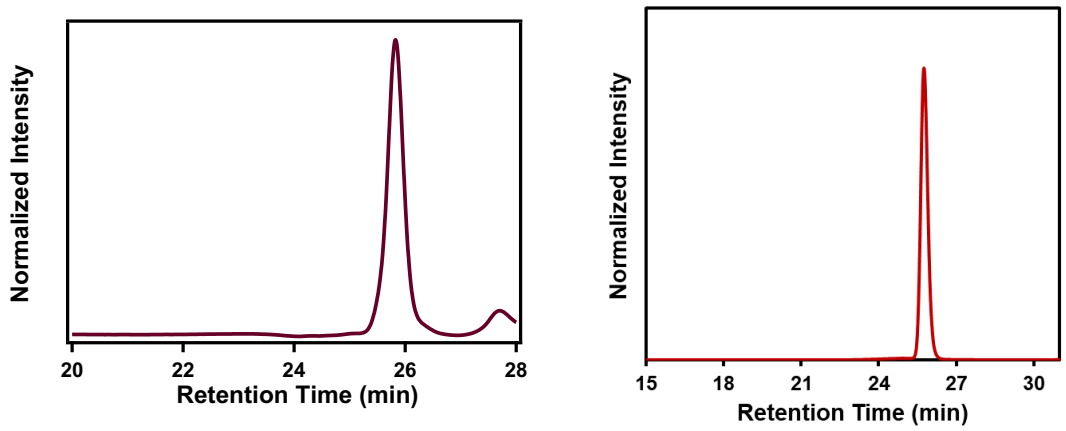

Figure S22. (Left) GPC of **MC 2**, synthesized at 25 mM, in THF showing a single narrow elution band corresponding to successful macrocyclization. was corroborated by rerunning the sample after washing the GPC column (Right) Furthermore, no resonances corresponding to smaller molecular weight species were observed via MALDI-MS or ^{1}H NMR analysis of the sample.

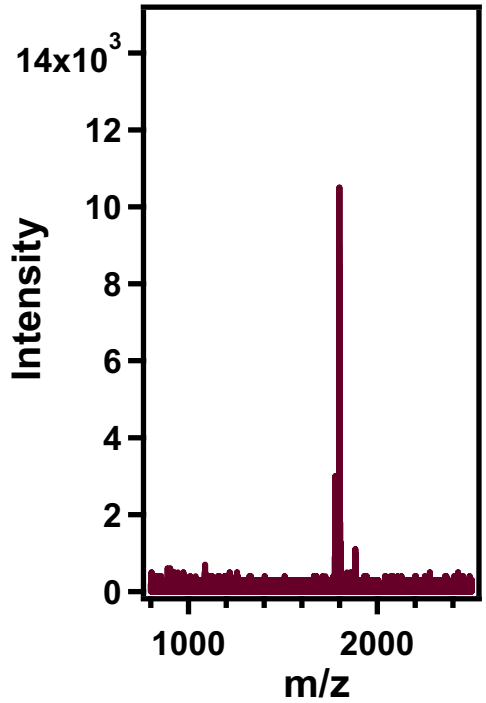

Figure S23. MALDI-MS of **MC 2**, synthesized at 25 mM, showing the desired $[M+H]^+$, $[M+Na]^+$, and $[M+K]^+$ adducts. (*m/z*=1774.61 $[M+H]^+$; *m/z*= 1796.40 $[M+Na]^+$; *m/z*= 1813.94 $[M+K]^+$).

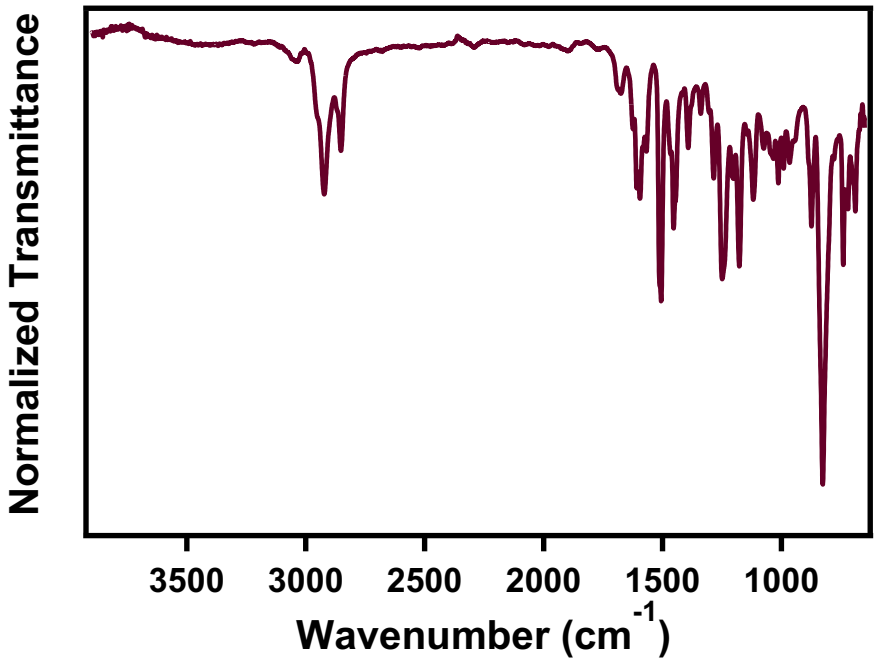

Figure S24. FT-IR spectra of **MC 2** synthesized at 25 mM with respect to **S1**. The observations made in this spectra are consistent with previous reports.[1-2]

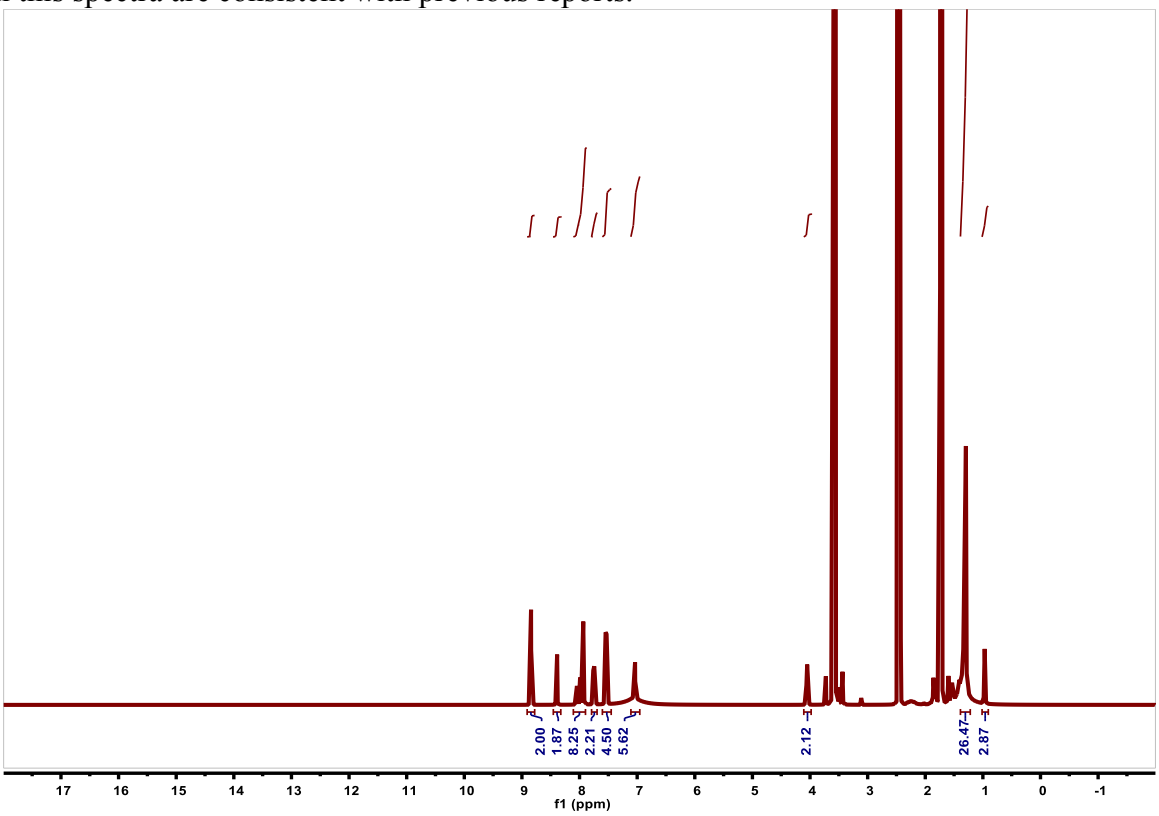

Figure S25. ^{1}H NMR (THF-d_8, 500 MHz, 298 K) of **MC 2**.

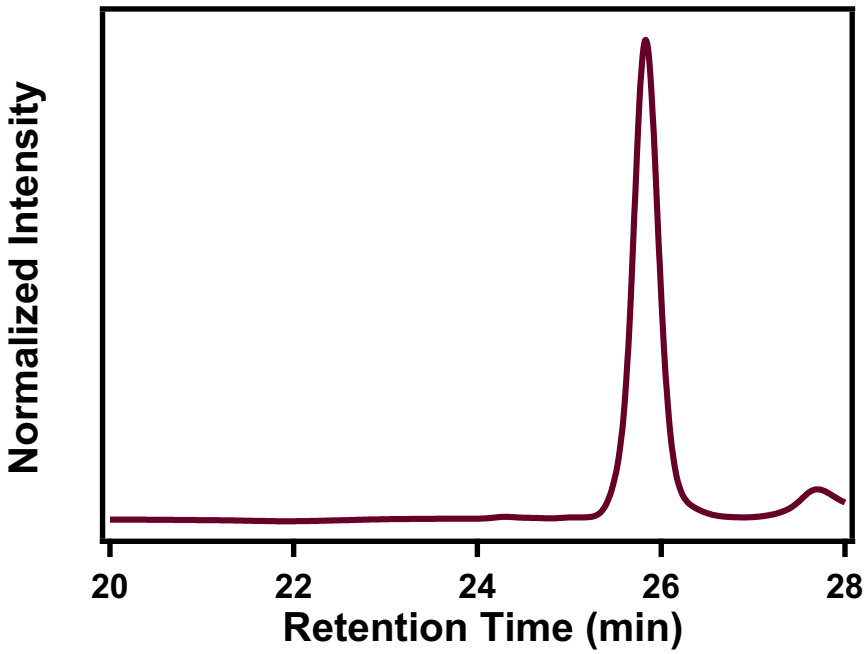

Figure S26. GPC of **MC 2**, synthesized at 12.5 mM, in THF showing a single narrow elution band corresponding to successful macrocyclization. was corroborated by rerunning a representative sample after washing the GPC column (Figure S23 Right) Furthermore, no resonances corresponding to smaller molecular weight species were observed via MALDI-MS or ^{1}H NMR analysis of the sample.

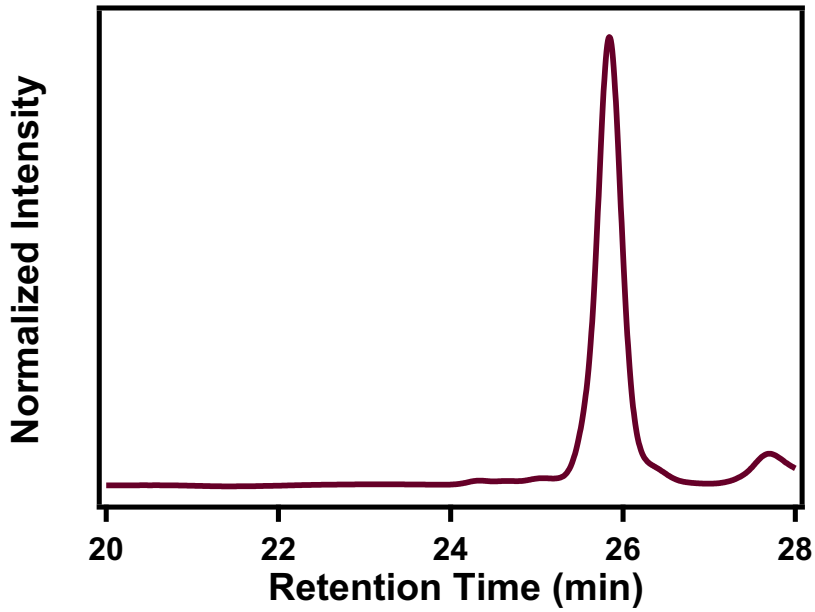

Figure S27. GPC of **MC 2**, synthesized at 8.5 mM, in THF showing a single narrow elution band corresponding to successful macrocyclization. was corroborated by rerunning a representative sample after washing the GPC column (Figure S23 Right) Furthermore, no resonances corresponding to smaller molecular weight species were observed via MALDI-MS or ^{1}H NMR analysis of the sample.

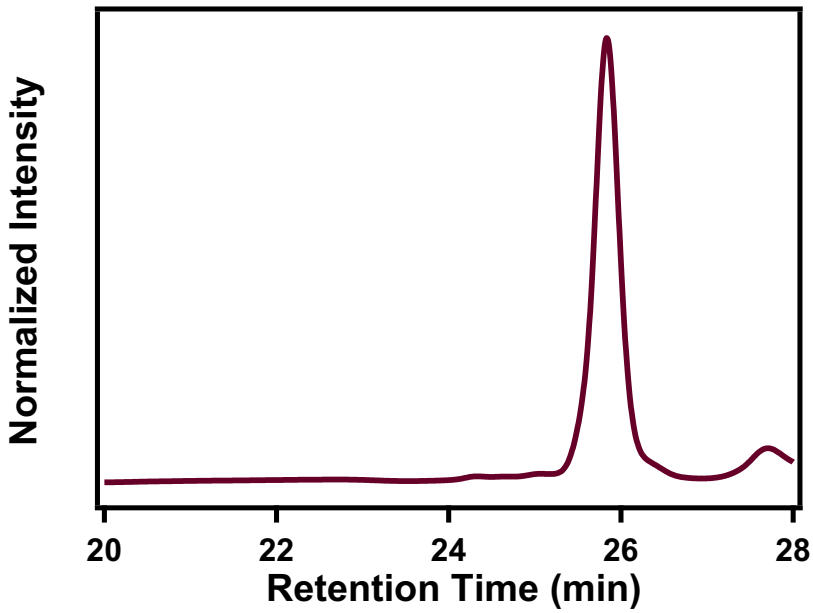

Figure S28. GPC of **MC 2**, synthesized at 6.4 mM, in THF showing a single narrow elution band corresponding to successful macrocyclization. was corroborated by rerunning a representative sample after washing the GPC column (Figure S23 Right) Furthermore, no resonances corresponding to smaller molecular weight species were observed via MALDI-MS or ^{1}H NMR analysis of the sample.

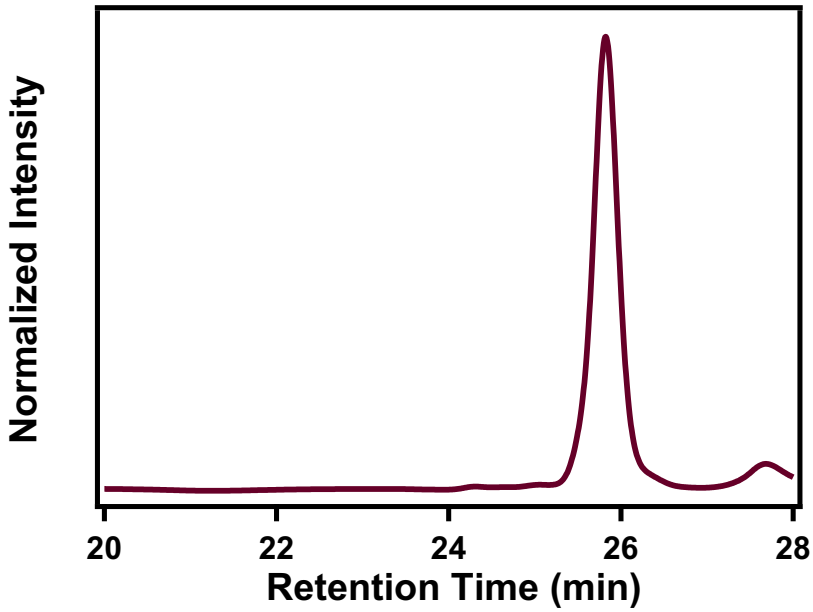

Figure S29. GPC of **MC 2**, synthesized at 5.1 mM, in THF showing a single narrow elution band corresponding to successful macrocyclization. was corroborated by rerunning a representative sample after washing the GPC column (Figure S23 Right) Furthermore, no resonances corresponding to smaller molecular weight species were observed via MALDI-MS or ^{1}H NMR analysis of the sample.

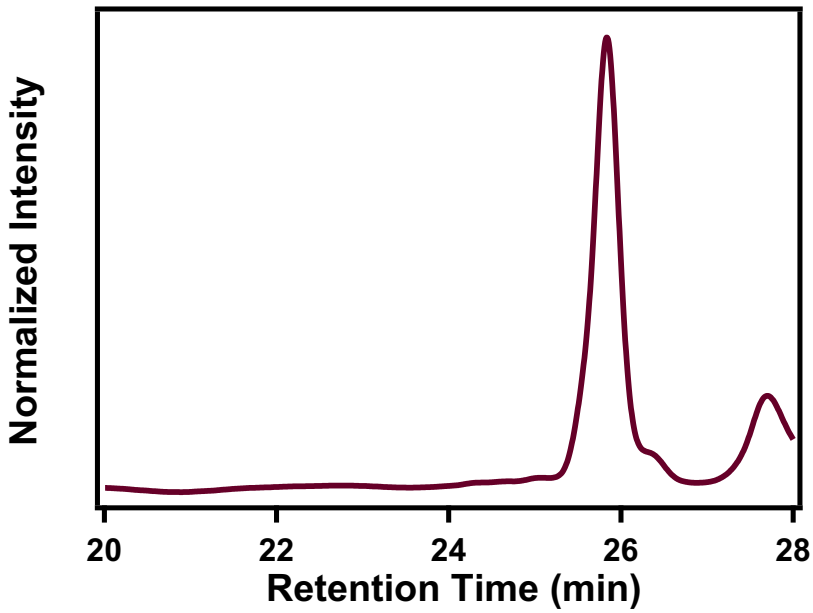

Figure S30. GPC of **MC 2**, synthesized at 3.4 mM, in THF showing a single narrow elution band corresponding to successful macrocyclization. was corroborated by rerunning a representative sample after washing the GPC column (Figure S23 Right) Furthermore, no resonances corresponding to smaller molecular weight species were observed via MALDI-MS or ^{1}H NMR analysis of the sample.

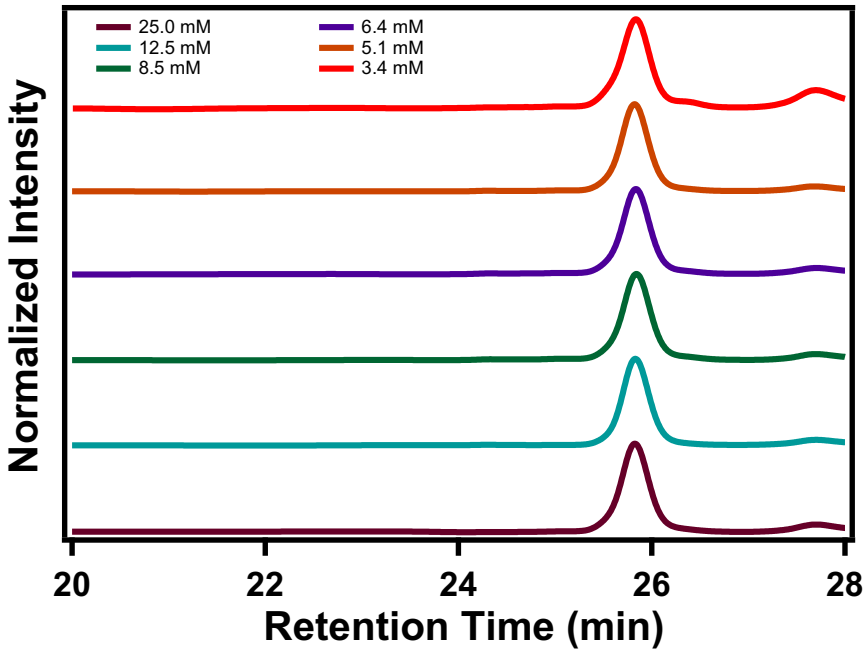

Figure S31. Overlaid GPC traces from all diluted syntheses of **MC 2**, showing no concentration dependence on macrocycle formation.

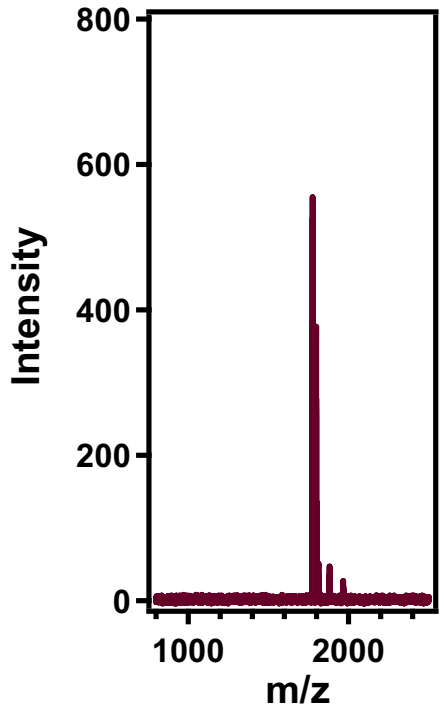

Figure S32. MALDI-MS of **MC 2**, synthesized at 12.5 mM, showing the desired $[M+H]^+$, $[M+Na]^+$, and $[M+K]^+$ adducts. (*m/z*=1774.61 $[M+H]^+$; *m/z*= 1796.44 $[M+Na]^+$; *m/z*= 1813.92 $[M+K]^+$).

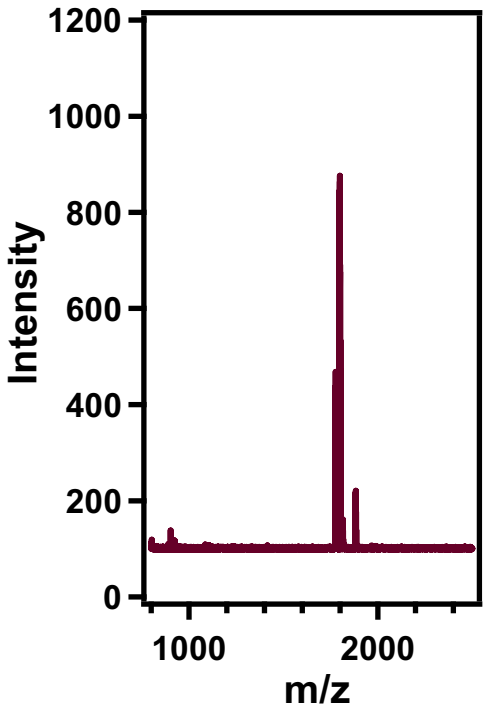

Figure S33. MALDI-MS of **MC 2**, synthesized at 8.5 mM, showing the desired $[M+H]^+$, $[M+Na]^+$, and $[M+K]^+$ adducts. (*m/z*=1774.64 $[M+H]^+$; *m/z*= 1796.72$[M+Na]^+$; *m/z*= 1813.64 $[M+K]^+$).

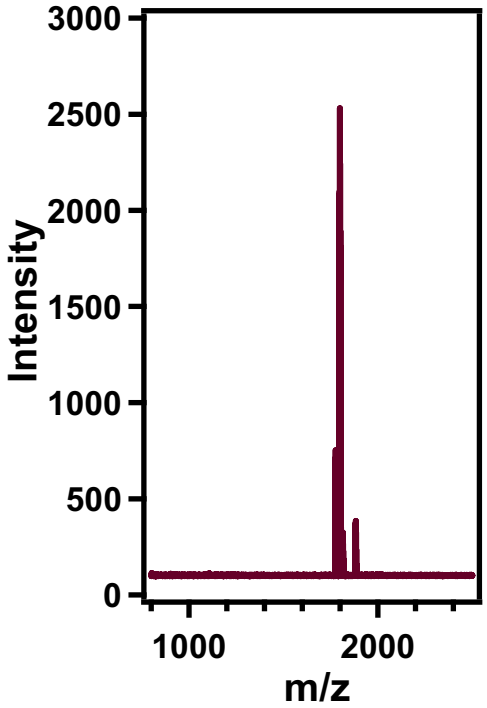

Figure S34. MALDI-MS of **MC 2**, synthesized at 6.4 mM, showing the desired $[M+H]^+$, $[M+Na]^+$, and $[M+K]^+$ adducts. (*m/z*=1774.66 $[M+H]^+$; *m/z*= 1796.48 $[M+Na]^+$; *m/z*= 1813.90 $[M+K]^+$).

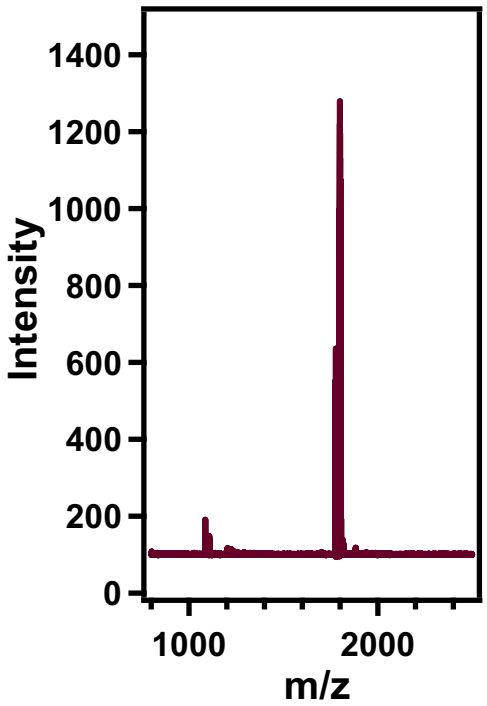

Figure S35. MALDI-MS of **MC 2**, synthesized at 5.1 mM, showing the desired $[M+H]^+$, $[M+Na]^+$, and $[M+K]^+$ adducts. (*m/z*=1774.62 $[M+H]^+$; *m/z*= 1796.44 $[M+Na]^+$; *m/z*= 1813.86 $[M+K]^+$). Peaks around *m/z*=1000 do not correspond to reaction of DFP or **S1** but are instrument artifacts observed in control samples. Furthermore **MC 2** formation was confirmed by ^{1}H NMR.

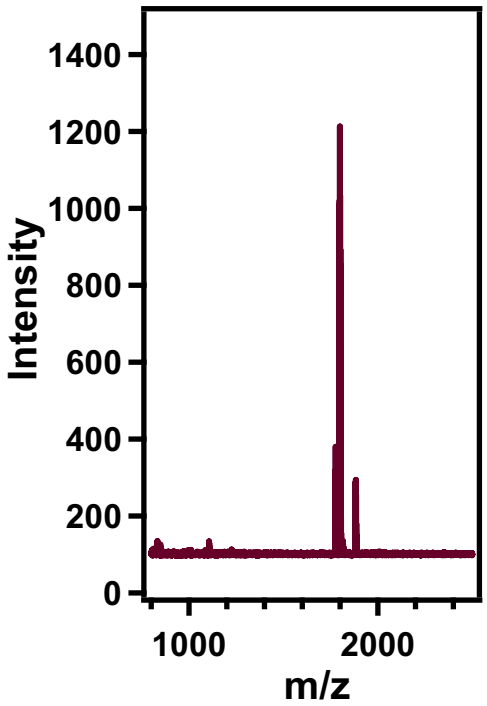

Figure S36. MALDI-MS of **MC 2**, synthesized at 3.4 mM, showing the desired $[M+H]^+$, $[M+Na]^+$, and $[M+K]^+$ adducts. (*m/z*=1774.62 $[M+H]^+$; *m/z*= 1796.50 $[M+Na]^+$; *m/z*= 1813.86 $[M+K]^+$).

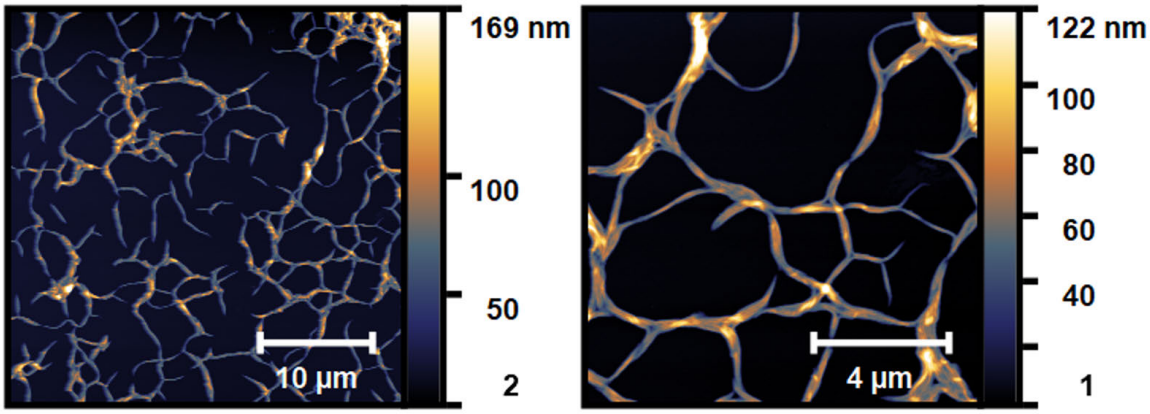

Figure S37. Atomic force microscopy images of a drop cast aliquot of from the **MC 2** reaction at 3.4 mM showing the formation of high-aspect ratio nanotubes.

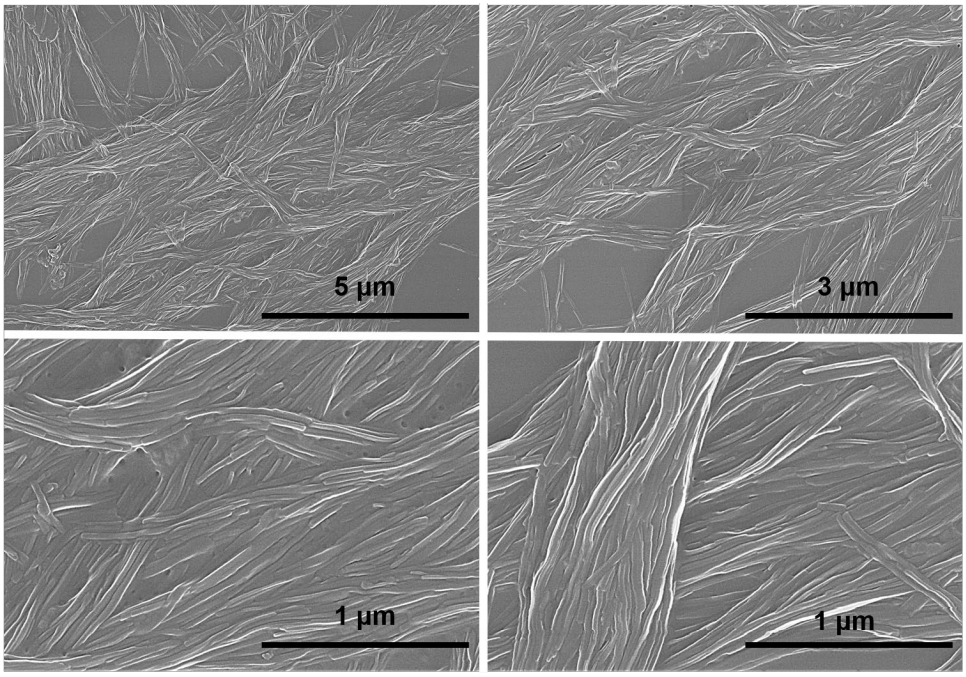

Figure S38. Scanning electron microscopy images of a drop cast aliquot of from the **MC 2** reaction at 3.4 mM showing the formation of high-aspect ratio nanotubes.

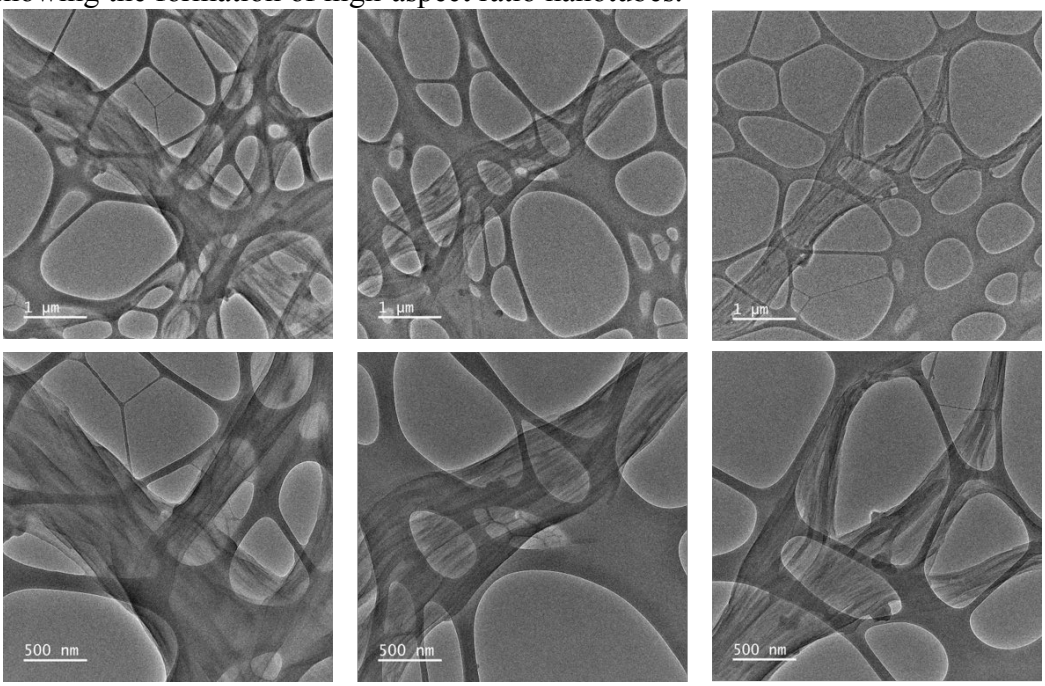

Figure S39. Transmission electron microscopy images of a drop cast aliquot of from the **MC 2** reaction at 25 mM showing the formation of high-aspect ratio nanotubes.

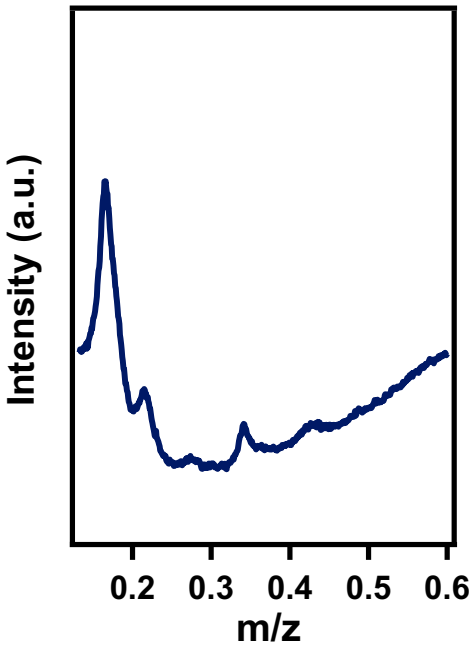

Figure S40. *In-Situ* WAXS pattern of the **MC 2** reaction run at 25 mM.

E. Kinetic Experiments Characterization

I. Characterization of MC 1 Kinetics

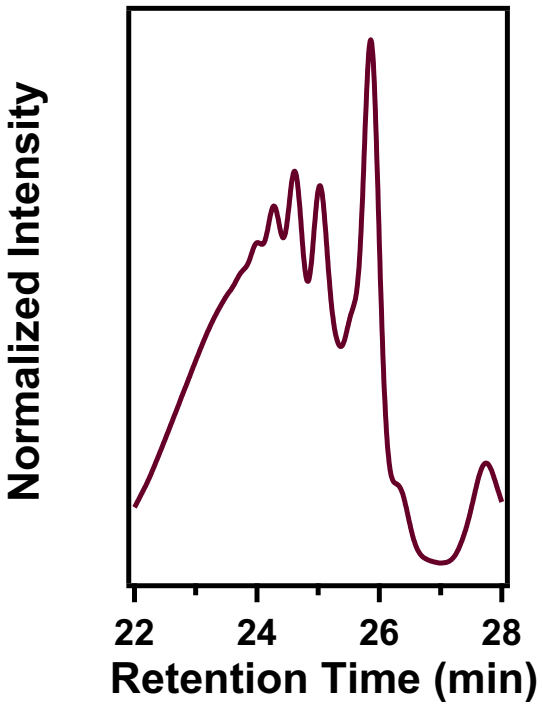

Figure S41. GPC trace of the **MC 1** reaction after 2 minutes depicting the presence of varying imine-linked structures.

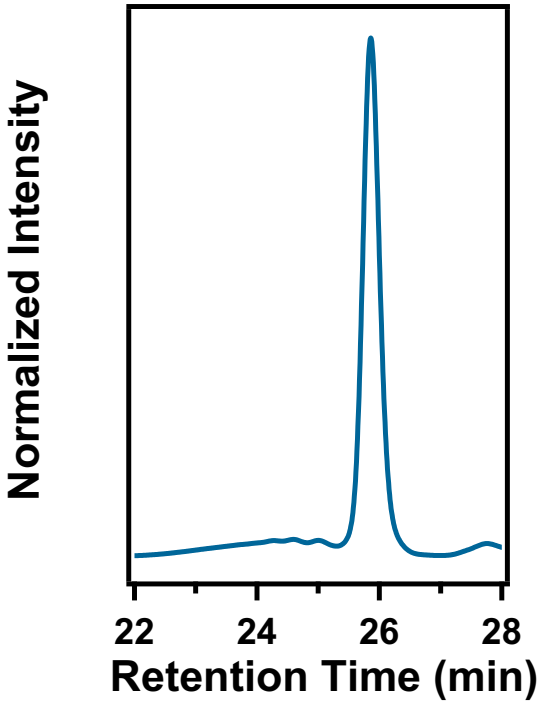

Figure S42. GPC trace of the **MC 1** reaction after 15 minutes depicting successful macrocyclization.

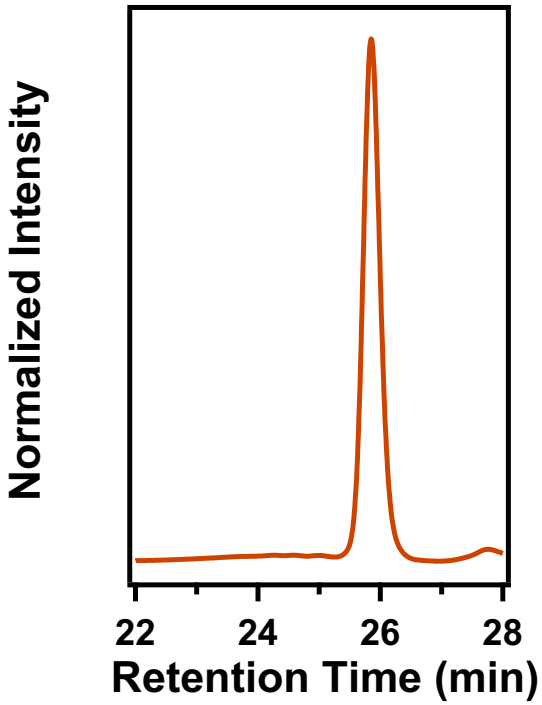

Figure S43. GPC trace of the **MC 1** reaction after 30 minutes depicting successful macrocyclization.

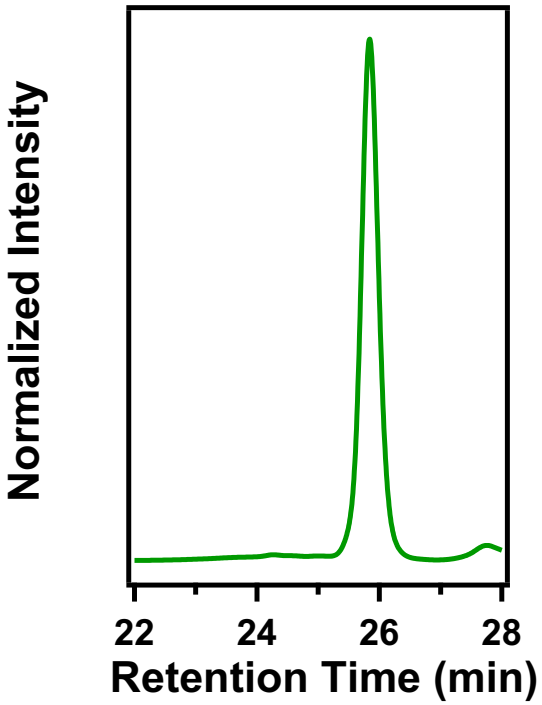

Figure S44. GPC trace of the **MC 1** reaction after 60 minutes depicting successful macrocyclization.

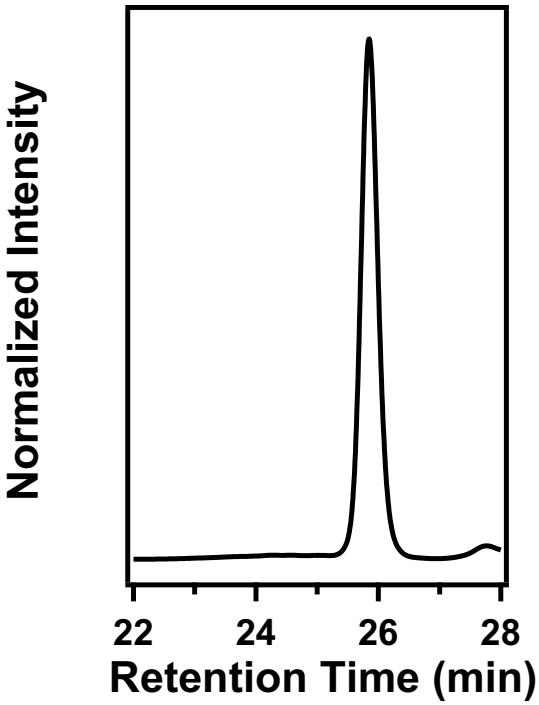

Figure S45. GPC trace of the **MC 1** reaction after 120 minutes depicting successful macrocyclization.

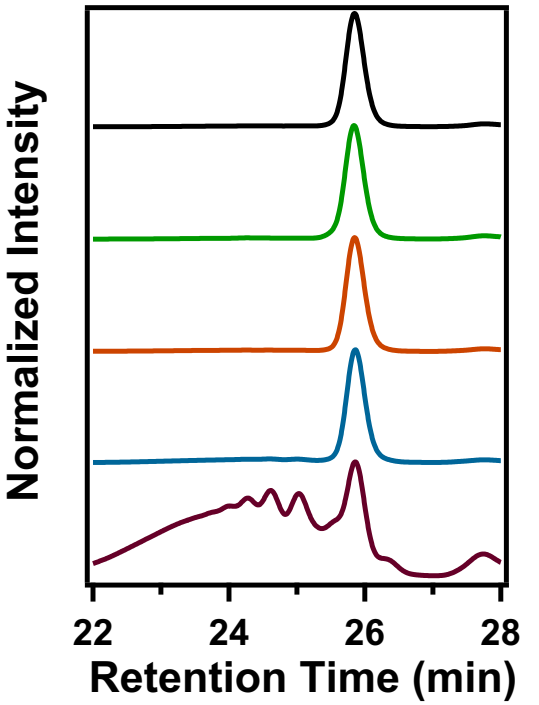

Figure S46. GPC traces of all **MC 1** reaction kinetic data. Overall, the GPC kinetic traces are consistent with previous reports of macrocycle formation,[1] but shown different time dependences than the TR-XRD data due to having more catalyst added and being run at a higher concentration.

II. Characterization of MC 2 Kinetics

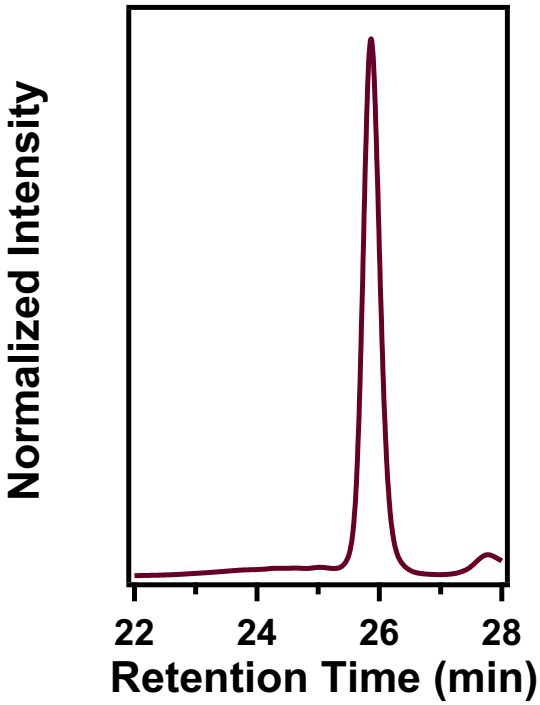

Figure S47. GPC trace of the **MC 2** reaction after 2 minutes depicting successful macrocyclization.

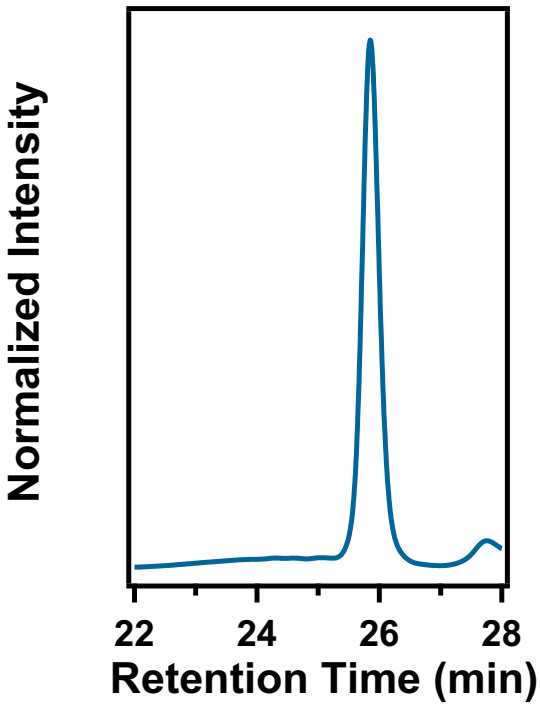

Figure S48. GPC trace of the **MC 2** reaction after 15 minutes depicting successful macrocyclization.

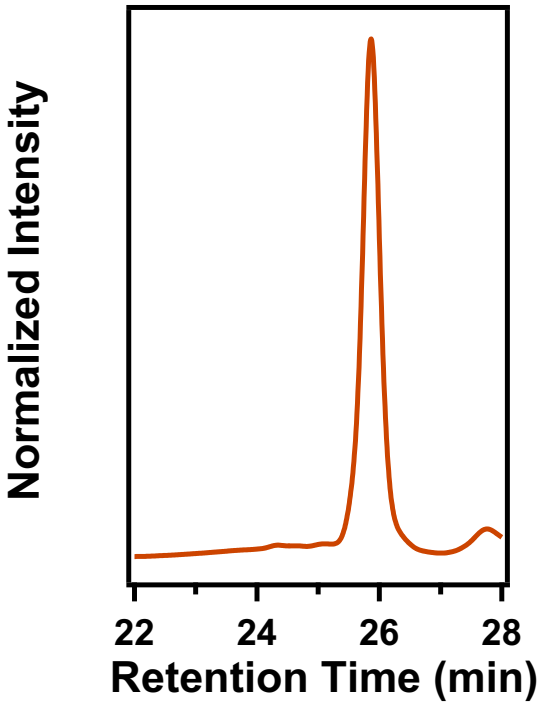

Figure S49. GPC trace of the **MC 2** reaction after 30 minutes depicting successful macrocyclization.

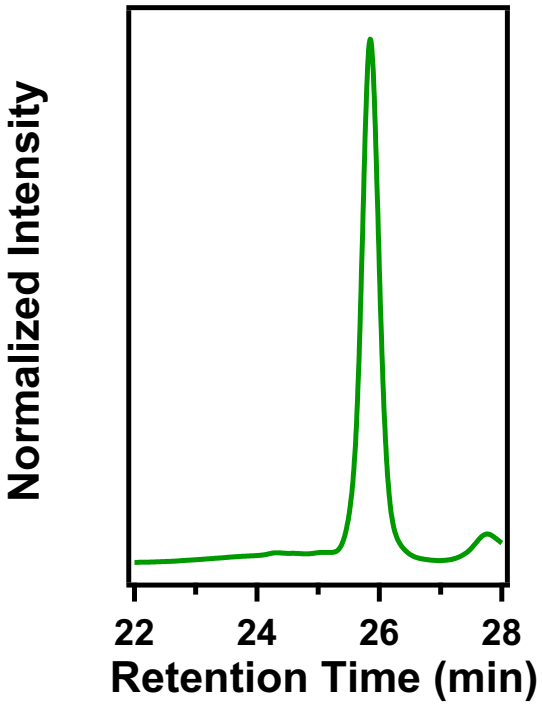

Figure S50. GPC trace of the **MC 2** reaction after 60 minutes depicting successful macrocyclization.

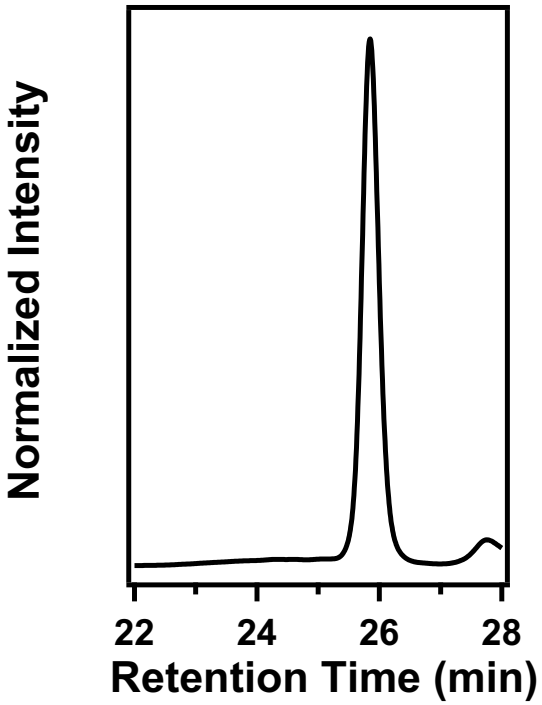

Figure S51. GPC trace of the **MC 2** reaction after 120 minutes depicting successful macrocyclization.

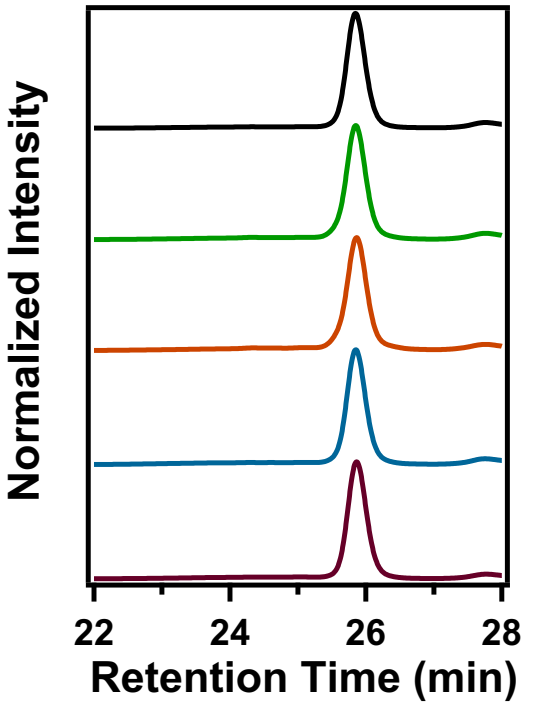

Figure S52. GPC traces of all **MC 2** reaction kinetic data. Overall, the GPC kinetic traces are consistent with previous reports of macrocycle formation,[1] but shown different time dependences than the TR-XRD data due to having more catalyst added and being run at a higher concentration.

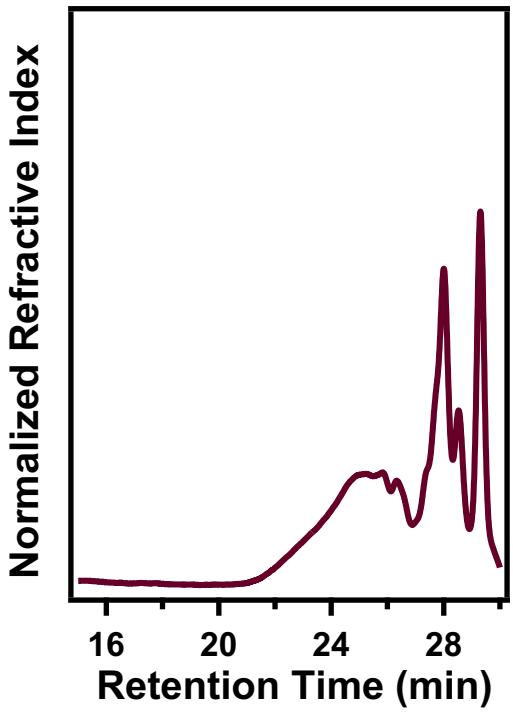

Figure S53. GPC trace of the **MC 2** reaction at 3.4 mM, with 0.005 equivalents of CF_3CO_2H, after 2 minutes of reaction time, thereby highlighting the polymeric intermediate in the formation of the desired macrocycle.

F. Scrambling Experiment Characterization

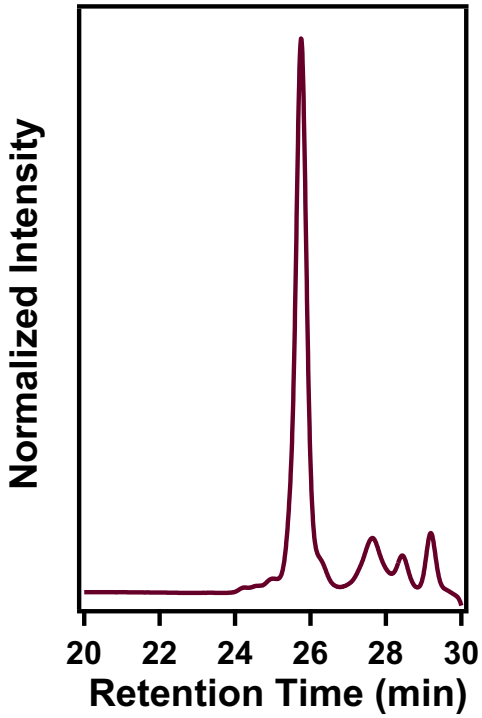

Figure S54. GPC trace of the scrambling experiment at 25 mM, showing the formation of macrocycles as well as small oligomers.

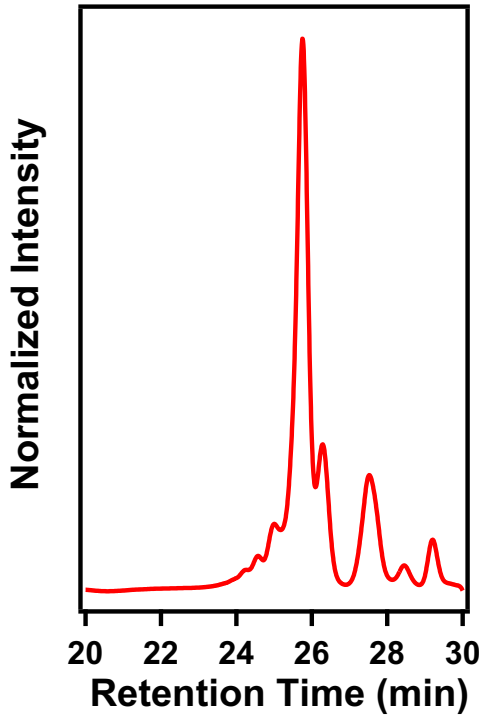

Figure S55. GPC trace of the scrambling experiment at 12.5 mM, showing the formation of macrocycles as well as small oligomers.

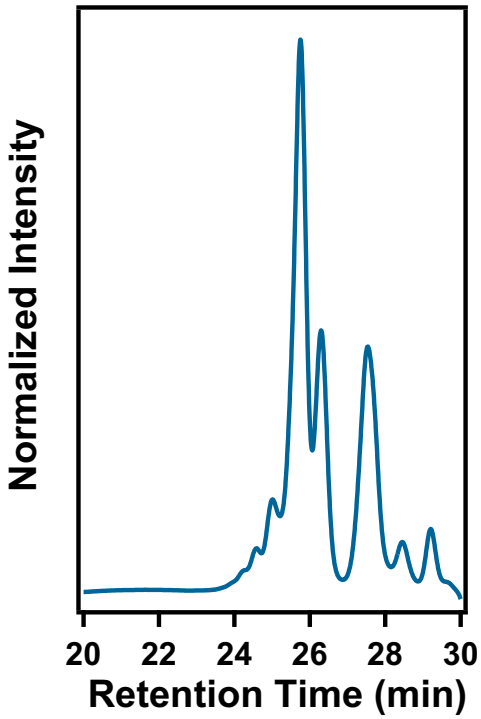

Figure S56. GPC trace of the scrambling experiment at 8.5 mM, showing the formation of macrocycles as well as small oligomers.

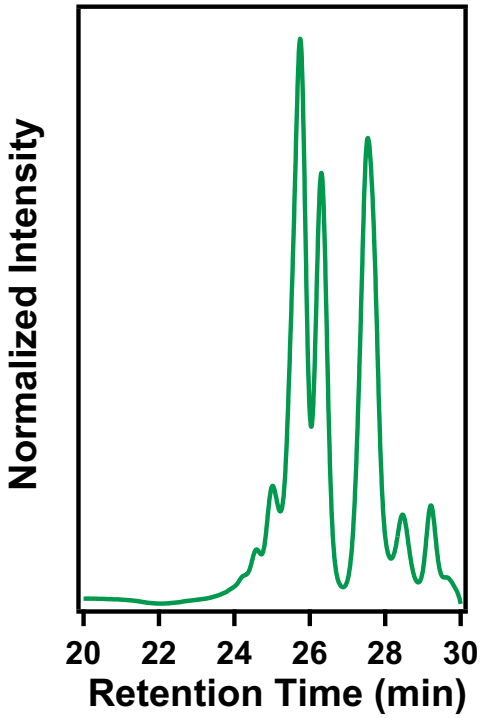

Figure S57. GPC trace of the scrambling experiment at 6.4 mM, showing the formation of macrocycles as well as small oligomers.

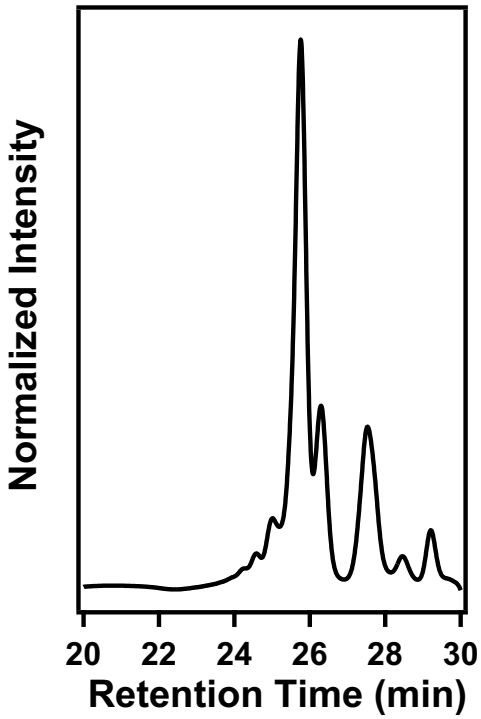

Figure S58. GPC trace of the scrambling experiment at 5.1 mM, showing the formation of macrocycles as well as small oligomers.

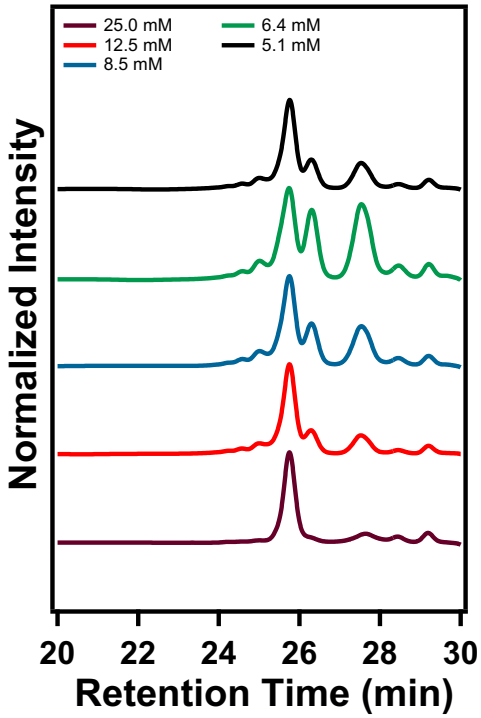

Figure S59. GPC of all scrambling experiments showing the formation of macrocycles as well as small oligomers regardless of reaction concentration.

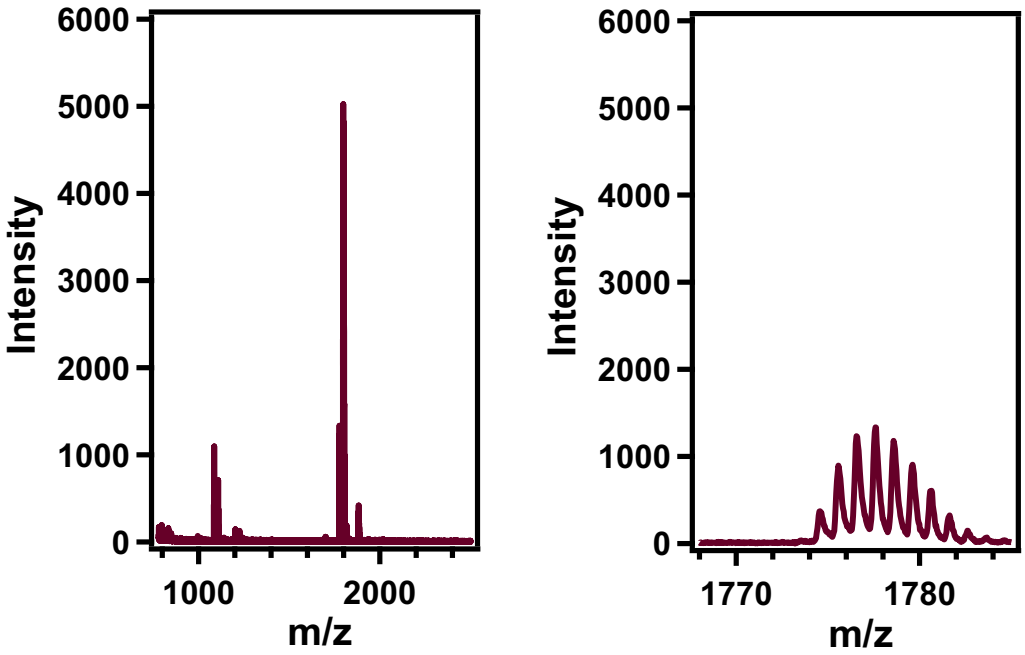

Figure S60. MALDI-MS of the scrambling reaction at 25 mM showing the formation of the MC 2 ([M+H]$^+$ *m/z*=1774.24, [M+Na]$^+$ *m/z*=1796.42, [M+K]$^+$ *m/z*=1813.90), as well as oligomers corresponding to IDA monomer incorporation ([2•**S1**+ **IDA**+H]$^+$ *m/z*=1083.64).

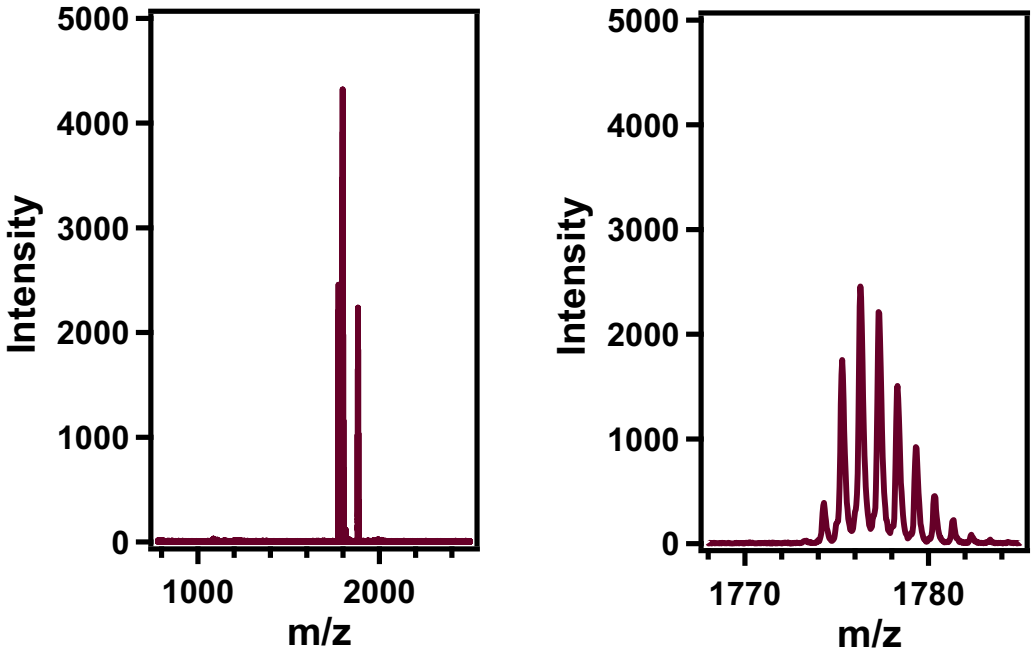

Figure S61. MALDI-MS of the scrambling reaction at 12.5 mM showing the formation of the **MC 2** ([M+H]$^+$ *m/z*=1774.28, [M+Na]$^+$ *m/z*=1796.56, [M+K]$^+$ *m/z*=1813.88).

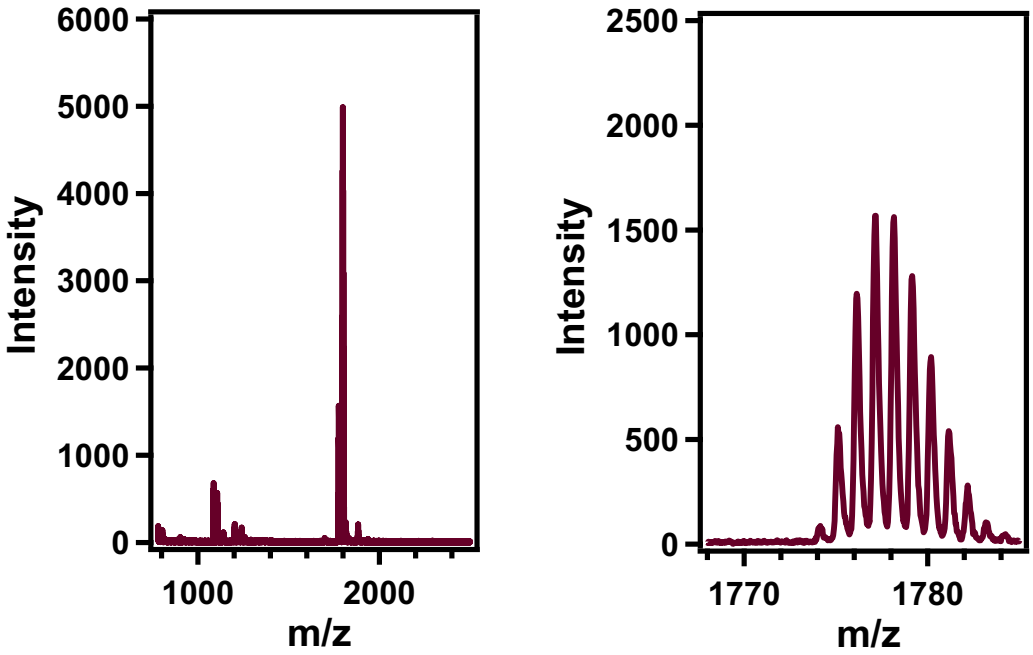

Figure S62. MALDI-MS of the scrambling reaction at 8.5 mM showing the formation of the **MC 2** ([M+H]$^+$ *m/z*=1774.28, [M+Na]$^+$ *m/z*=1796.47, [M+K]$^+$ *m/z*=1813.85), as well as oligomers corresponding to IDA monomer incorporation ([2•**S1+ IDA**+H]$^+$ *m/z*=1083.64, [2•**S1+ IDA**+Na]$^+$ *m/z*=1105.63).

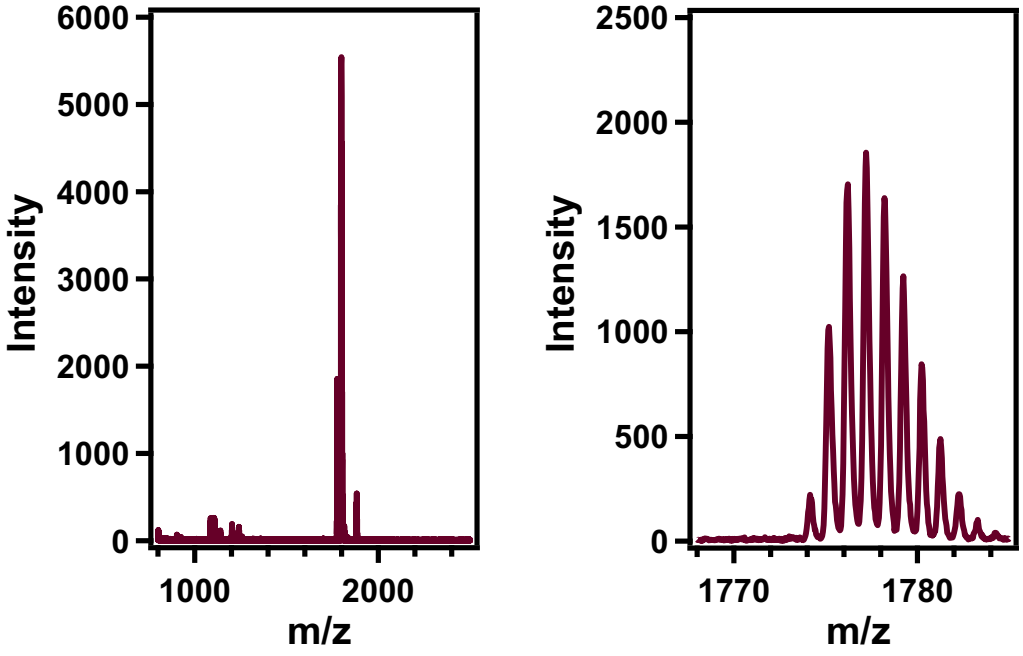

Figure S63. MALDI-MS of the scrambling reaction at 6.4 mM showing the formation of the **MC 2** ([M+H]$^+$ *m/z*=1774.34, [M+Na]$^+$ *m/z*=1796.44, [M+K]$^+$ *m/z*=1813.90), as well as oligomers corresponding to IDA monomer incorporation ([2•**S1+ IDA**+H]$^+$ *m/z*=1083.82, [2•**S1+ IDA**+Na]$^+$ *m/z*=1105.93).

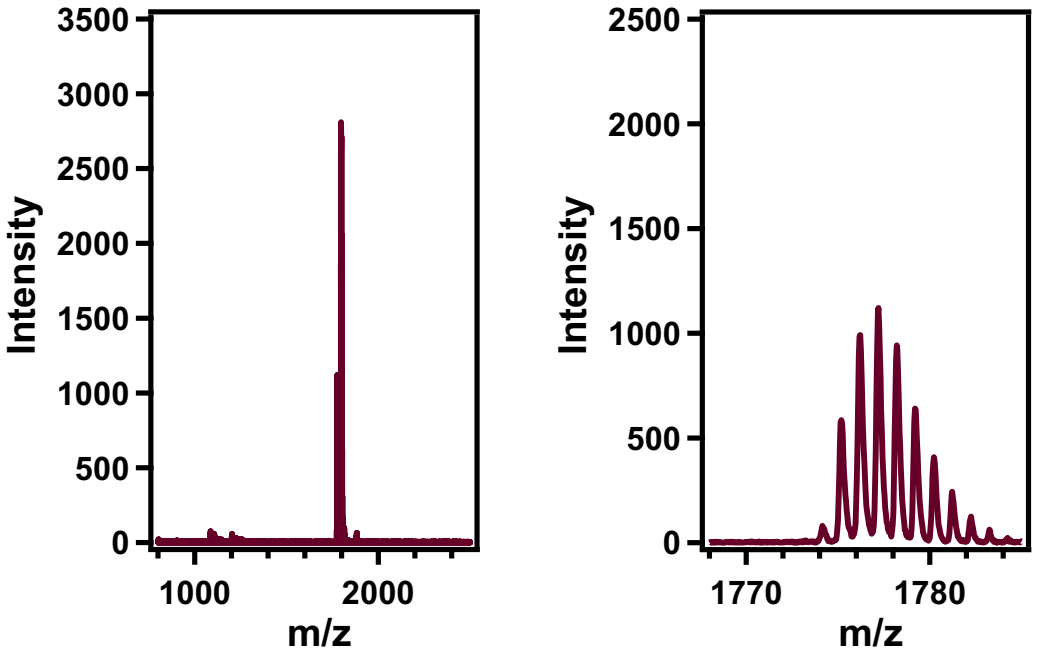

Figure S64. MALDI-MS of the scrambling reaction at 5.1 mM showing the formation of the **MC 2** ($[M+H]^+$ *m/z*=1774.30, $[M+Na]^+$ *m/z*=1796.50, $[M+K]^+$ *m/z*=1813.85).

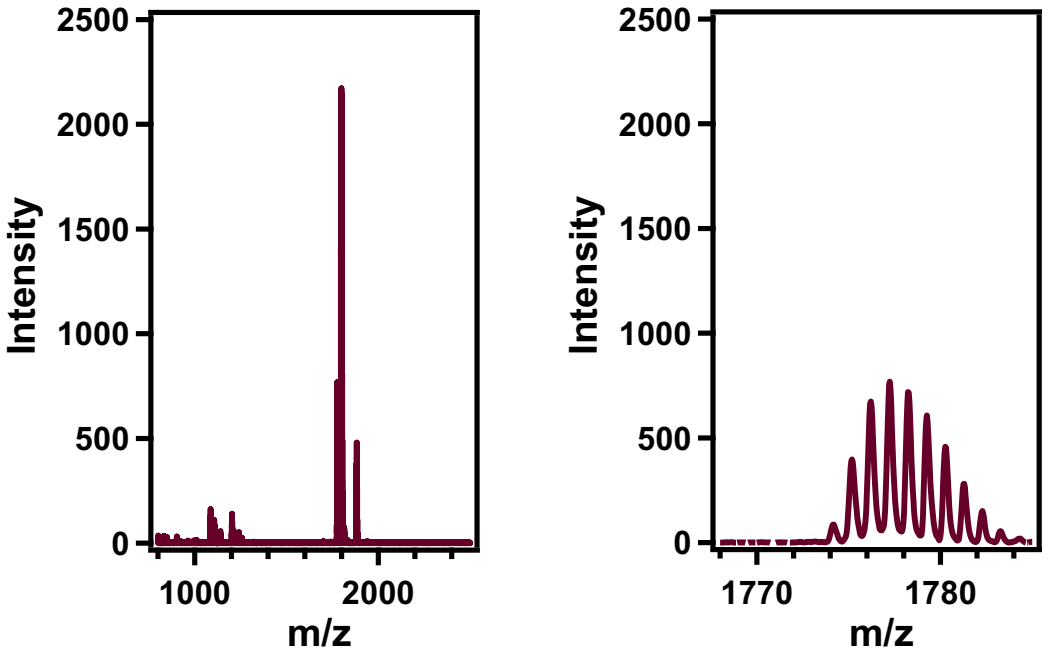

Figure S65. MALDI-MS of the scrambling reaction at 3.4 mM showing the formation of the **MC 2** ($[M+H]^+$ *m/z*=1774.26, $[M+Na]^+$ *m/z*=1796.42, $[M+K]^+$ *m/z*=1813.92), as well as oligomers corresponding to IDA monomer incorporation ($[2•\mathbf{S1}+\mathbf{IDA}+H]^+$ *m/z*=1083.90, $[2•\mathbf{S1}+\mathbf{IDA}+Na]^+$ *m/z*=1105.90).

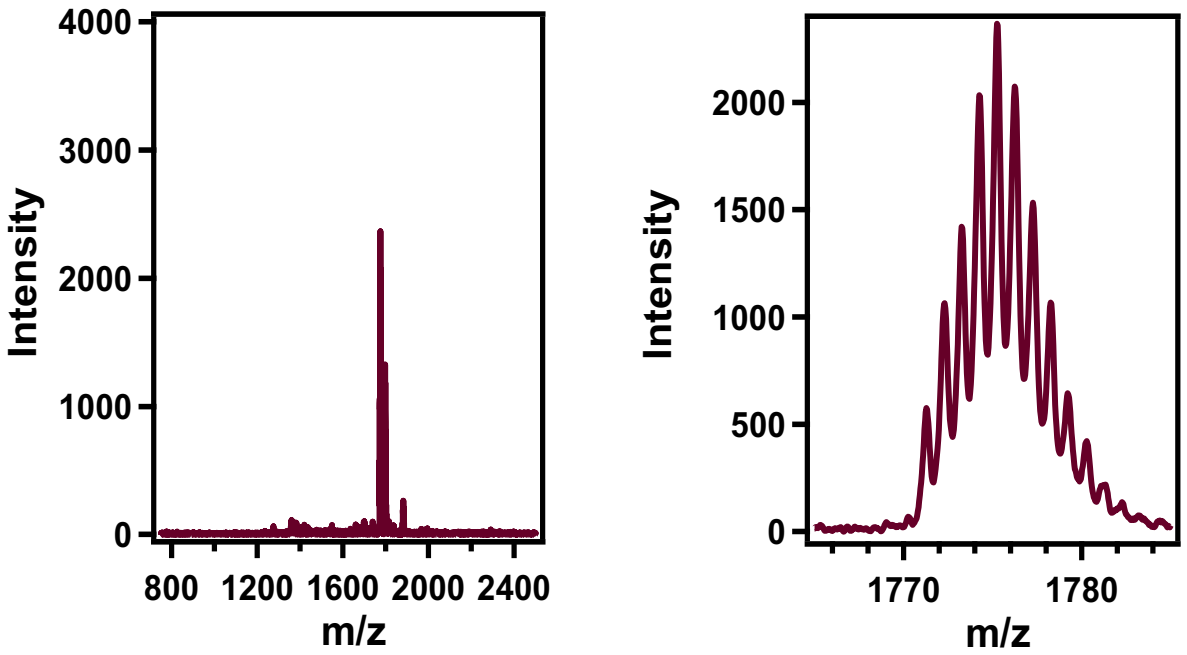

Figure S66. MALDI-MS of a 1:1 mixture of **MC 1** and **MC 2**, showing that when both macrocycles are present, they can both be detected.

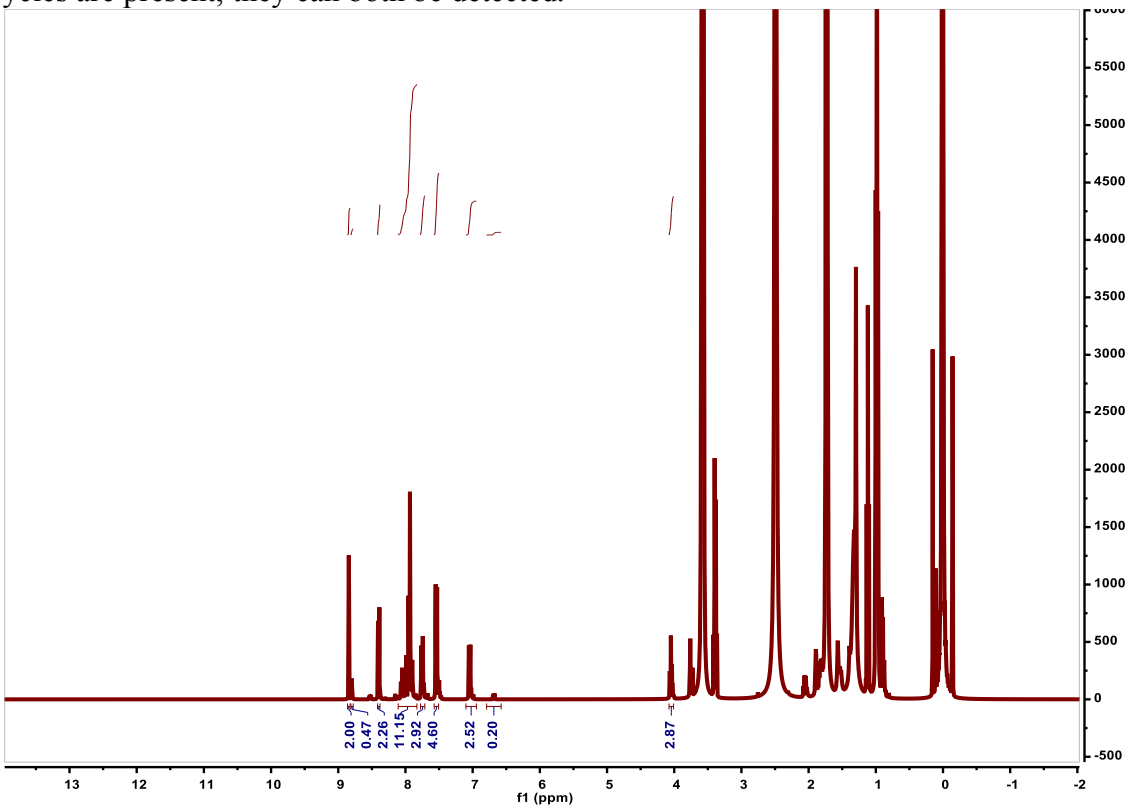

Figure S67. ^{1}H NMR (THF-d_8, 500 MHz, 298 K) of the scrambling experiment showing the formation of the **MC 2** and oligomers containing IDA moieties. Oligomers containing IDA moieties were removed by precipitating the solid into CH_2Cl_2, after which the ^{1}H NMR spectra was analogous to that of the direct **MC 2** synthesis.

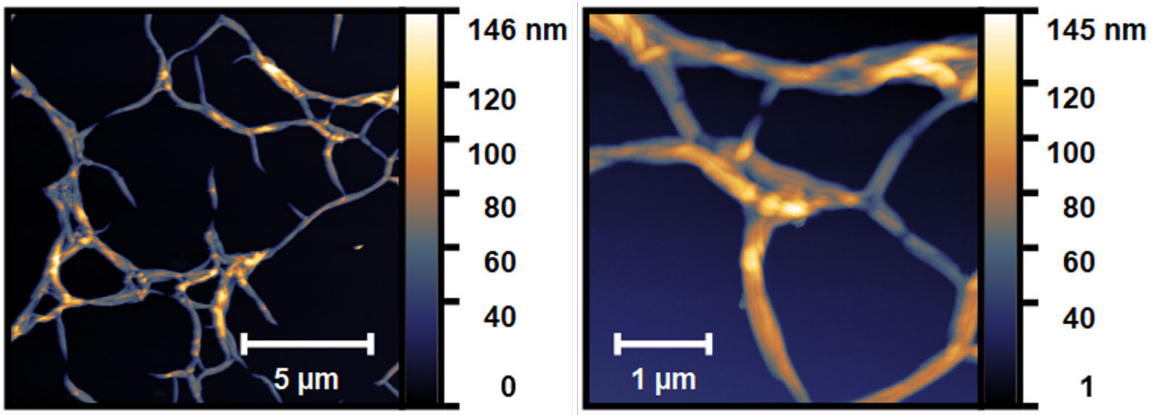

Figure S68. Atomic force microscopy images of a drop cast aliquot of from the scrambling macrocyclization reaction at 3.4 mM showing the formation of high-aspect ratio nanotubes, further supporting the formation of **MC 2** which have previously demonstrated self-assembly ability.

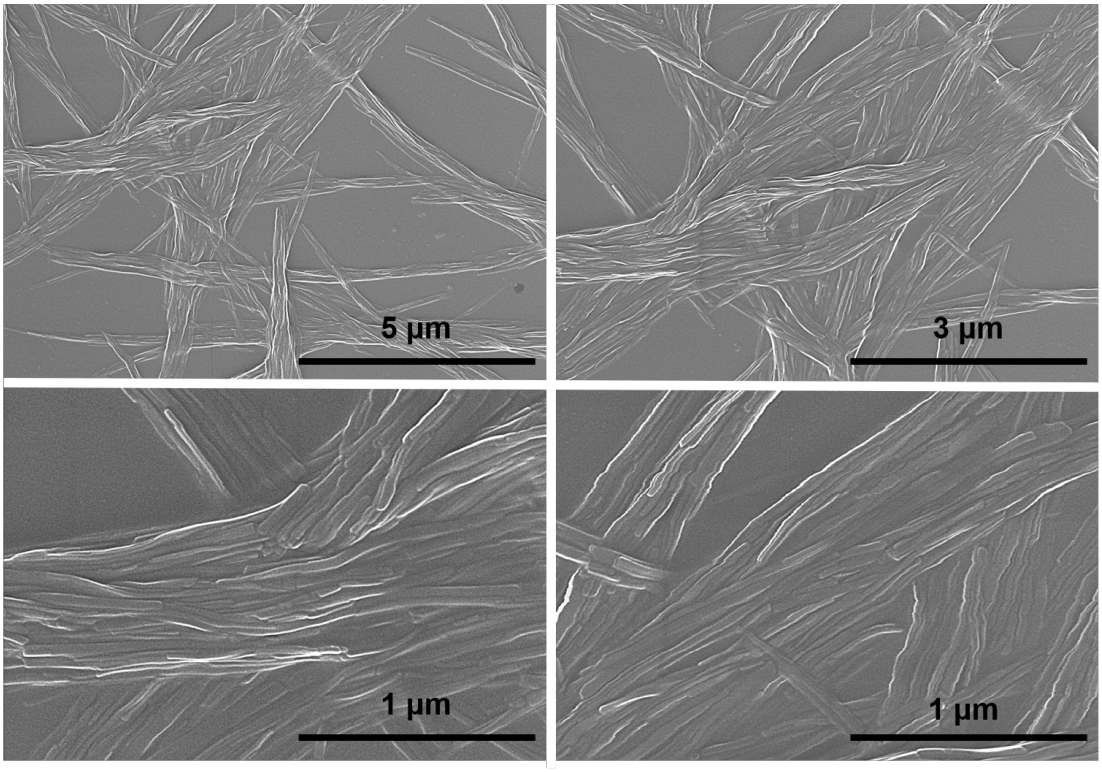

Figure S69. Scanning electron microscopy images of a drop cast aliquot of from the scrambling macrocyclization reaction at 3.4 mM showing the formation of high-aspect ratio nanotubes, further supporting the formation of **MC 2** which have previously demonstrated self-assembly ability.

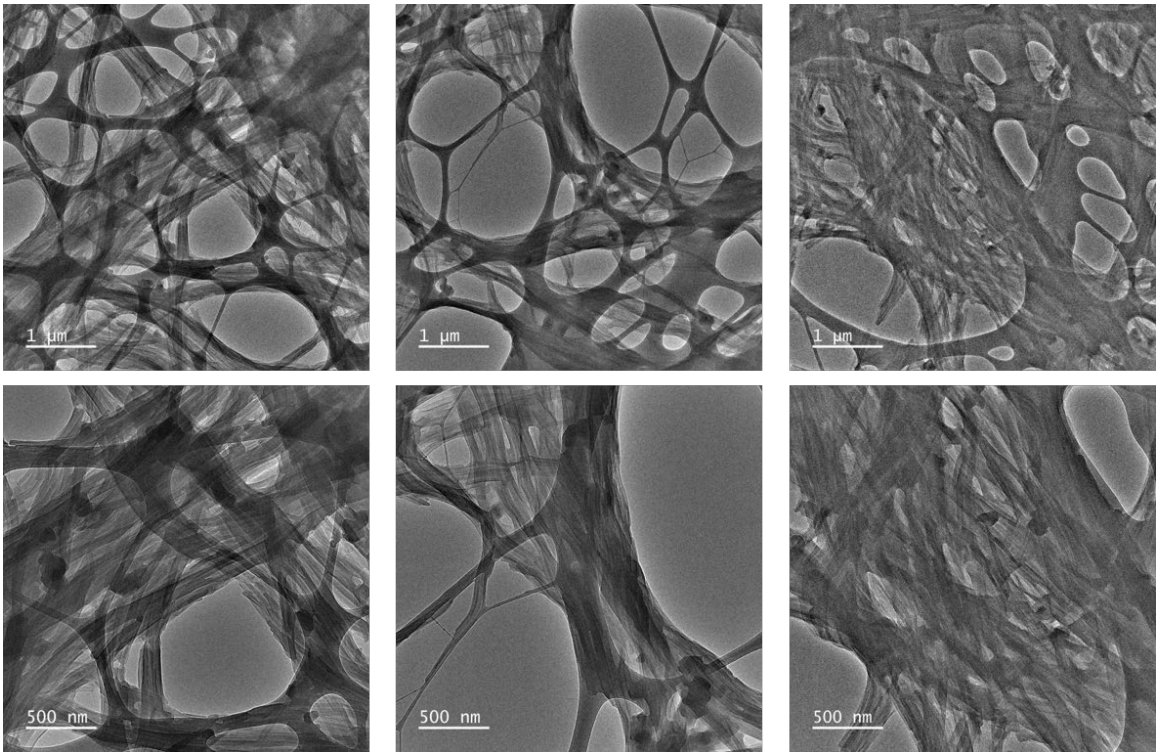

Figure S70. Transmission electron microscopy images of a drop cast aliquot of from the scrambling macrocyclization reaction at 25 mM showing the formation of high-aspect ratio nanotubes, further supporting the formation of **MC 2** which have previously demonstrated self-assembly ability.

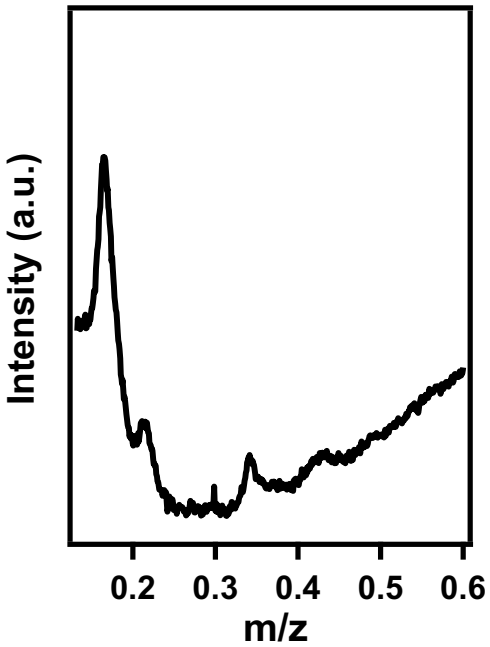

Figure S71. *In-Situ* WAXS pattern of the scrambling reaction run at 25 mM.

G. Competition Experiment Characterization

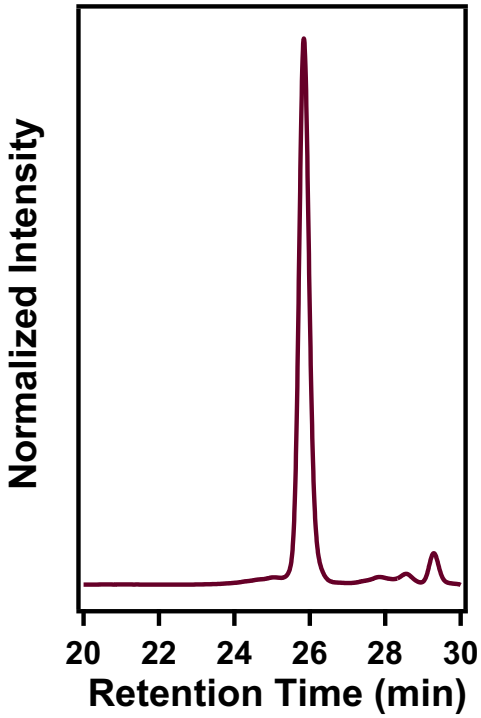

Figure S72. GPC trace of the competition experiment at 25 mM, showing mainly the formation of macrocycles as well as low quantities of small oligomers.

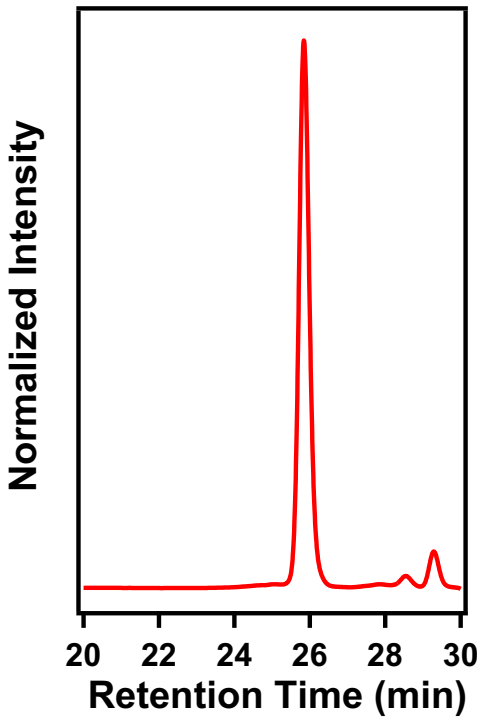

Figure S73. GPC trace of the competition experiment at 12.5 mM, showing mainly the formation of macrocycles as well as low quantities of small oligomers.

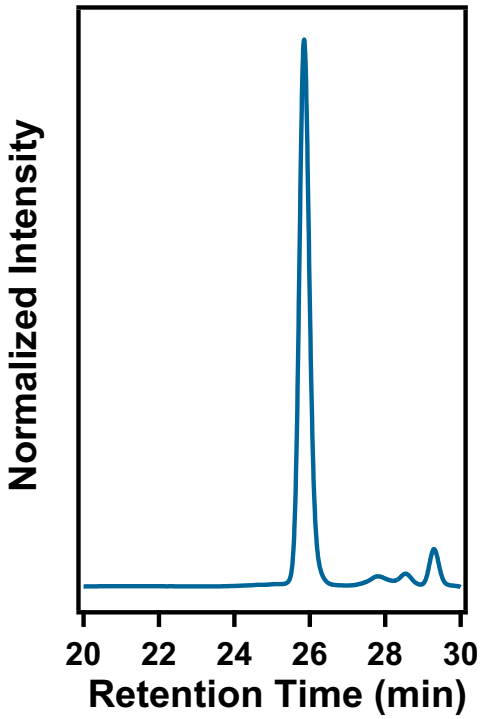

Figure S74. GPC trace of the competition experiment at 8.5 mM, showing mainly the formation of macrocycles as well as low quantities of small oligomers.

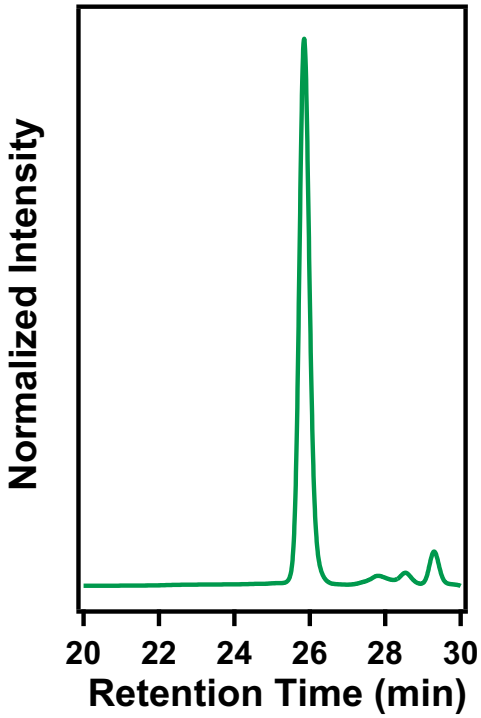

Figure S75. GPC trace of the competition experiment at 6.4 mM, showing mainly the formation of macrocycles as well as low quantities of small oligomers.

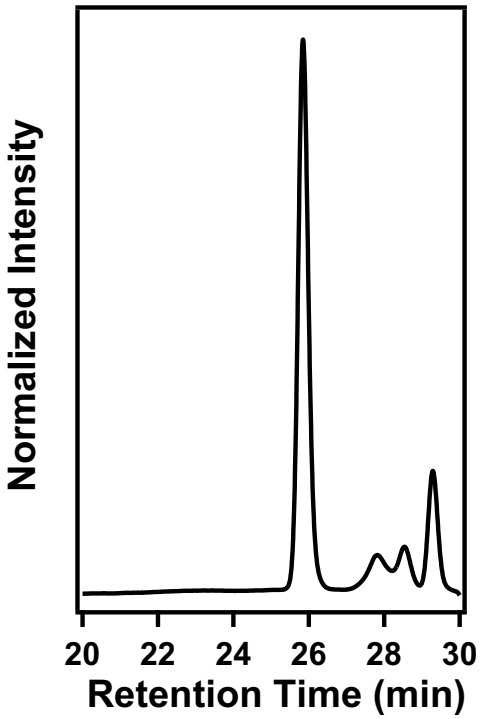

Figure S76. GPC trace of the competition experiment at 5.1 mM, showing mainly the formation of macrocycles as well as low quantities of small oligomers.

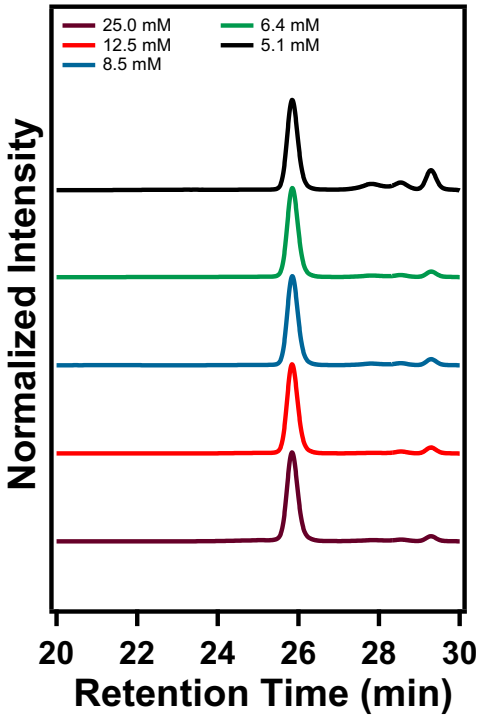

Figure S77. GPC traces of all competition experiments showing the formation of macrocycles as evident by the narrow elution band at ~26 minutes.

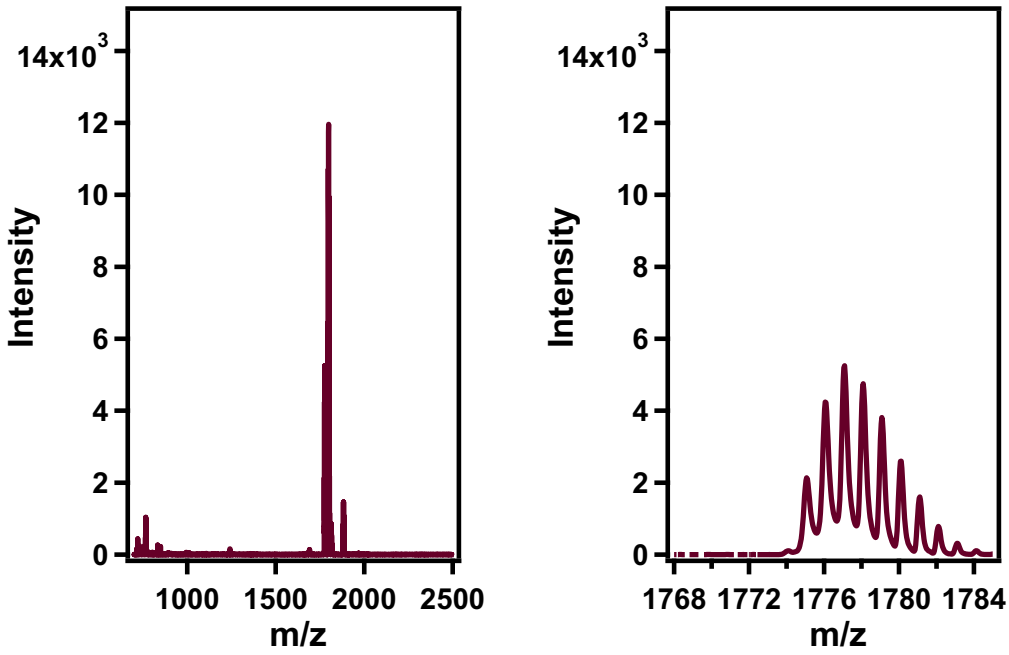

Figure S78. MALDI-MS of the competition reaction at 25 mM showing the formation of the **MC 2** ([M+H]$^+$ *m/z*=1774.28, [M+Na]$^+$ *m/z*=1796.52, [M+K]$^+$ *m/z*=1813.81) as well as a small oligomer corresponding to the reaction of IDA monomers ([**S1**+2**IDA**+H]$^+$ *m/z*=725.37).

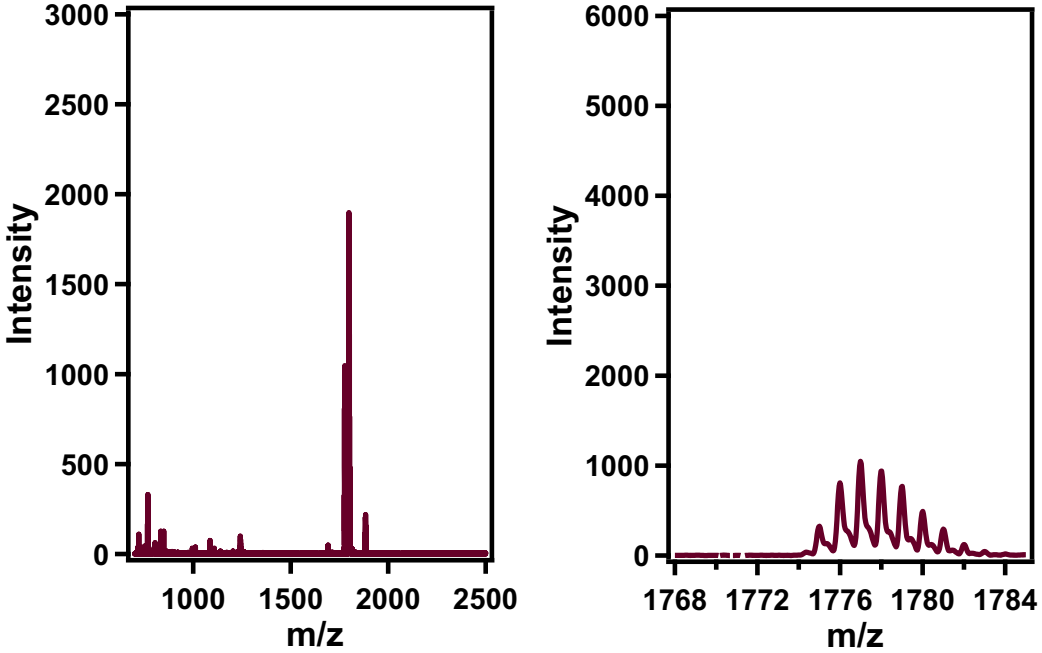

Figure S79. MALDI-MS of the competition reaction at 12.5 mM showing the formation of the **MC 2** ([M+H]$^+$ *m/z*=1774.32, [M+Na]$^+$ *m/z*=1796.50, [M+K]$^+$ *m/z*=1813.92) as well as a small oligomer corresponding to the reaction of IDA monomers ([**S1**+2•**IDA**+H]$^+$ *m/z*=725.35).

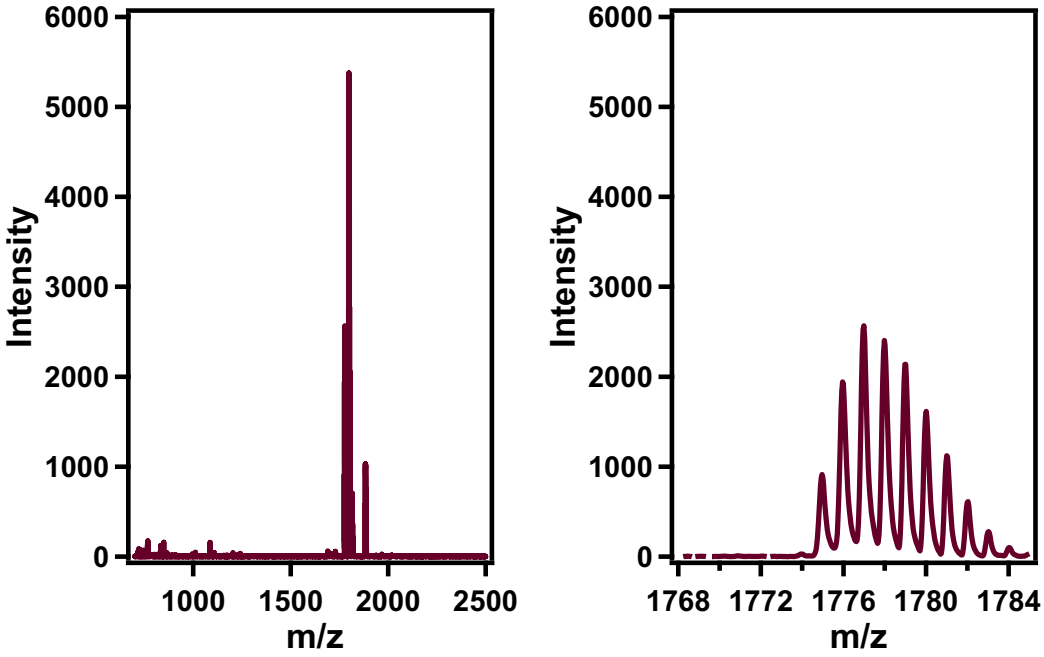

Figure S80. MALDI-MS of the competition reaction at 8.5 mM showing the formation of the **MC 2** ($[M+H]^+$ *m/z*=1774.61, $[M+Na]^+$ *m/z*=1796.44, $[M+K]^+$ *m/z*=1813.90).

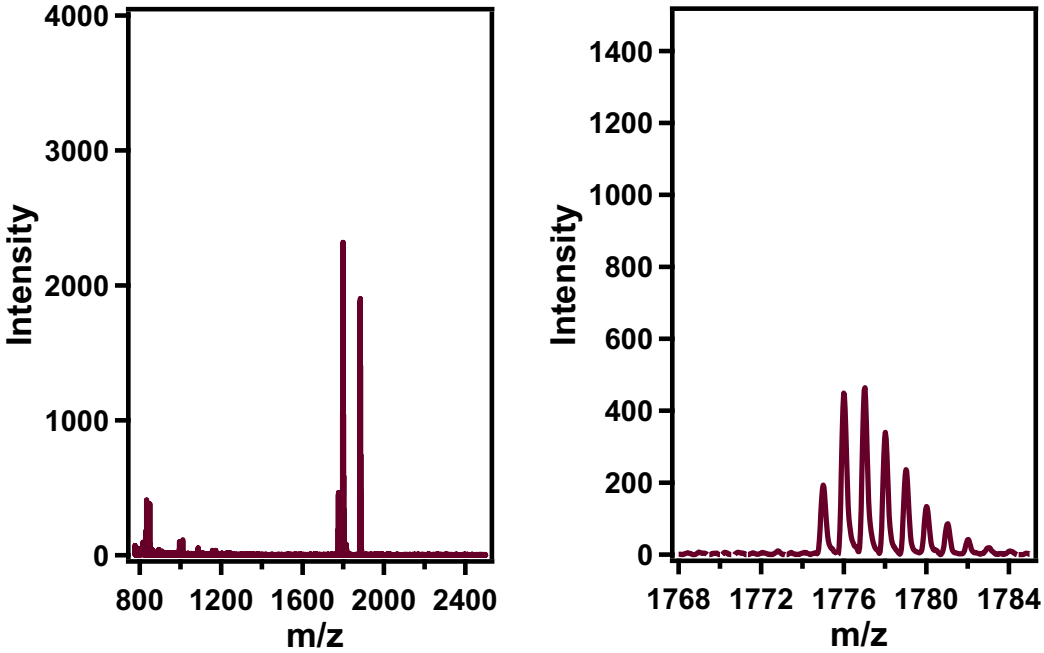

Figure S81. MALDI-MS of the competition reaction at 6.4 mM showing the formation of the **MC 2** ($[M+H]^+$ *m/z*=1774.54, $[M+Na]^+$ *m/z*=1796.48, $[M+K]^+$ *m/z*=1813.93) as well as a small oligomer corresponding to the reaction of IDA monomers ($[$**S1**+2•**IDA**$+H]^+$ *m/z*=725.39 and $[$**S1**+2•**IDA**$+Na]^+$ *m/z*=748.36).

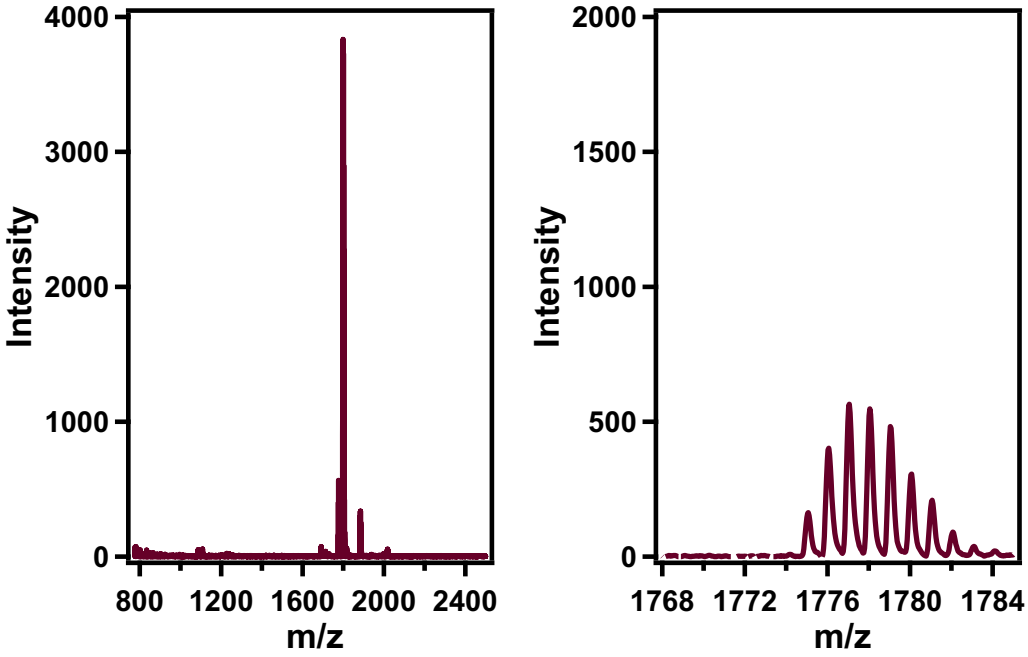

Figure S82. MALDI-MS of the competition reaction at 5.1 mM showing the formation of the **MC 2** ([M+H]$^+$ *m/z*=1774.62, [M+Na]$^+$ *m/z*=1796.48, [M+K]$^+$ *m/z*=1813.90).

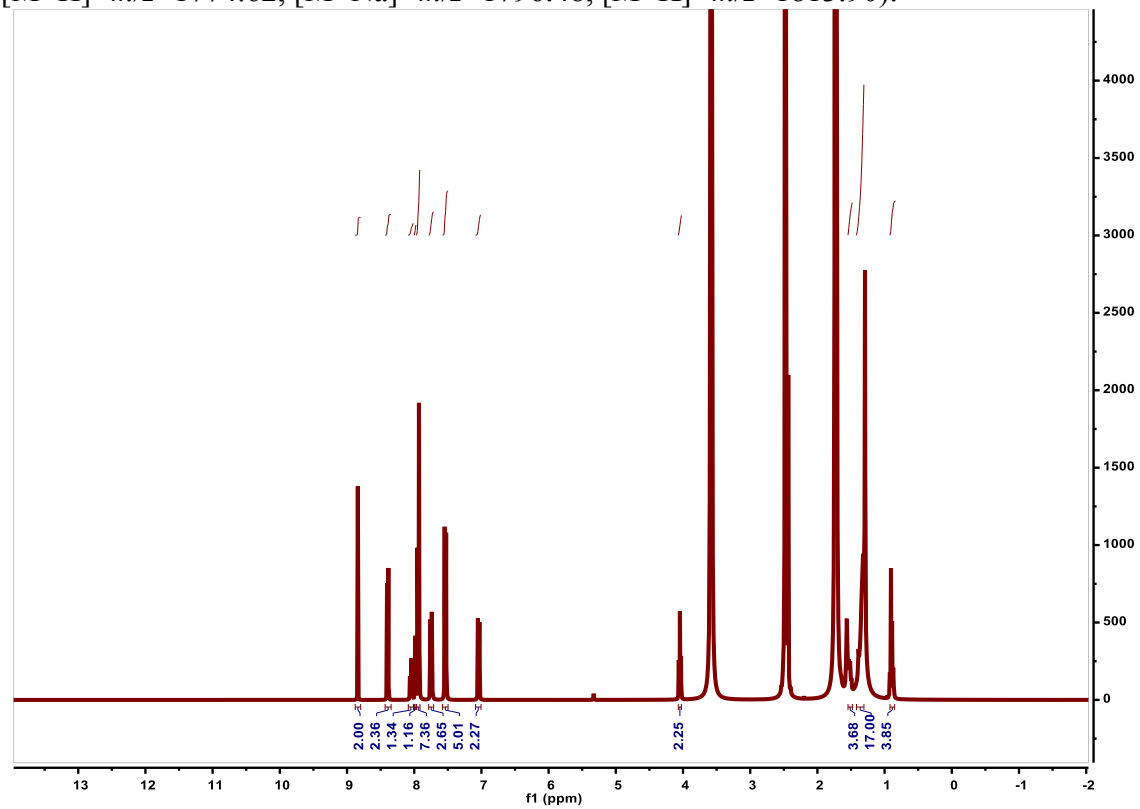

Figure S83. ^{1}H NMR (THF-d_8, 500 MHz, 298 K) of the macrocycles resulting of the competition experiment. Small oligomers containing IDA moieties were removed from the sample prior to analysis.

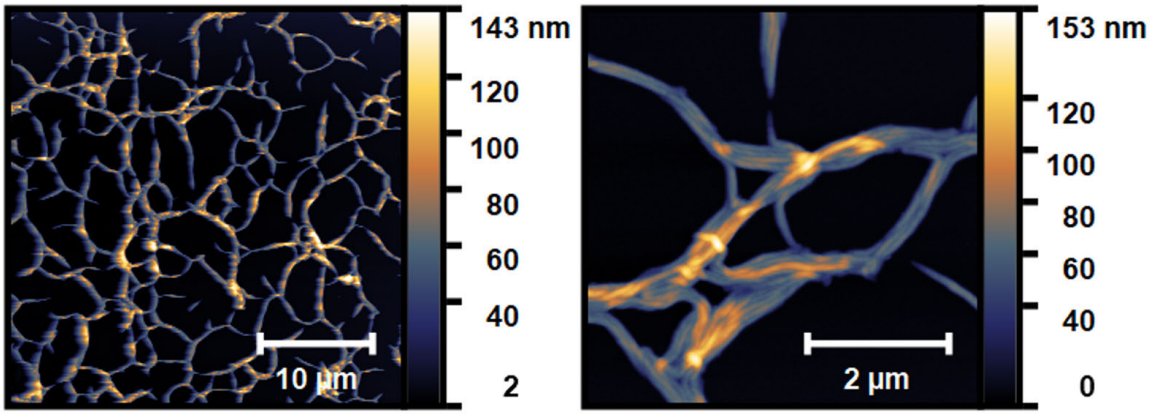

Figure S84. Atomic force microscopy images of a drop cast aliquot of from the competition macrocyclization reaction at 5.1 mM showing the formation of high-aspect ratio nanotubes, further supporting the formation of **MC 2** which have previously demonstrated self-assembly ability.

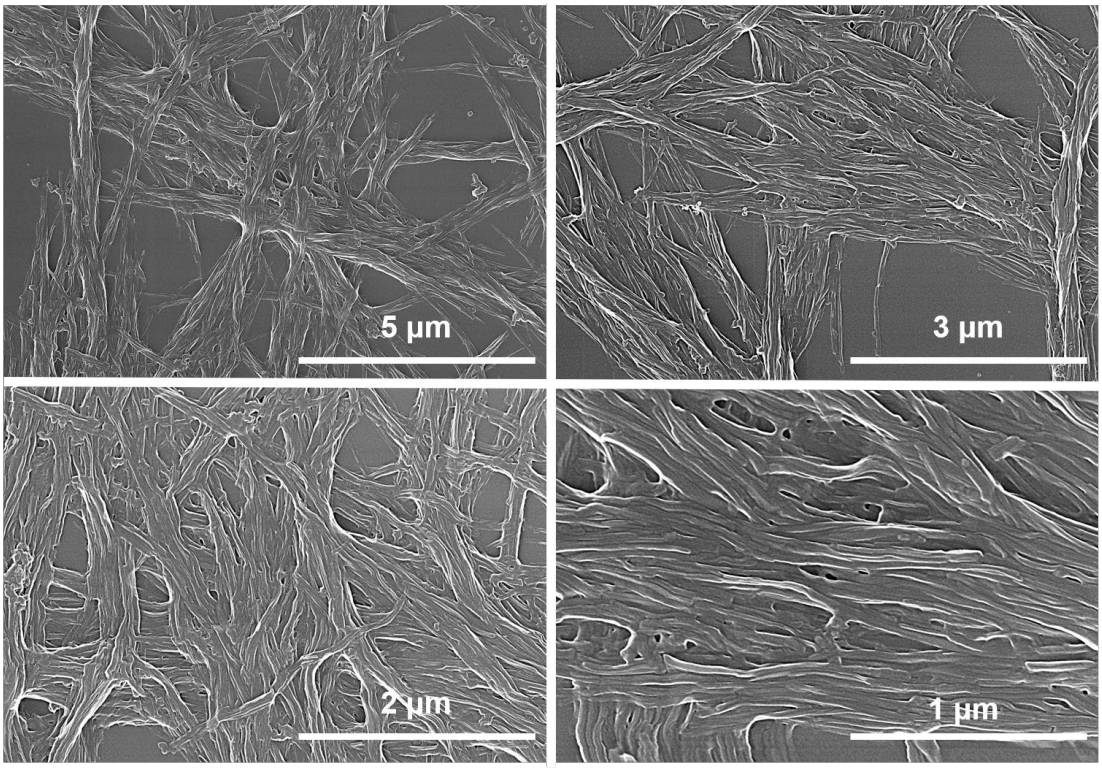

Figure S85. Scanning electron microscopy images of a drop cast aliquot of from the competition macrocyclization reaction at 5.1 mM showing the formation of high-aspect ratio nanotubes, further supporting the formation of **MC 2** which have previously demonstrated self-assembly ability.

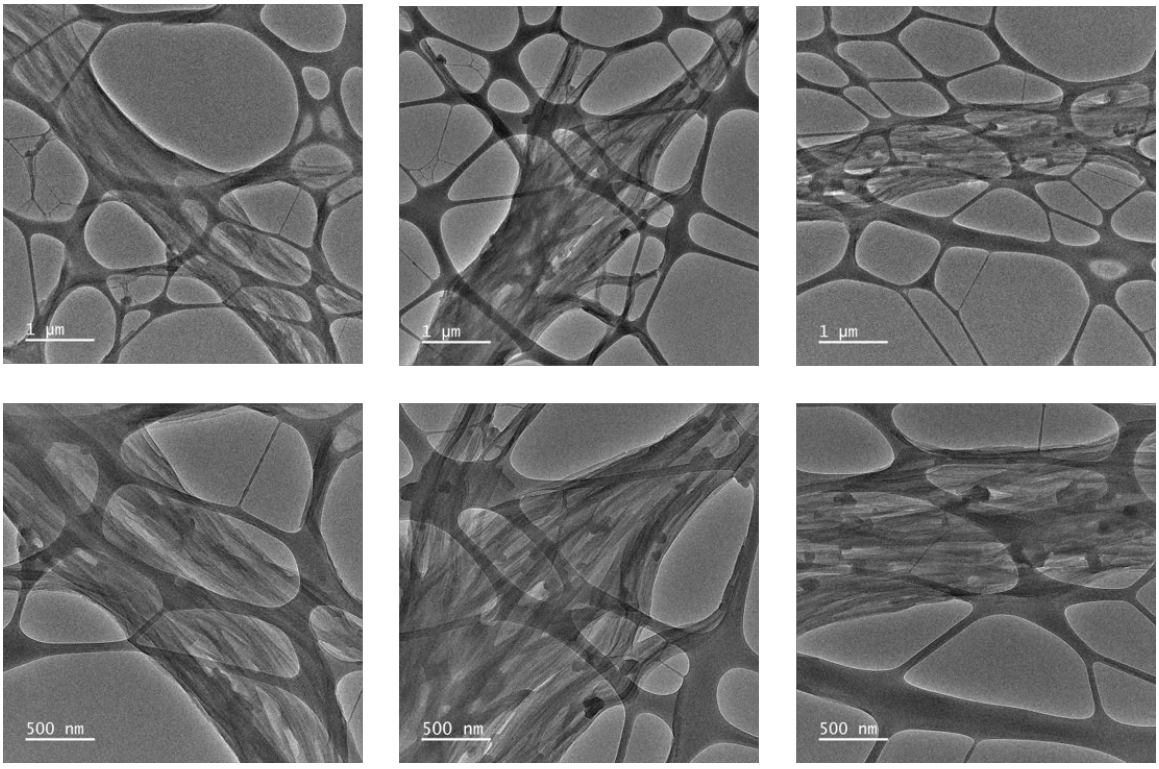

Figure S86. Transmission electron microscopy images of a drop cast aliquot of from the competition macrocyclization reaction at 25 mM showing the formation of high-aspect ratio nanotubes, further supporting the formation of **MC 2** which have previously demonstrated self-assembly ability.

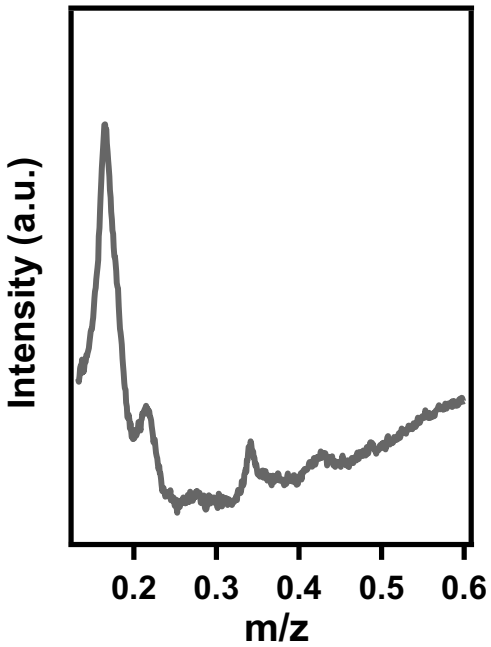

Figure S87. *In-Situ* WAXS pattern of the competition reaction run at 25 mM.

H. Monomer Exchange Experiments Characterization

I. Monomer Exchange of MC 2

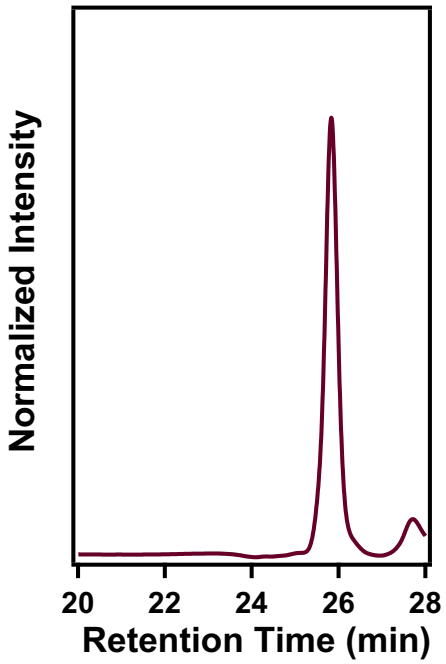

Figure S88. GPC trace of the monomer exchange reaction beginning with the **MC 2** depicting the formation of macrocycles.

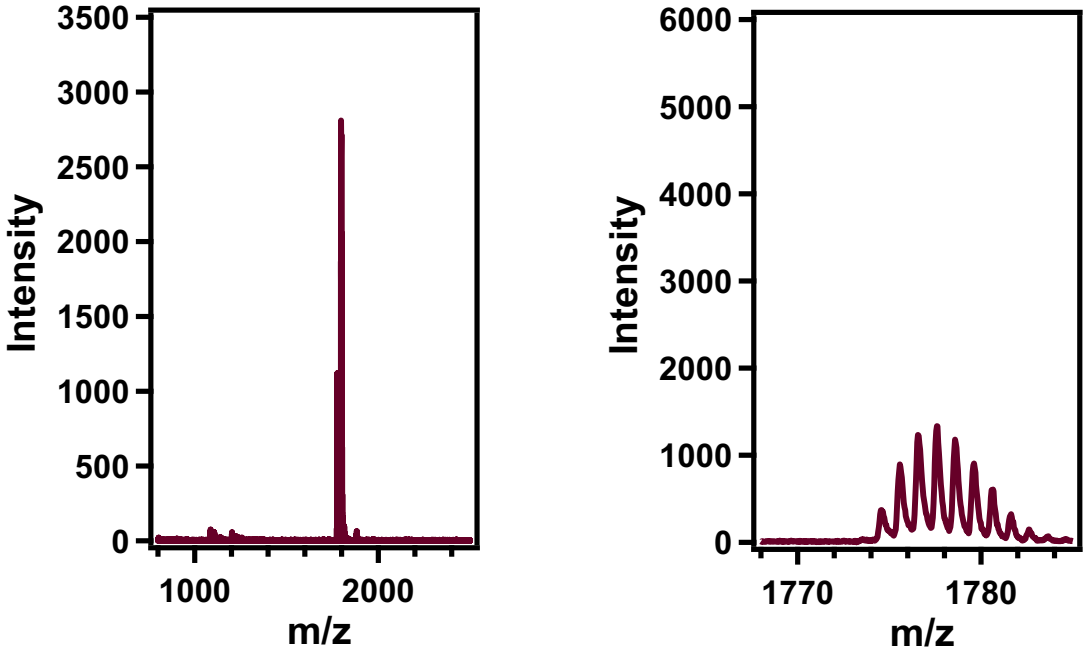

Figure S89. MALDI-MS of the monomer exchange reaction beginning with the MC 2, showing full recovery of the initial **MC 2** ($[M+H]^+$ *m/z*=1774.64, $[M+Na]^+$ *m/z*=1796.51).

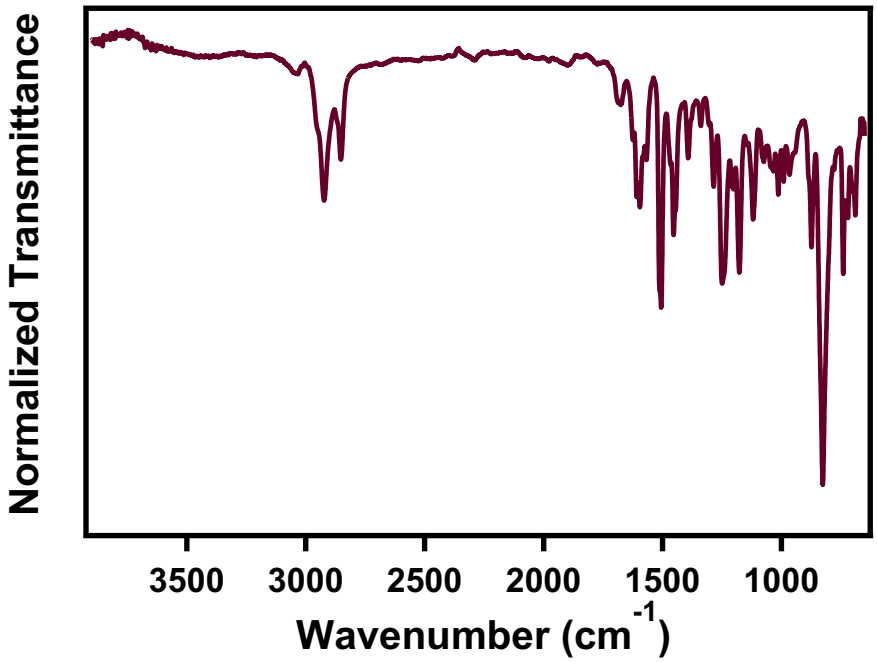

Figure S90. FT-IR spectra of the macrocycles resulting from the attempted monomer exchange reaction beginning with **MC 2**.

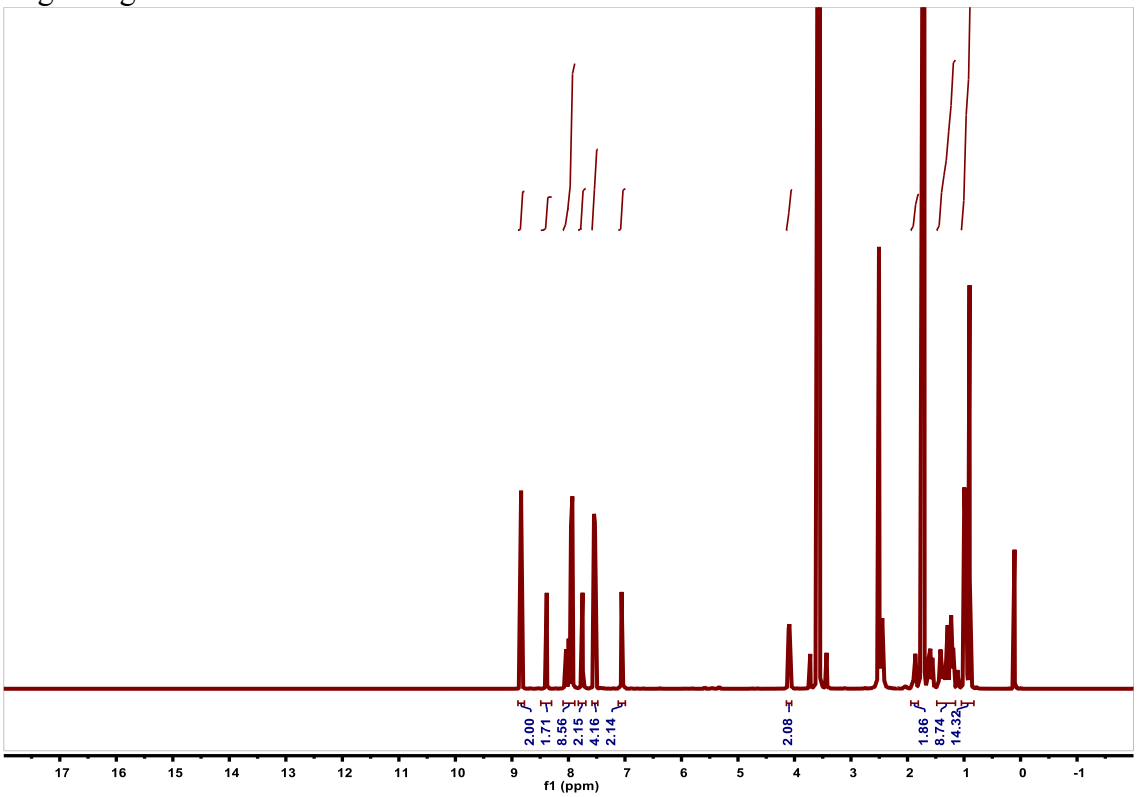

Figure S91. ^{1}H NMR (THF-d_8, 500 MHz, 298 K) of the macrocycles resulting from the attempted monomer exchange reaction beginning with **MC 2**. Rather than observing intercalation of the IDA moieties into **MC 2**, full recovery of **MC 2** was demonstrated.

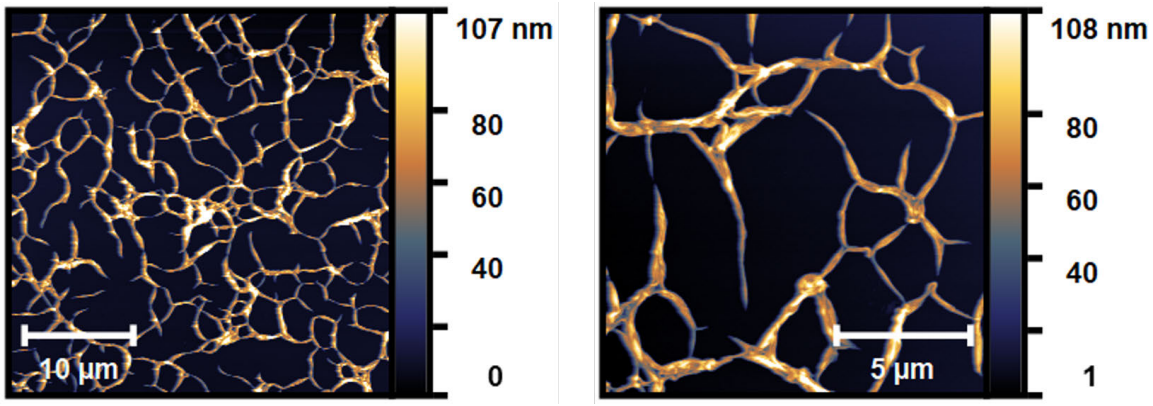

Figure S92. Atomic force microscopy images of a drop cast aliquot of from the monomer exchange reaction beginning with **MC 2**, showing the formation of high-aspect ratio nanotubes as seen in previous **MC 2** samples.

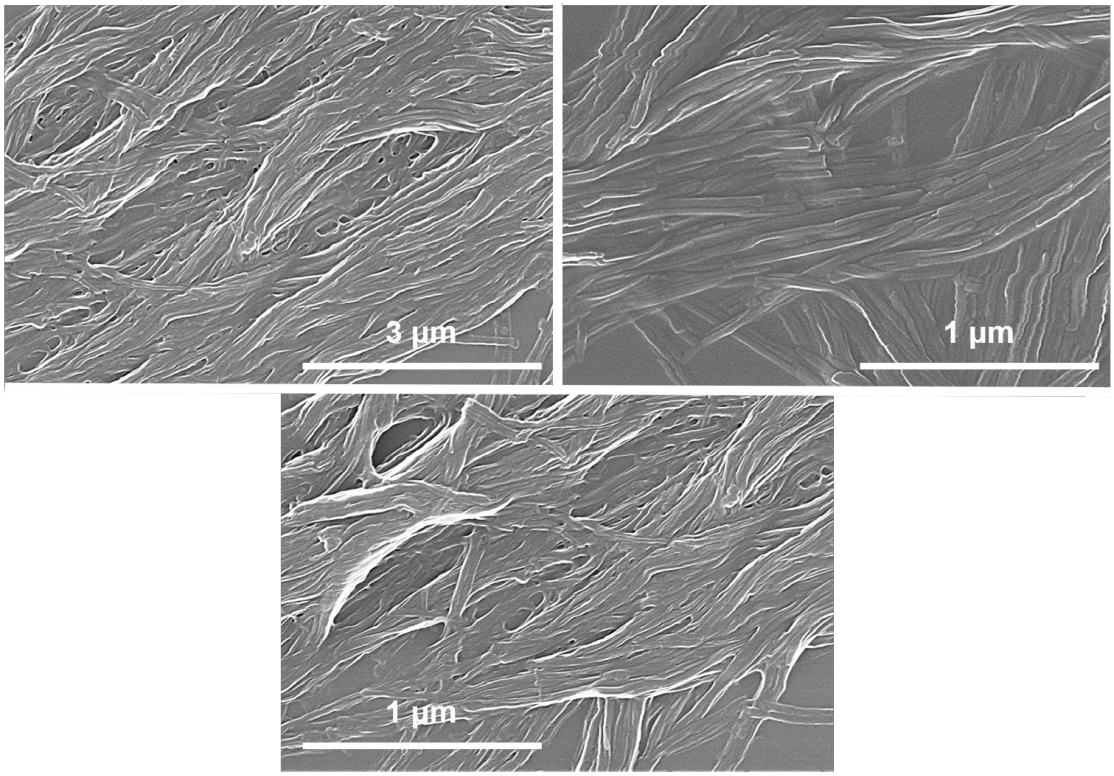

Figure S93. Scanning electron microscopy images of a drop cast aliquot of from the monomer exchange reaction beginning with **MC 2**, showing the formation of high-aspect ratio nanotubes as seen in previous **MC 2** samples.

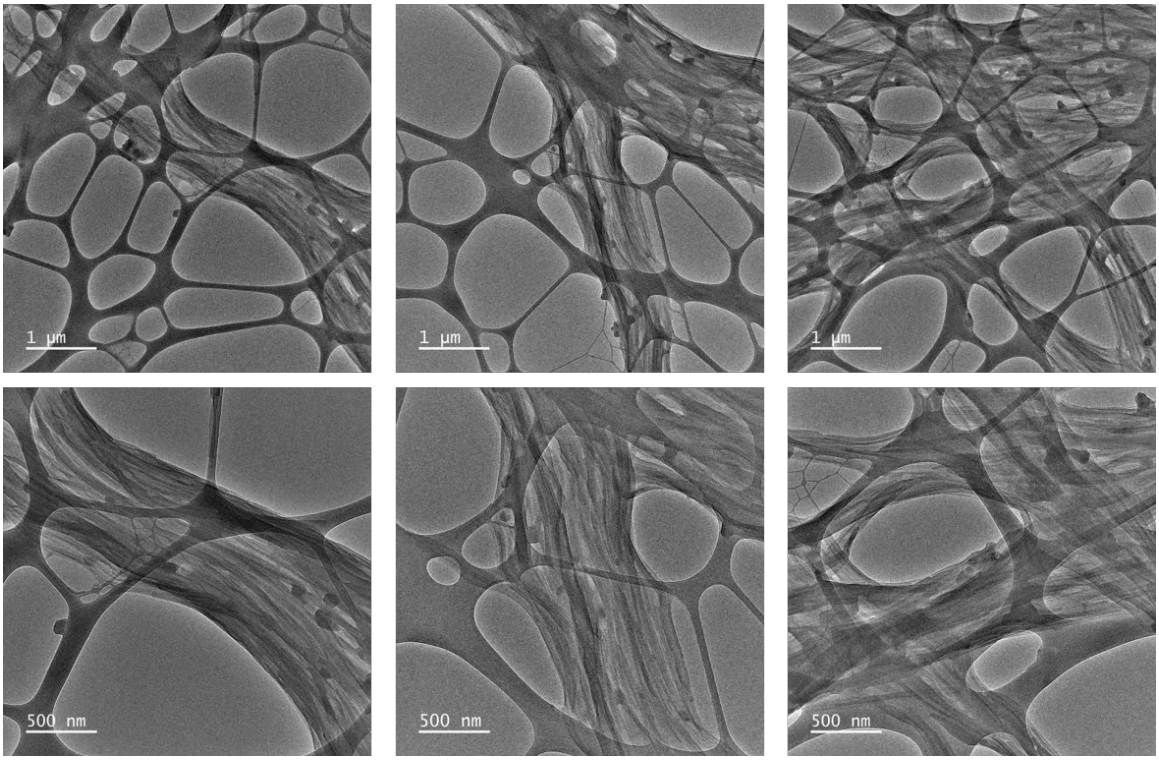

Figure S94. Transmission electron microscopy images of a drop cast aliquot of from the monomer exchange reaction beginning with **MC 2**, showing the formation of high-aspect ratio nanotubes as seen in previous **MC 2** samples.

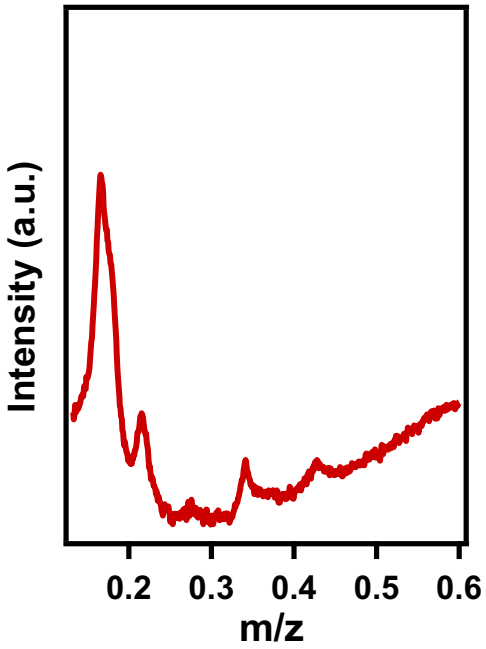

Figure S95. *In-Situ* WAXS pattern of the monomer exchange reaction beginning with the **MC 2.**

II. Monomer Exchange of MC 1

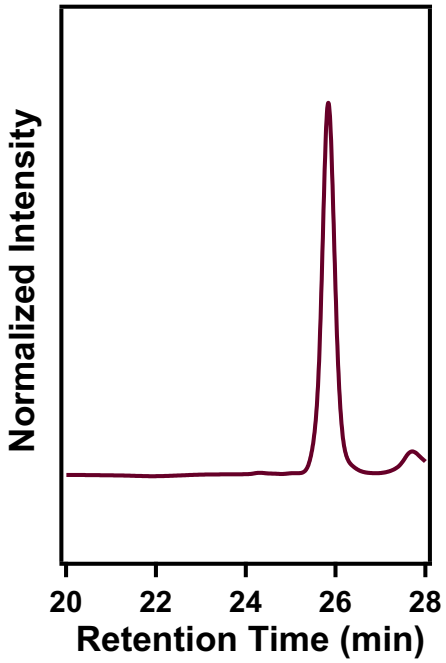

Figure S96. GPC trace of the monomer exchange reaction beginning with the **MC 1**, showing a narrow elution band corresponding to the formation of macrocycles.

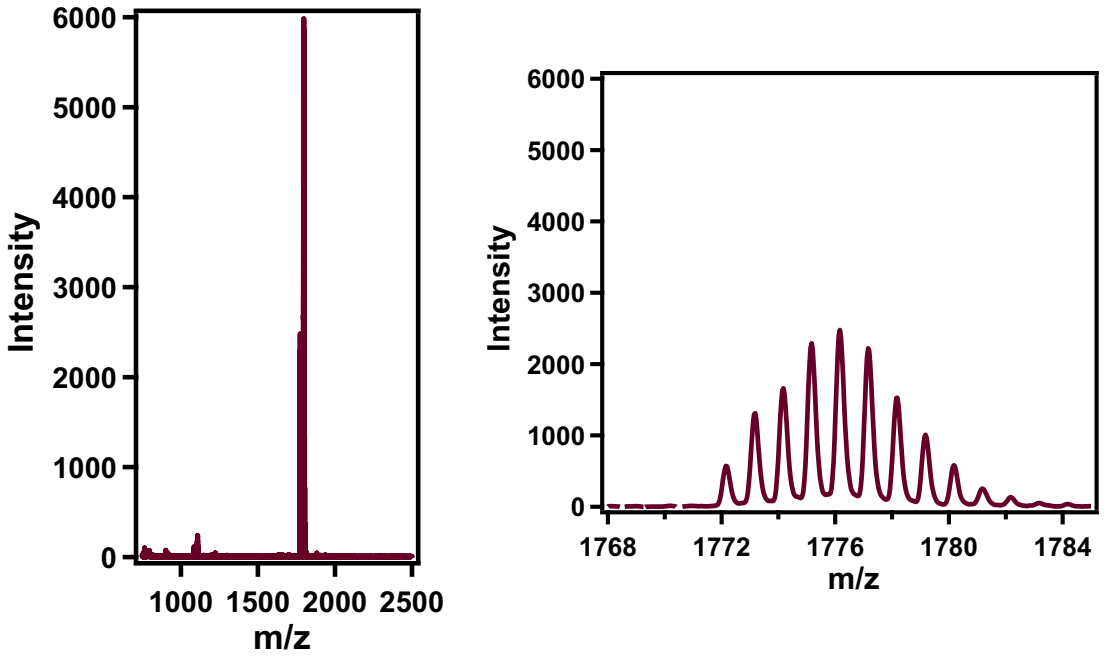

Figure S97. MALDI-MS of the monomer exchange reaction beginning with **MC 1**, showing the neither the retainment of the **MC 1**, nor the full conversion to the **MC 2** (*m/z*=1772.18). A full comparison of the MALDI-MS spectra of **MC 1**, **MC 2**, and this linker exchange can be found in the main text (Figure 5D).

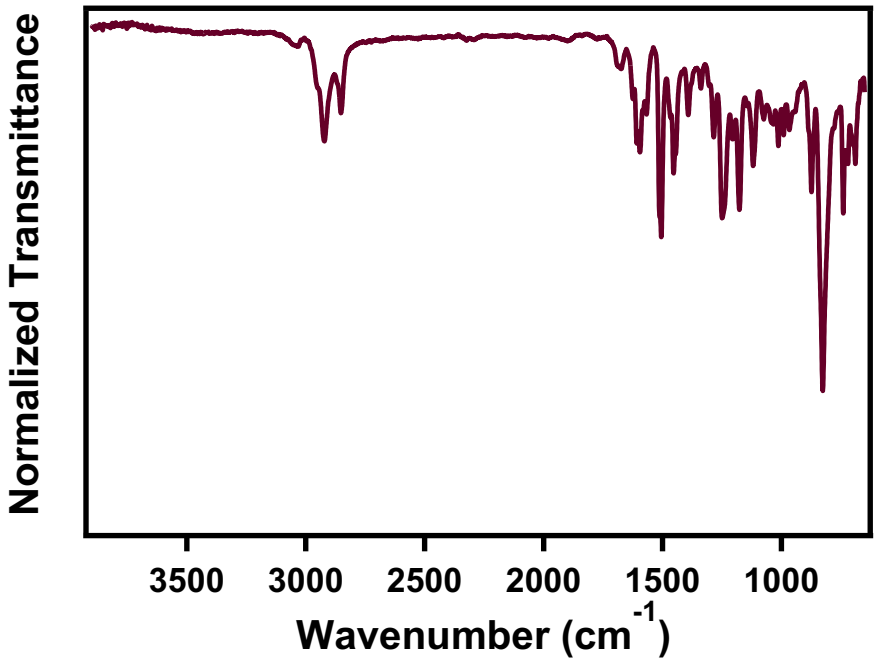

Figure S98. FT-IR spectra of the macrocycles resulting from the attempted monomer exchange reaction beginning with **MC 1**.

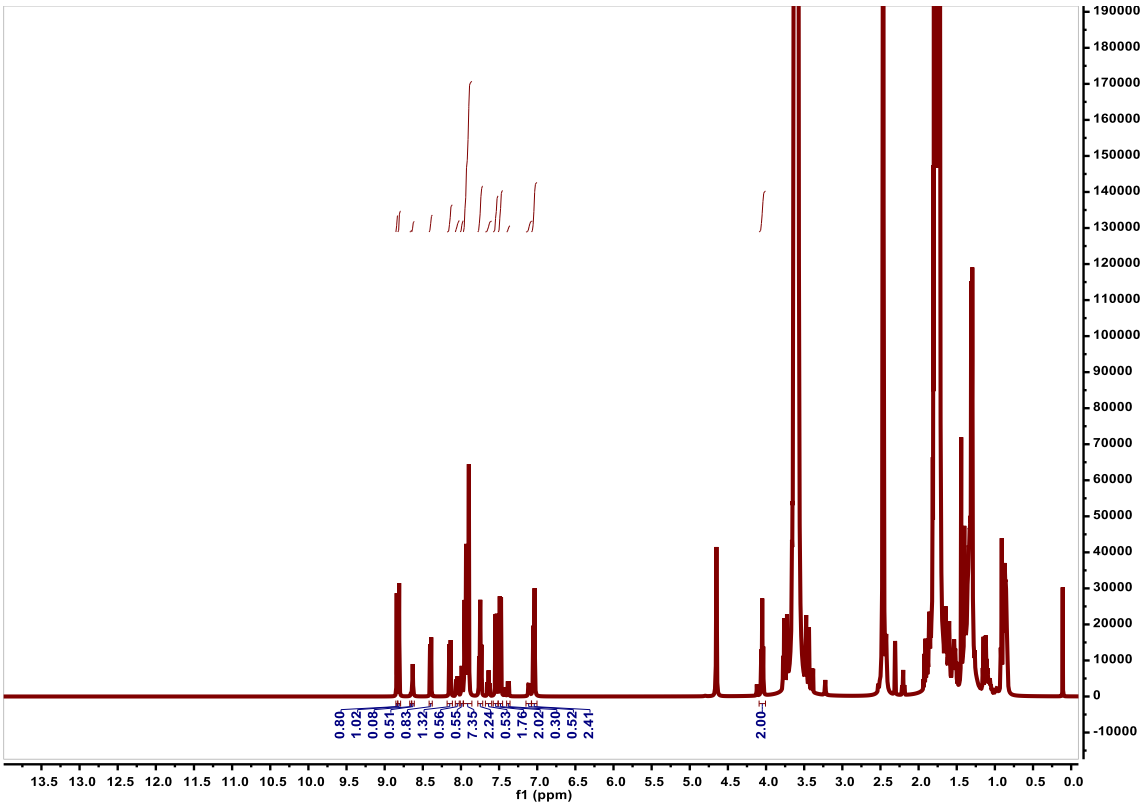

Figure S99. ^{1}H NMR (THF-d_8, 500 MHz, 298 K) of the mixture of macrocycles resulting from the monomer exchange reaction beginning with **MC 1**.

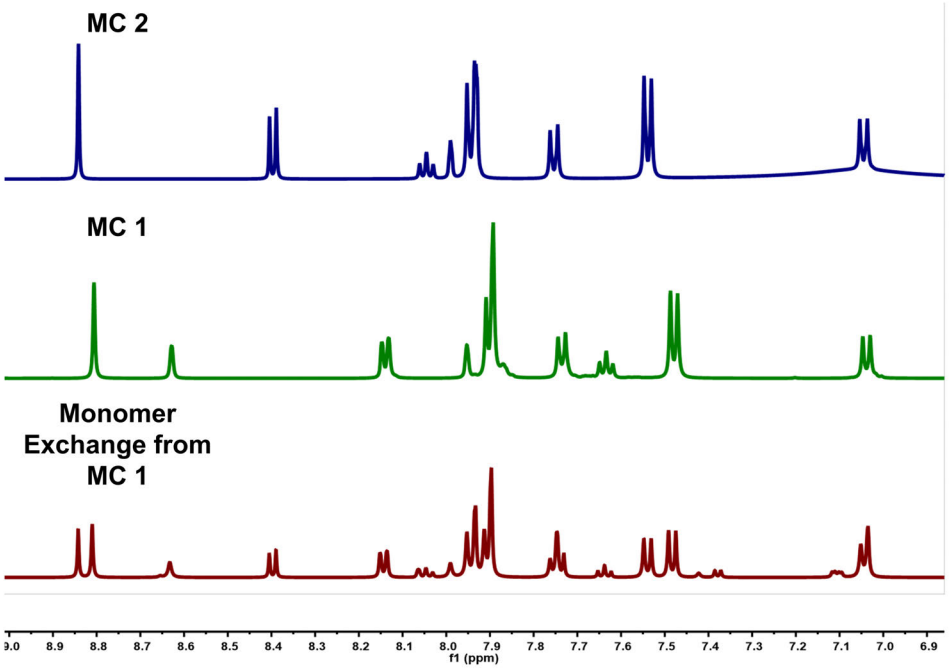

Figure S100. Comparison of ^{1}H NMR spectra from the isolated **MC 2**, the isolated **MC 1**, and the result of the monomer exchange reaction beginning with **MC 1**.

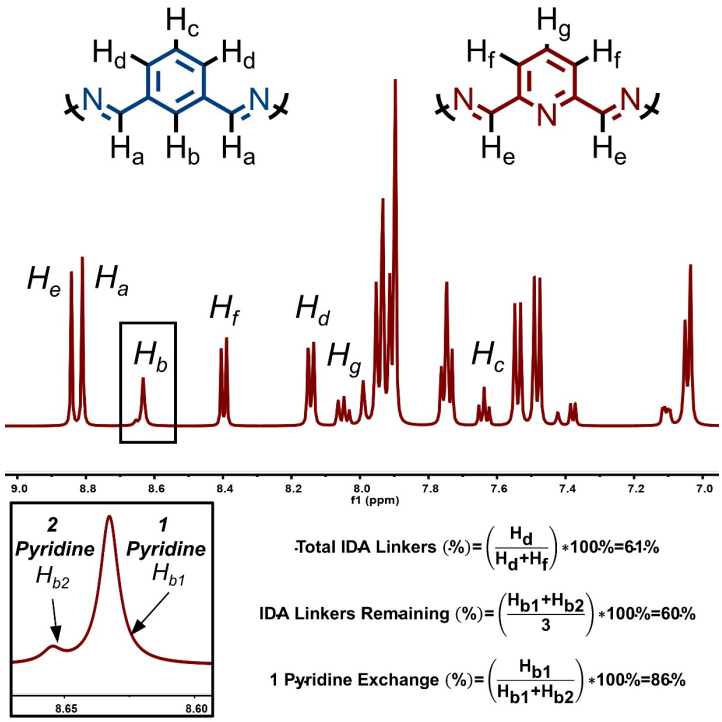

Figure S101. Quantification of monomer exchange via ^{1}H NMR. Furthermore, the small secondary peaks ~7.1 ppm and ~7.4 ppm correspond to species bearing two pyridine moieties and match with the assignment of 14% of macrocycles existing as such.

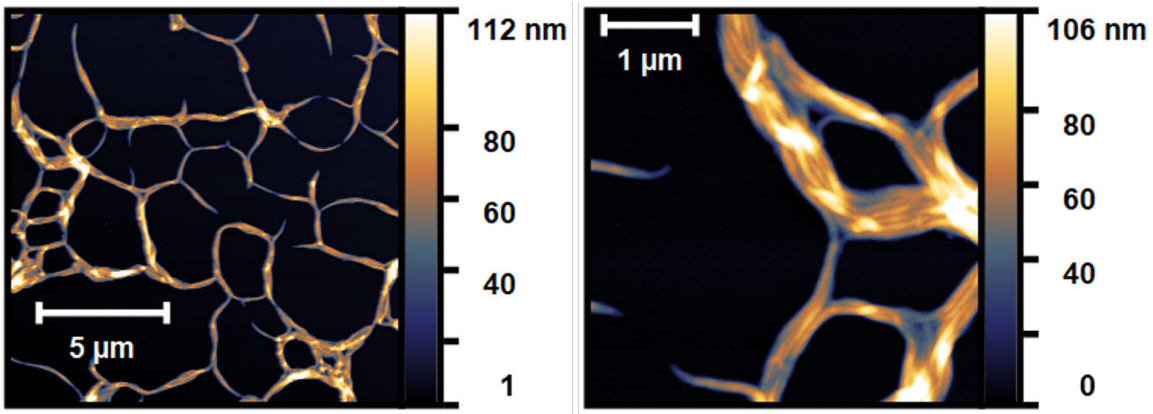

Figure S102. Atomic force microscopy images of a drop cast aliquot of from the monomer exchange reaction beginning with **MC 1**, showing the formation of high-aspect ratio nanotubes.

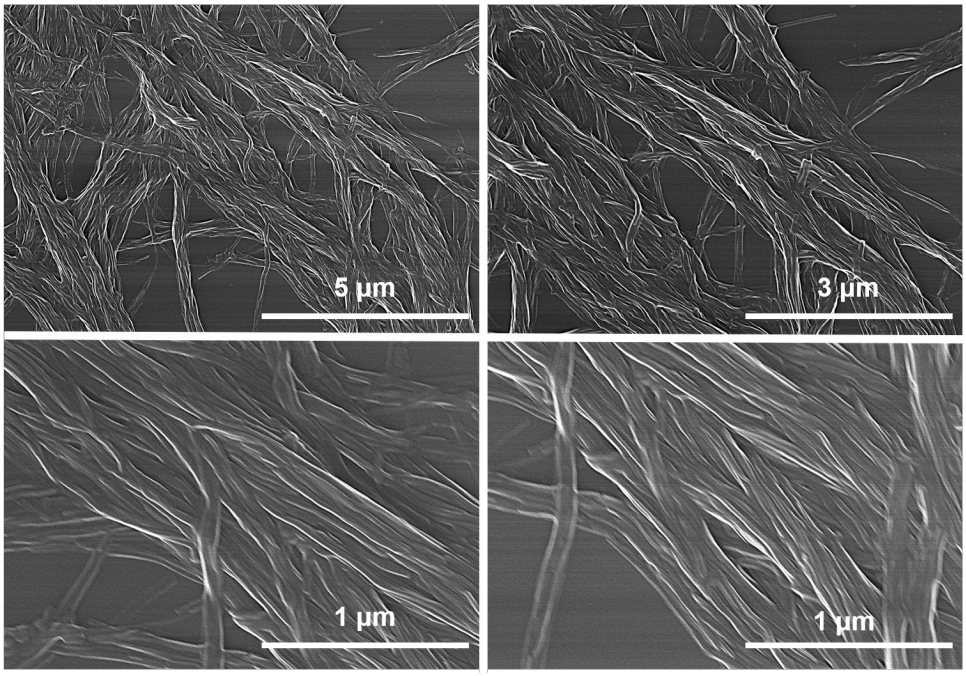

Figure S103. Scanning electron microscopy images of a drop cast aliquot of from the monomer exchange reaction beginning with **MC 1**, showing the formation of high-aspect ratio nanotubes.

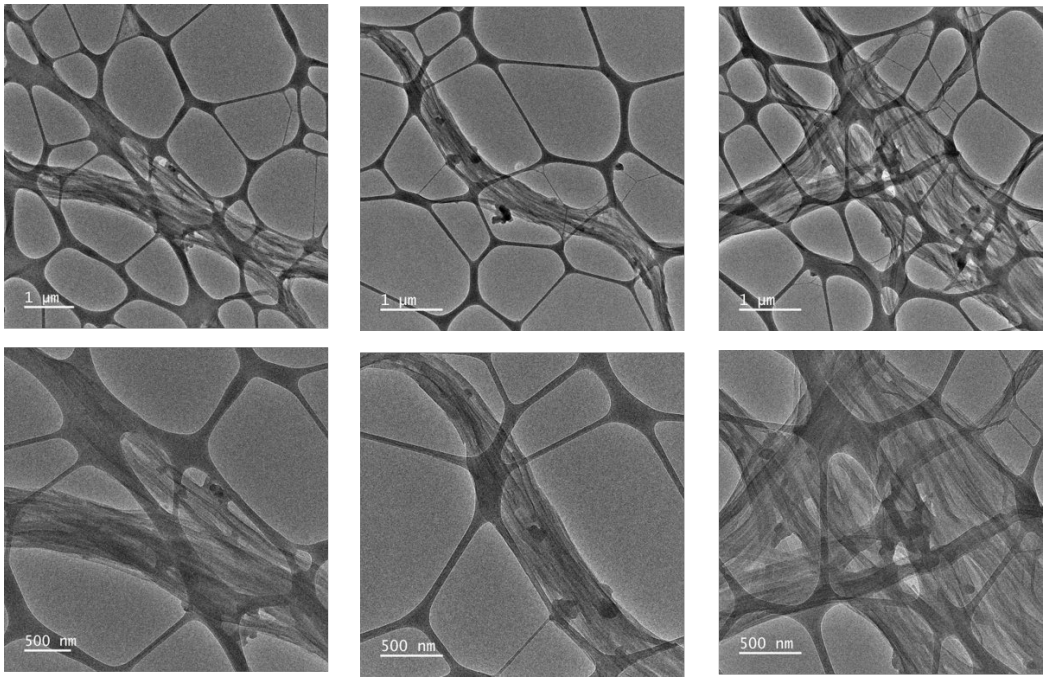

Figure S104. Transmission electron microscopy images of a drop cast aliquot of from the monomer exchange reaction beginning with **MC 1**, showing the formation of high-aspect ratio nanotubes.

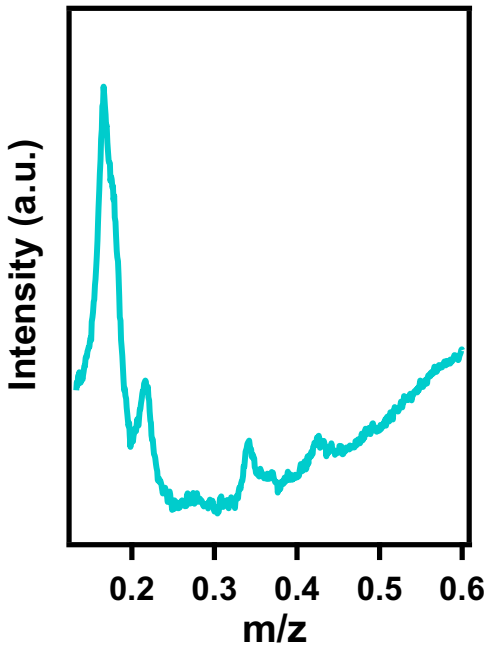

Figure S105. *In-Situ* WAXS pattern of the monomer exchange reaction beginning with the **MC 1**.

III. Synthesis and Monomer Exchange of 5-Br-MC 1

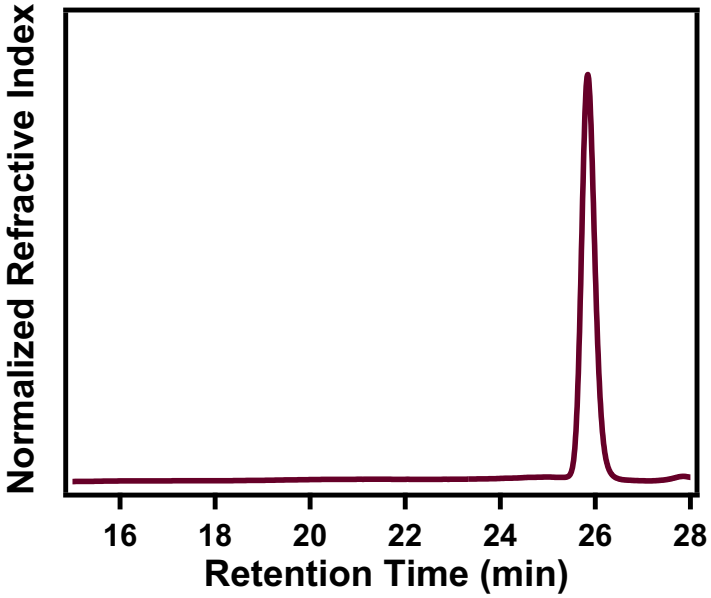

Figure S106. GPC trace of the synthesized 5-Br-IDA MC, showing a single narrow elution band corresponding to successful macrocyclization.

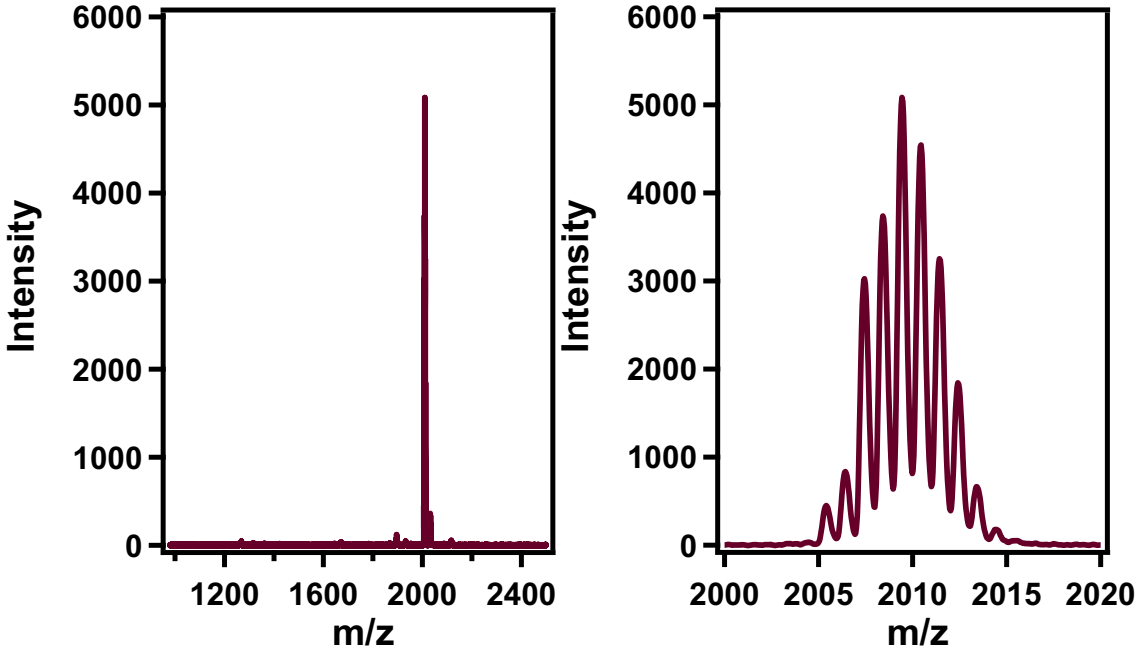

Figure S107. MALDI-MS of 5-Br-IDA MC, showing the desired $[M+H]^+$ adduct (*m/z*=2005.72).

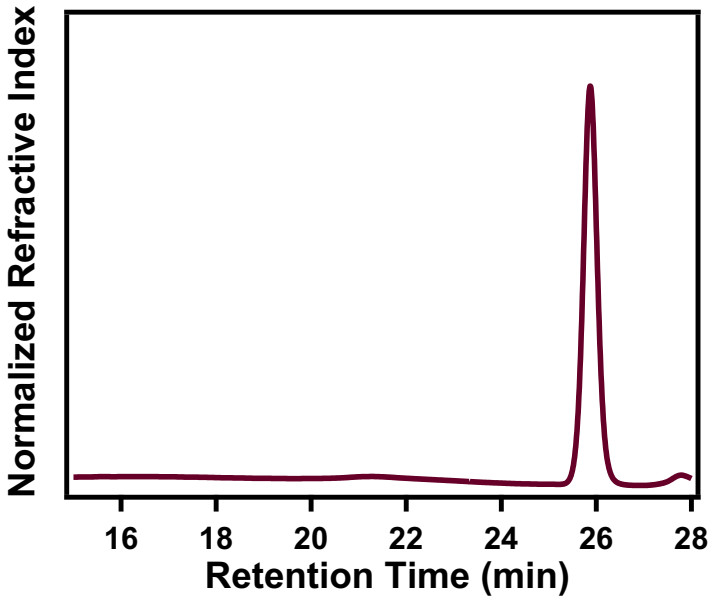

Figure S108. GPC trace of the macrocycles resulting from monomer exchange of the 5-Br-IDA MC with IDA. The narrow elution band corresponds to macrocycle products.

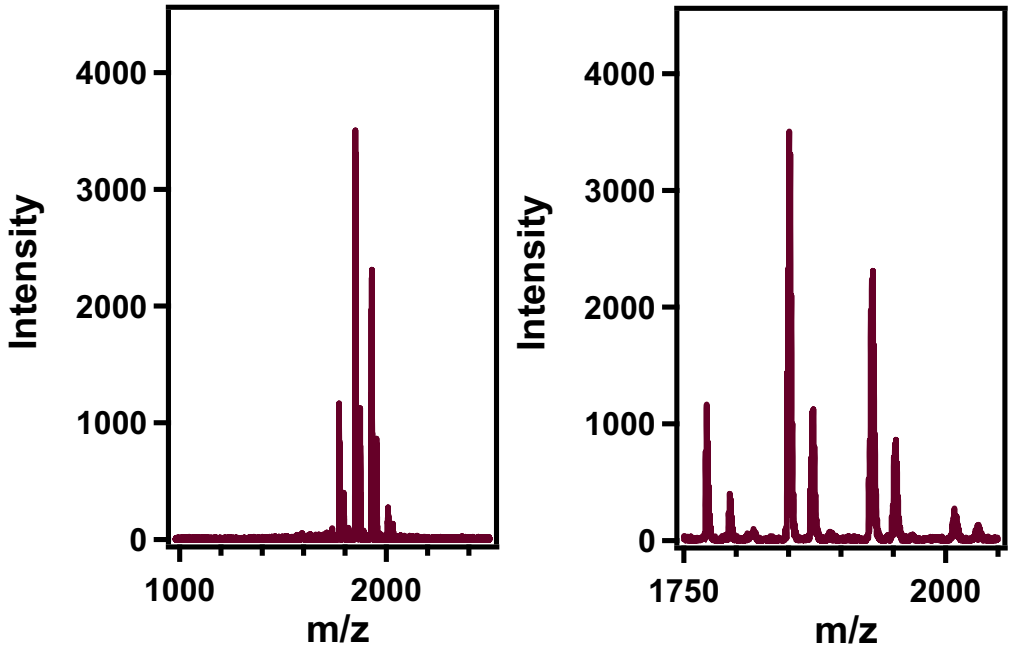

Figure S109. MALDI-MS of the monomer exchange reaction beginning with 5-Br-MC 1, showing the statistical incorporation of IDA monomers into the system ([3•**S1**+3•**IDA**+H]$^+$ *m/z*=1771.74, [3•**S1**+3•**IDA**+Na]$^+$ *m/z*=1794.86, [3•**S1**+2•**IDA**+1•**5-Br-IDA**+H]$^+$ *m/z*=1848.92, [3•**S1**+2•**IDA**+1•**5-Br-IDA**+Na]$^+$ *m/z*=1871.89, [3•**S1**+1•**IDA**+2•**5-Br-IDA**+H]$^+$ *m/z*=1927.83, [3•**S1**+1•**IDA**+2•**5-Br-IDA**+Na]$^+$ *m/z*=1950.82, [3•**S1**+3•**5-Br-IDA**+H]$^+$ *m/z*=2005.75, [3•**S1**+3•**5-Br-IDA**+Na]$^+$ *m/z*=2028.71).

I. Small Molecule ^{1}H NMR Studies

I. Small Molecule Competition ^{1}H NMR Study

Scheme S10. Scheme of small molecule competition study between IDA, DFP, and Aniline under conditions typical for macrocycle synthesis.

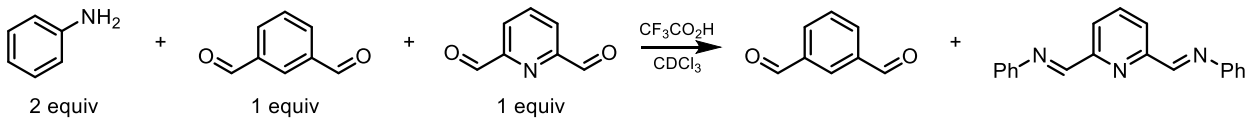

Small Molecule Competition Study:
Aniline (0.025 g, 0.27 mmol), IDA (0.018 g, 0.13 mmol), and DFP (0.018 g, 0.13 mmol) were dissolved in previously dried $CDCl_3$ to a final concentration of 20 mM with respect to aniline. A 1,4-dichlorobenzene (0.015 g) was added to the solution. CF_3CO_2H (34 uL of a 2M solution in $CDCl_3$, 0.5 equiv) was added to the solution, a 1 mL aliquot was placed into an NMR tube and the tube was inverted 3-4 times to ensure proper mixing of the solution. The reaction mixture was then monitored over the course of two hours via ^{1}H NMR spectrometry. HRMS of the reaction mixture after 120 minutes confirmed the presence of a pyridine-2,6-diimine species and unreacted isophthalaldehyde.

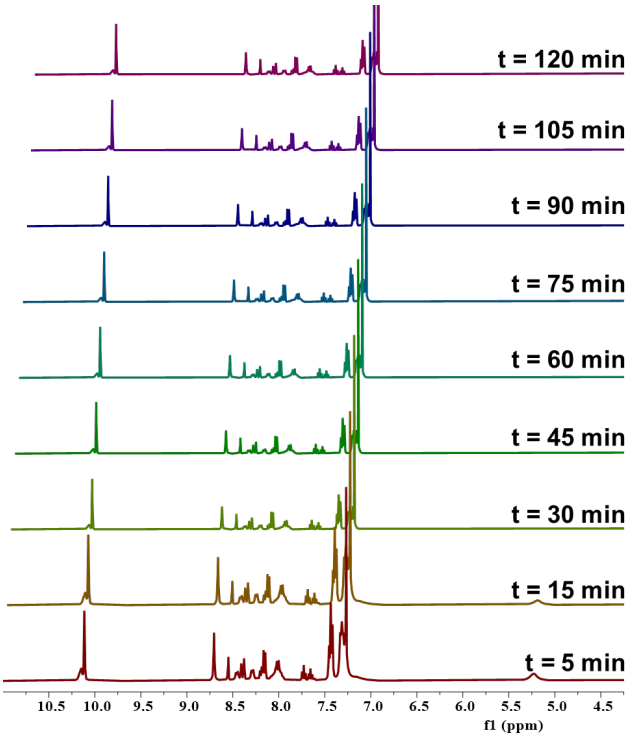

Figure S110. Stacked ^{1}H NMR spectra (400 MHz, $CDCl_3$, 298 K) of the small molecule competition study over the course of two hours. No appreciable changes in the spectra are observed from 5 min. to 2 h. of reaction time indicating that the rapidly formed pyridine-2,6-diimine species is both kinetically and thermodynamically favored.

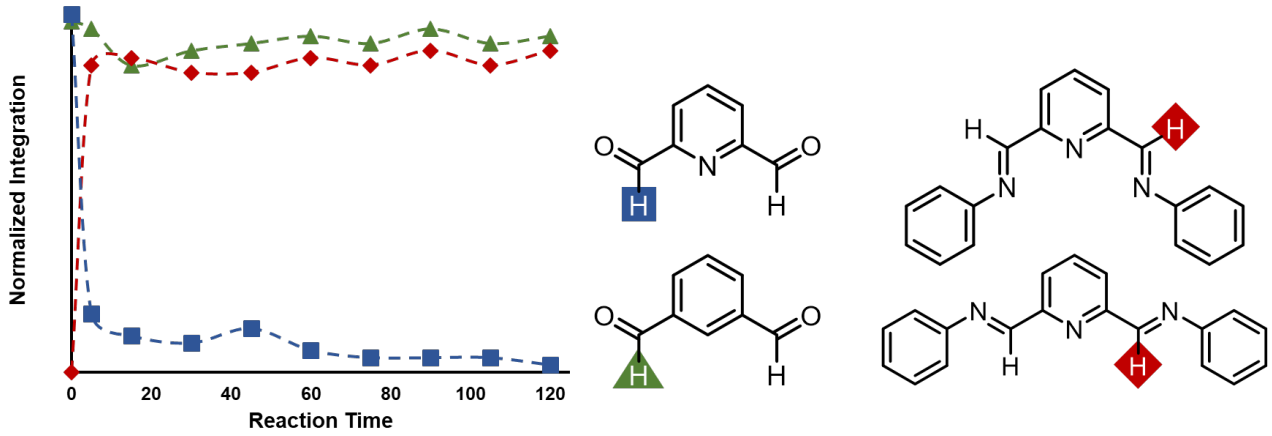

Figure S111. Normalized integrations of the aldehydic protons of both IDA and DFP, along with the integrations of the imine C-H proton with respect to the included 1,4-dichlorobenzene internal standard. The results of the small molecule competition study indicate that DFP is rapidly consumed due to its enhanced electrophilicity relative to IDA, and that the resulting pyridine-2,6-diimine species is thermodynamically favored relative to the benzene-1,3-diimine analogue.

II. Small Molecule Scrambling ^{1}H NMR Study

Scheme S11. Scheme of small molecule scrambling study between IDA, DFP, and Aniline under conditions typical for macrocycle synthesis.

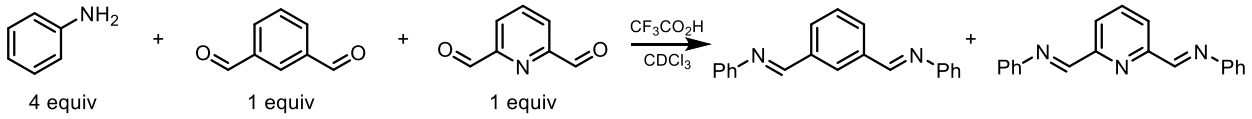

Small Molecule 'Scrambling' Study:
Aniline (0.025 g, 0.27 mmol), IDA (0.009 g, 0.07 mmol), and DFP (0.009 g, 0.07 mmol) were dissolved in previously dried $CDCl_3$ to a final concentration of 20 mM with respect to aniline. A 1,4-dichlorobenzene (0.02 g) was added to the solution. CF_3CO_2H (16 uL of a 2M solution in $CDCl_3$, 0.5 equiv) was added to the solution, a 1 mL aliquot was placed into an NMR tube and inverted 3-4 times to ensure proper mixing of the solution. The reaction mixture was then monitored over the course of two hours via ^{1}H NMR spectrometry. HRMS of the reaction mixture after 120 minutes confirmed the presence of both pyridine-2,6-diimine and benzene-1,3-diimine species.

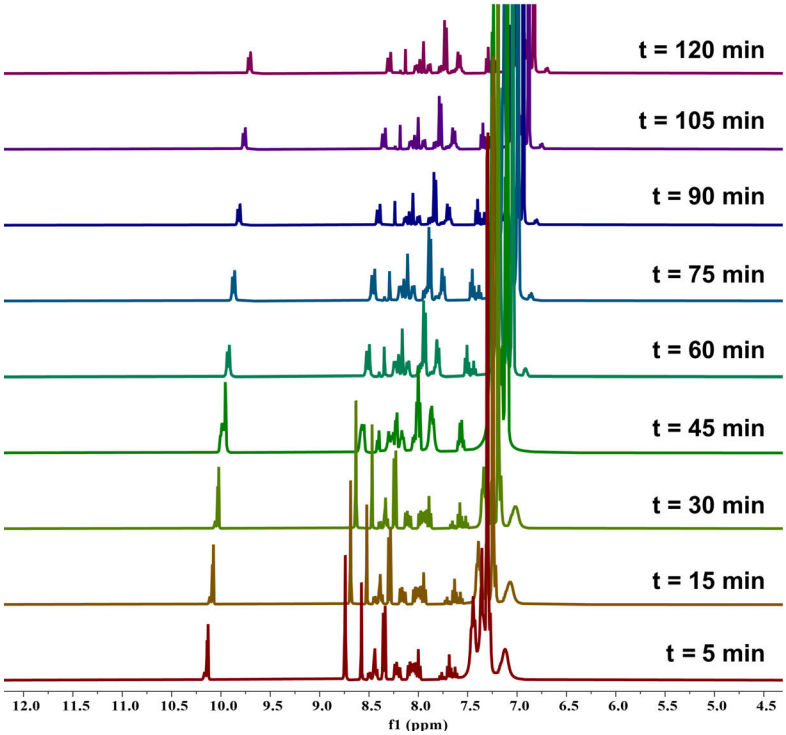

Figure S112. Stacked ^{1}H NMR spectra (400 MHz, $CDCl_3$, 298 K) of the small molecule 'scrambling' study over the course of two hours. Consumption of the pyridine-2,6-dicarboxaldehyde monomer mainly occurred prior to the first spectra being recorded, and the consumption of isophthalaldehyde began at ~45 min of reaction time. At elevated reaction times, two aldehydic species are observed, one in which IDA had reacted with 1 equiv of aniline and one in which IDA had not reacted with aniline. Resonances corresponding to the DFP aldehydes were almost completely consumed upon the first measurement. Integration relative to an internal standard yielded that the IDA imine resonance corresponded to structures with both one and two imines, which was further corroborated by mass spectrometry (Figure S113).

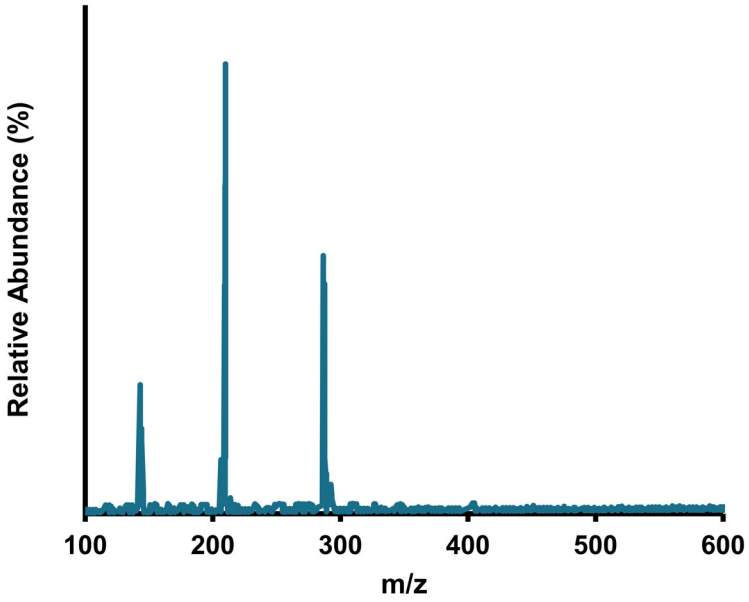

Figure S113. Mass spectrum of the results of the small molecule 'scrambling' reaction yielding peaks 135.3 ($[IDA+H]^+$), 210.3 ($[IDA+1•Aniline+H]^+$), 285.4 ($[IDA+2•Aniline+H]^+$), 286.5 ($[DFP+2•Aniline+H]^+$) matching with the changes observed via ^1H NMR.

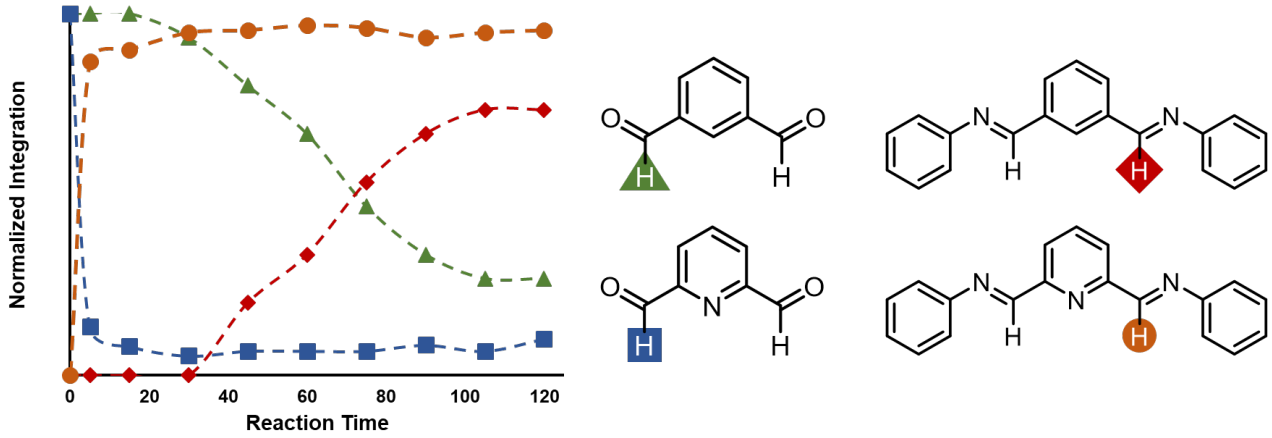

Figure S114. Normalized integrations of the aldehydic protons of both IDA and DFP, along with the integrations of the imine C-H protons with respect to the included 1,4-dichlorobenzene internal standard. The results of the small molecule scrambling study indicate that both imines can be formed in solution, albeit at different reaction times. These results contradict the macrocycle competition study in which both **MC 2** and **MC 1** could not both be formed under reaction relevant conditions. These results suggest that an antagonistic effect exists between the kinetically favored **MC 2** nanotubes and the kinetically sluggish **MC 1** species.

J. References

1. Chavez, A. D.; Evans, A. M.; Flanders, N. C.; Bisbey, R. P.; Vitaku, E.; Chen, L. X.; Dichtel, W. R., Equilibration of Imine-Linked Polymers to Hexagonal Macrocycles Driven by Self-Assembly. *Chem. Eur. J.* **2018,** *24* (16), 3989-3993.
2. Strauss, M. J.; Asheghali, D.; Evans, A. M.; Li, R. L.; Chavez, A. D.; Sun, C.; Becker, M. L.; Dichtel, W. R., Cooperative Self-Assembly of Pyridine-2,6-Diimine-Linked Macrocycles into Mechanically Robust Nanotubes. *Angew. Chem. Int. Ed.* 10.1002/anie.201907668.